Master of Science Thesis

A Study on Frequency Dependency and Spatial Modeling of Wireless Channels

Jia Chen (4032268)

International Research Centre for
Telecommunication and Radar (IRCTR)
Faculty of Electrical Engineering
Mathematics and Computer Science
Delft University of Technology,
the Netherlands

Department of Radio Access Innovation
KPN, the Netherlands

Supervisor: Dr.ir. Homayoun Nikookar (TU Delft)
Dr.ir. Zoubir Irahhauten (KPN)

Delft, the Netherlands
June, 2011

A Study on Frequency Dependency and Spatial Modeling of Wireless Channels

THESIS

submitted in partial fulfillment of the
requirements for the degree of

MASTER OF SCIENCE

in

TELECOMMUNICATIONS

by

Jia Chen B. Sc.
born in Wuhan, P.R. China

This work was performed at:

International Research Centre for Telecommunications and Radar
Department of Telecommunications
Faculty of Electrical Engineering, Mathematics and Computer Science
Delft University of Technology

Telecommunications Department
Faculty of Electrical Engineering, Mathematics and Computer Science
Delft University of Technology
Delft, the Netherlands

DELFT UNIVERSITY OF TECHNOLOGY

DEPARTMENT OF

TELECOMMUNICATIONS

The undersigned hereby certify that they have read and recommend to the Faculty of Electrical Engineering, Mathematics and Computer Science for acceptance a thesis entitled **"A study on frequency dependency and spatial modeling of wireless channels"** by **Jia Chen B.Sc.** in partial fulfillment of the requirements for the degree of **Master of Science**.

Dated: June 15th, 2011

Chairman: _____

Prof. dr. O. Yarovoy

Committee members: _____

Dr. ir. H. Nikookar

_____

Dr. ir. Z. Irahhauten

_____

Dr. ir. G. Janssen

_____

Ing. M. Klepper

Abstract

There are many different wireless communication systems operating simultaneously, such as GSM, WiFi, LTE and etc. Each of these wireless communication systems operates at different frequency bands and with different bandwidths. As we know, the successful implementation of wireless communication technology requires a good understanding of the propagation characteristics of the wireless channel, which may vary from one environment to another. According to the previous research, the channel modeling for different wireless communication systems is well developed at the corresponding working frequency bands. However, there are few researches on the frequency dependency of the wireless channel models. In fact, the signal's pathloss in free space transmission is strongly frequency dependent and also the scattering and diffraction mechanisms have close relationship to the frequency. Therefore, the channel parameters should be characterized differently at different frequency bands, which need to be noticed and investigated.

In this Msc. thesis project, the statistical method is utilized for our channel modeling work. We firstly design a UWB channel measurement system and then utilize it to gather a large number of channel measurements at three different indoor scenarios, which is used later for the channel modeling studies. Because of the use of circular array at the receiver side, the multipath angular information is estimated and this makes the spatial modeling of wireless channel possible. This extra angular information is important for communication systems, such as MIMO, smart antenna and in other fields such as radar as well. For the modeling part, we choose the statistical approach to model the wireless channel and also study the related frequency dependency issues. At the beginning, a wideband spatial channel model is proposed. After that, we discuss the methods for both modeling and estimating of channel

parameters, such as multipath amplitude, *rms* delay spread and angular spread. This work can be seen as a good reference for telecom companies developing future LTE band outdoor channel measurements as well as related channel modeling efforts. In the end, the bandwidth effect and frequency dependency of wireless channels are studied and the measured data is used to validate the models. According to the analysis result, we find the bandwidth can have serious influence on the accuracy of channel parameter's estimation and this thesis provides a guide to choose the right method to model them in different bandwidths. For the channel frequency dependency study, although it has been found that no significant frequency dependency exist comparing the channel parameters at different frequency bands, we analyze the reasons from different aspects and also give the recommendations for the future works.

Acknowledgements

I would like to deliver my deepest appreciation to those who have supported me throughout the thesis process. Firstly, I would like to express my sincere thanks to my supervisor, Dr. H. Nikookar and daily mentor, Dr. Z. Irahhauten, for their guidance, encouragement and continuous support during the whole thesis project. I also would like to express my gratitude to the IRCTR lab technicians: P. Aubry, P. Hakkaart, J.H. Zijderveld and W.F. van der Zwan, for their guidance and assistance during the measurement system design and channel measurements. I am also very grateful to the PhD students, Yiyin Wang and Kaifeng Guo, for their invaluable suggestions.

Furthermore, I would like to thank my KPN manager Mr. Matthijs Klepper, who provided me this precious opportunity to work on this interesting project and allow me to work with all the wonderful people at KPN. Additionally, I want to thank my thesis committee, Prof.dr. O. Yarovyi and Dr. G. Janssen, for taking time to give feedback on my thesis. I am very grateful to all MTSR and WMC members and all my fellow students, for the pleasant and stimulating atmosphere.

Last but not least, I would like to thank my family for their support and encouragement. Also I want to say thank you to my friends who give me help during the whole project.

Table of Contents

Chapter 1

Introduction

1-1 Background

The world is now in a stage of major telecommunication revolutions. The needs for multimedia communications and new flexible communication capabilities with high data rates and high Quality of Service (QoS) requirements become increasingly important. For instance, mobile communication is evolving from 2nd (GSM) to 3rd (UMTS) generation and consequently to the 4th generation (LTE) and LTE advance providing broadband wireless applications in the coming decade. Each of these wireless communication systems uses its own technology and operates at different frequency bands with different bandwidths. As we know, the successful implementation of wireless communication technology, such as LTE, transmitting over wireless channels requires a good understanding of the propagation characteristics of the radio channel, which may vary from one environment to another. The radio propagation mechanisms in indoor and/or outdoor environments are complex. These signals propagating in the wireless environment may undergo attenuation, reflection, refraction and diffraction. In general, because of these effects, the transmitted signal arrives at the receiver through various paths having different amplitudes, delays and phases and these would influence the communication system's performance operating on such channel. For example, signal transmission usually results in delayed and attenuated echoes of each transmitted signal, which in digital communication systems causes inter-symbol interference and eventually limits the transmission rate of the data. In addition to this, the received signal also suffers from noise and interference. That is why a designer of communication systems must understand the channel characteristic or built a well matched channel model before designing the communication systems.

There are several methods to model the wireless channel, such as deterministic, statistical and the geometry-based stochastic modeling. However, the most common way is statistical modeling approach. The main reason of using such method is it balances between the accuracy and complexity of channel modeling. The deterministic method, such as ray tracing, usually only considers free space transmitting and reflection mechanisms but neglects the effects from diffraction and scattering mechanisms, which is not enough to describe accurately the complex real mobile channel environment. On the opposite, the statistical method is based on real measurements and therefore it can reflect the real wireless channel to some extent. The statistical method is usually done by measuring the wireless channel in the environment, proposing mathematical channel models and finally statistically analyzing the measured data to validate such developed channel models. Therefore, multidimensional (such as delay, position, azimuth/elevation angle and etc.) probability functions of channel impulse response are used in this model.

The channel parameters modeling, such as power/amplitude fading distribution, *rms* delay spread and angular spread can be good indicators to reflect the multipath propagation channel. For example, the small-scale fading phenomenon has serious influence on the received signal power (there is more than 15dB power attenuation). Therefore, the fading parameter combined with the pathloss and scattering could be good information for calculating the mobile system's minimum transmitting power, which can satisfy all users in the network to communicate successfully. The time dispersion parameter or *rms* delay spread indicates how the received power is distributed with respect to time. Delay spread restricts transmitted data rates and could limit the capacity of the system. For the angular spread parameter, people begin to pay attention on it since the MIMO technology is developed. Because of the inventions of different beamforming technologies, the multipath signals' angles of arrival (AoA) can be estimated. This multipath AoA parameter can improve the system's performance. For instance, if the AoA of the strongest signal is known, the antenna array's main beam can be formed to that direction to increase the receiving power by using, for example, digital beamforming method. As a result, well studying the channel and finally building a well matched channel model is very important for developing wireless communication systems, such as LTE.

1-2 Motivation and Goals

According to the previous work, the channel modeling for different wireless communication technology is well studied and channel models are developed separately for different frequency bands. However, there are seldom researches on the frequency dependency of the wireless channel and less people focus on the study of frequency correlation. As we know, the signal's pathloss in free space transmission is really frequency dependent and the amplitude or angle of rough surface reflected multipath is also having close relation to frequency, such as scattering, diffraction phenomenon. Therefore, the channel parameters might be characterized differently on different frequency band. Meanwhile, the meaning for the frequency dependency study is also very important. As the fast development of wireless communication field, there will be many new technologies and systems invented and operated in different new frequency bands, respectively. Therefore, considering the channel modeling issue in new frequency band, can we directly utilize the channel model developed on currently occupied frequency band (such as GSM band) to the new frequency band (such as LTE band)? The answer is yes if a frequency dependent channel model can be developed. Furthermore, the frequency diversity, such as multiband OFDM, is a very promising technology used in the next generation's mobile system. The idea of frequency diversity is using different sub-bands or sub-carriers to transmit signals simultaneously. Thus, if we know the frequency correlation among these sub-bands, it is very important and useful for us to improve such system's performance. In this regard, it is imperative to know the frequency dependency of the channel parameters, such as power/amplitude fading, *rms* delay spread and angular spread.

There are also several meaningful reasons for spatial channel modeling. Since the development of antenna array, it gives the door to estimate signals' AoAs. Through mapping these arrives angles to the channel environment, the propagation route of each multipath can be exactly known, which help us better understand the wireless channel. The signal's AoA estimation is also essential for smart antenna technology. The principle is through estimating the angle of strongest signal path and then rotating the main beam to that direction to receive the highest signal strength. Furthermore, the multipath angular spread information has close relationship to the communication system's performance, because both the multipath angular spread and antenna spacing determine the spatial correlation of the antenna array in MIMO system and therefore influence the its capacity. These are the motivations for this Msc. thesis project.

Through the whole thesis project, we conduct a study on frequency dependency and spatial modeling of wireless channel. The goals of the thesis are:

- To understand and master the basic knowledge about channel measurements and channel modeling.
- To design a measurement set-up, which can measure the wireless channel in several different frequency bands simultaneously and such system can be used to study the channel parameters, such as channel fading, delay and angle information.
- To conduct the measurements in different scenarios.
- To process the measured data in order to estimate the channel parameters.
- To develop the wideband channel spatial model and know the way to study the channel parameters, such as multipath fading distribution, *rms* delay spread and angular spread.
- To study the frequency dependency of wireless channel parameters

1-3 Conclusions

The purpose of this section is to highlight the contributions of this thesis.

- The UWB channel measurement set-up is specifically designed for the wireless channel frequency dependency study. During the system development, the related theoretical and practical problems are discussed.
- The real channel measurements are successfully achieved in three different indoor environments. In total 2016 channel impulse responses are collected for further modeling analysis.
- The wideband spatial channel model is proposed, which represents each multipath by its amplitude, time delay and also angle of arrival.
- The methods of both estimating and modeling the wideband channel parameters, such as multipath amplitude, time delay are discussed in this thesis. Furthermore, through studying the principle of antenna array and high resolution angle estimation algorithm, we successfully design the antenna array at receiving side

and apply the MUSIC DoA algorithm on the real measured signal to estimate the AoA information.

- The principle, meaning and method to investigate the frequency dependency of wireless channel are explained. And then the issues of bandwidth effects and frequency correlation on the wireless channel's power fading and *rms* delay spread are discussed, which makes it to further understand the wireless multipath channel. Furthermore, the frequency dependency of the channel parameters, such as amplitude fading, *rms* delay spread and angular spread are studied in different frequency bands. Although the frequency dependency of channel parameters is not significant in our researched frequency bands, this research can still be good information and reference for further wireless channel's frequency dependency studies, such as investigating the frequency dependency among those frequency bands with larger centre frequency differences.

1-4 Thesis Outline

The rest of the thesis is organized as follows. In Chapter 2, the basic knowledge on the radio wave propagation is given and followed by a literature survey of wireless channel model. In Chapter 3, the channel measurement set-up is given and related technical issues are discussed. The data processing methods to estimate channel parameters and the spatial channel modeling are given in Chapter 4. In Chapter 5, the study on frequency dependency of wireless channel is given and followed by validation. Finally, the conclusions and recommendations are listed in Chapter 6. The appendix is attached in the end of the thesis report. Figure 1.1 illustrates the organization of the Msc. thesis project.

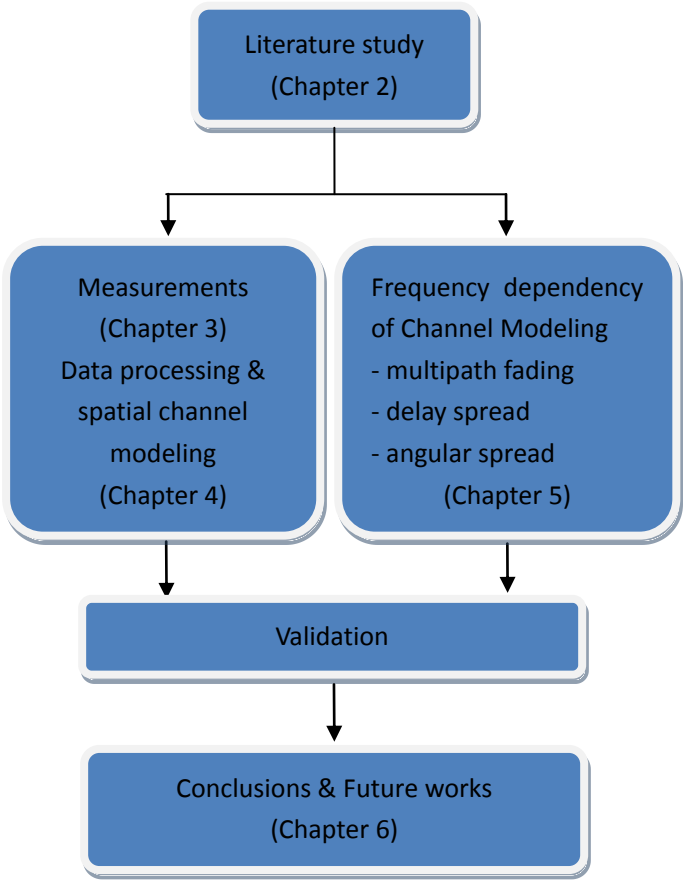

Figure 1.1 Organization of the thesis

Chapter 2

Background on Wireless Channel

The radio channel is defined as the signal paths from a radio transmitter to a receiver. Since the radio propagation mechanisms in both outdoor and indoor environments are complex, a transmitted signal usually experiences the influence of several propagation mechanisms such as reflection, diffraction and scattering [1]. Therefore, the transmitted signal arrives at the receiver through different paths rather than only the direct path. This is known as multipath propagation. The transmitted signal through different paths will undergo different propagation mechanisms and thus suffer from different amplitude attenuations, arrival time delays, arrival angles and phase shifts. Therefore, the characteristics of wireless channel will seriously influence the design of wireless communication system. For example, in wideband communication system, the delayed and attenuated echoes of each transmitted signal will result in inter-symbol interference and eventually limit the rate of the wireless transmission. In narrow band transmission, the wireless medium causes fluctuations in the magnitude and phase of the received signal [2]. Thus, developing a well-established channel model is very important for the wireless communications.

The characterization of the wireless channel propagation is based on the mathematical model of the channel, which can be built in time or frequency domain. In this chapter, an overview of the wireless channel will be given. Followed by a different mathematical channel models of the channel will be followed.

2-1 Wireless Propagation Channel

2-1-1 Description of Wireless Channel

In telecommunications, the wireless channel (radio channel) refers to a logical connection over a multiplexed medium. The channel is used to convey information signal, for example digital bit stream, from one or several senders (or transmitters) to one or several receivers.

For a radio communication system, the channel describes how the electromagnetic propagation of a transmitted wave induces a signal at the receiver. It is possible to express the channel in terms of an impulse response obtained at the receiver. Where communication takes place in an environment with a number of distinct propagation paths from the transmitter to the receiver, the channel impulse response can be described by a summation of weighted phasors [3]. Figure 2.1 shows a basic wireless communication scenario.

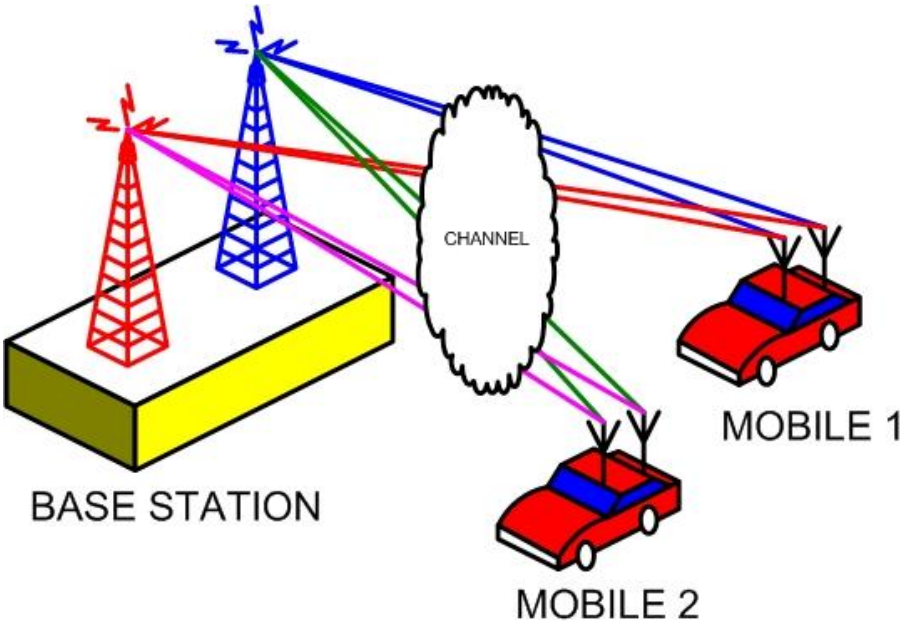

Figure 2.1: Basic wireless communication scenario

2-1-2 Description of Wireless Channel Propagation Mechanisms

Wireless propagation channel is the link between transmitter and receiver and the conditions of wireless channel can have important influence on the performance of wireless communication system. Therefore, understanding the wireless channel propagation mechanisms is vital for system designs.

A wireless channel contains a large number of paths transmitting signal from

transmitter to receiver, where the signal propagation will undergo one or several propagation mechanisms: free-space attenuation, large/small-scale fading, reflection, diffraction and scattering. The channel characteristics are determined by the interactions of multipath. Thus, in this section, the principles of wireless channel propagation are described [3].

Free space attenuation is the loss in signal strength of electromagnetic wave which would result from a line-of-sight path through free space, without obstacles nearby to cause reflection or diffraction. It does not include factors such as the gain of antennas used at the transmitter and receiver. The measurement range should be large enough for local large-scale variations (such as shadowing effects) to not have an influence on the estimation process. Achieving this is, however, not always feasible, especially for indoor measurement campaigns where the building structure often sets the limit [4]. The free space pathloss can be represented in (2.1):

$$L_{free} = +20\log\left(\frac{\lambda}{4\pi d}\right)[dB] \tag{2.1}$$

Large-scale fading, or shadowing, describes the variations of the small-scale averaged received signal power at a given distance. Shadowing is caused by a large obstruction such as hill or large building's obscuring the main signal path between the transmitter and the receiver. The ideal way of measuring shadowing would be to perform a large set of measurements for every Tx-Rx separation *d*, and study the statistics. However, because such a procedure is very time-consuming, few measurements have been performed in this way. Rather than that, shadowing can be defined as the variations of the small-scale averaged power around the distance-dependent decay, i.e., the residue power variations once the distance dependence has been subtracted [4]. The amplitude change caused by shadowing is often modeled by using a log-normal distribution with a standard deviation from the long distance pathloss model, represented in (2.2):

$$L(d) = PL(d) + X_{shadow}[dB], \quad X_{shadow} = N(0, \sigma_{shadow})\,[dB] \tag{2.2}$$

Small-scale fading is caused by constructive or destructive interference of multipath components impinging at the receiver. This phenomenon typically occurs during movements of a terminal over one or a few wavelengths. Thus, small-scale fading gives variations around the large-scale signal level. The probability distribution function of small-scale fading can be represented as Rayleigh, Rician, etc. according to the scenario. The total three types of propagation are shown in Figure 2.2 and

formula (2.3) [69]:

$$L(d) = PL(d) + X_{shadow} + X_{multipath} \quad [dB] \tag{2.3}$$

Reflection (see Figure 2.3), is the change in direction of a wave front at an interface between two different media, such as building surface, so that the wave front returns into the medium from which it is originated. The law of reflection says that for specular reflection, the angle at which is incident on the surface equals the angle at which it is reflected. And reflection of electromagnetic wave is either specular (mirror-like) or diffuse (retaining the energy, but loss the image) depending on the nature of the surface, such as material type, roughness, frequency and etc.

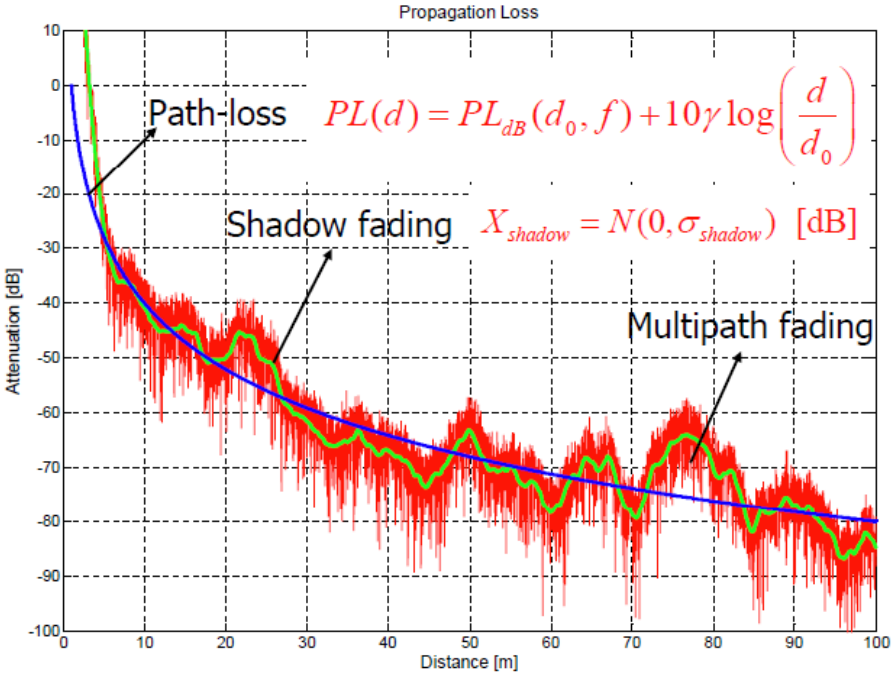

Figure 2.2: The three types of channel propagation loss [69]

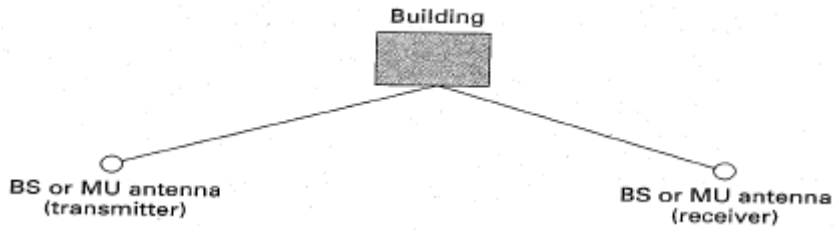

Figure 2.3: Reflection of the electromagnetic wave at a boundary

Diffraction [7] (see Figure 2.4), the figure is said to be diffracted when the wave has travelled round such obstacles as for instance building, hills, vegetation, roofs, road or

other structures. The phenomenon of diffraction occurs when a wave meets an edge with large dimensions compared to the wavelength, and it is one of the most important factors involved in the propagation of radio waves [11].

The phenomenon of diffraction can be explained by Huygen's principle, which states the all points on a wave front can be considered as point sources for the production of secondary wavelets, and these wavelets combine to produce a new wave front in the direction of propagation. Diffraction is caused by the propagation of secondary wavelets into a shadowed region. The field strength of a diffracted wave in the shadowed region is the vector sum of the electric field components of all the secondary wavelets in the space around the obstacle. *Geometrical Theory of Diffraction* (GTD) [12] shows that the additional attenuation due to diffraction has a frequency response of the form $10 * log_{10}(f)$ in the case of the diffraction by an edge. Diffraction has a strong influence in frequency bands not higher than 15 GHz. At higher frequencies, especially at frequency bands higher than 15 GHz, the attenuation due to diffraction may reach a considerable level compared to the attenuation due to reflection.

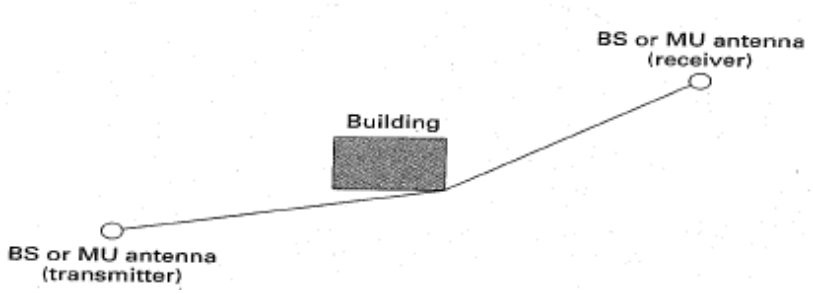

Figure 2.4: Diffraction of the electromagnetic wave at the edge of a building

Diffusion happens when the obstacles are of large size with respect to the wavelength ($\lambda < 2\ cm$) and their surfaces are often regarded as rough. This is the case with such obstacles as the balconies, the frontage windows, the urban furniture or the vegetation. The phenomenon of diffusion appears when an obstacle presents a number of irregularities of wavelength size.

Scattering [7], seeing Figure 2.5, is found that the actual received signal in a mobile radio environment is often stronger than what is predicted by reflection and diffraction models alone. This is because when a radio wave impinges on a rough surface, the reflected energy is spread out (diffused) in all directions due to scattering. Object such as lamp posts and trees tend to scatter energy in all directions, thereby providing additional radio energy at the receiver. According to [10], for narrowband

case, the surfaces roughness is usually indicated by a critical height (h_c) of surface protuberances for a given angle of incidence θ_i, given by

$$h_c = \frac{\lambda}{8\,sin\ \theta_i} \tag{2.4}$$

And a surface is considered smooth if its maximum to minimum protuberance $h < h_c$, otherwise, the surface is considered rough. Furthermore, the reflection coefficient of rough surface is defined as:

$$\Gamma_{rough} = \rho_s \Gamma \tag{2.5}$$

where the scattering loss factor is

$$\rho_s = \exp\left[-8\left(\frac{\pi\sigma_h \sin\ \theta_i}{\lambda}\right)^2\right] I_0\left[8\left(\frac{\pi\sigma_h \sin\ \theta_i}{\lambda}\right)^2\right] \tag{2.6}$$

As showed in (2.4) and (2.6), both the critical height and roughness are related to wavelength λ and therefore they are frequency dependent.

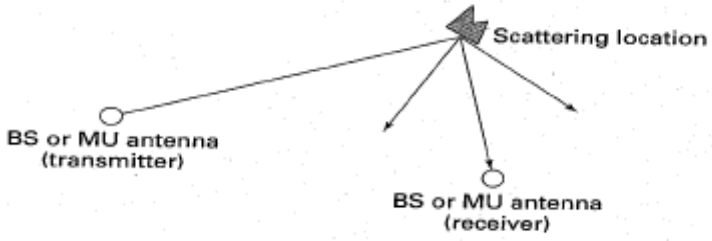

Figure 2.5: Scattering of the electromagnetic wave

2-1-3 Types of Wireless Channel

There are several ways to classify the wireless channel. One of the most commonly used classifications is on the channel's frequency bandwidth. Thus, the wireless channel can be divided into two types: narrowband and wideband channel.

One of the most important differences between wideband and narrow channel is the bandwidth. The feature of narrowband/wideband channel is determined by the signal bandwidth *BW* as well as the channel coherence bandwidth B_{coh} [69]. The characters of narrowband signal ($BW << B_{coh}$) are virtually constant channel response, no distortion and heavy fluctuations. The symbol time (T_{symbol}) is much larger than the maximum multipath delay (τ_{max}), which means the multipath cannot be resolved and all multipath contributions sum to a single complex amplitude. And the narrowband signal will suffer from flat fading. However, for wideband signal, the delay spread of a channel is larger than the symbol time, which is the inverse of signal bandwidth,

then the signal is wideband, which means that different paths may contain different symbols: $g(t-\tau_m) \neq g(t-\tau_n)$. In the extreme case of very short pulses, a single symbol may be active in only one path at a time. The received power is $|r(t_0)|^2 = \sum_{n=0}^{N} a_n^2(t_0)$ and multipath can be resolved [69]. In addition to the multipath effects encountered in narrowband systems, the performance of wideband transmissions is also limited by dispersion in the channel. Dispersion gives rise to frequency selective fading which means that two sufficiently spaced frequencies fade in an uncorrelated manner. This lack of correlation between frequency components within the information bandwidth results in a distorted frequency spectrum. Thus, there is a variation in received signal strength as a function of frequency, similar to the variation in signal strength with location. In digital system, the time-delayed echoes produce inter-symbol-interference.

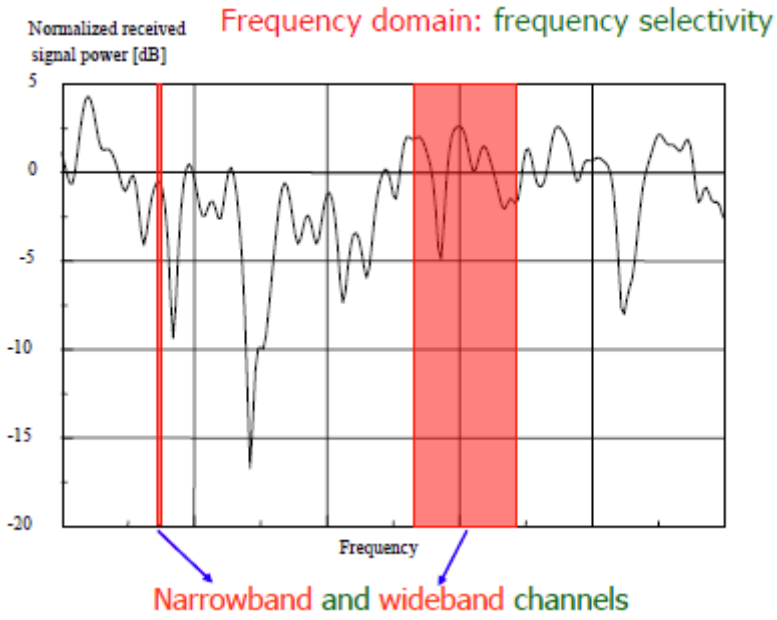

Figure 2.6: Comparison between Narrowband and Wideband channels in frequency domain [69]

2-2 Types of Wireless Channel Models

In order to understand the physical wireless channel, developing a well-matched channel model is very important. There is always trade-off on developing channel model. On one hand, the model should be as accurate as possible. On the other hand, in order to make the model easy to use, the simplicity of channel model should also be considered. According to the reference, the channel modeling can be classified into several ways: (1) Deterministic model, (2) pure statistical model and (3) Geometry-based stochastic channel model (GSCM) [9].

2-2-1 Deterministic Model

Most deterministic channel modeling approaches depend on solving Maxwell's equations under the boundary conditions imposed by a specific environment, thus this method requires information about the location, shape and electromagnetic properties of every object in the propagation environment. However, there is a large quantity of computations required to find solutions and the intensive calculations makes it difficult to change parameters in the model, which limits deterministic modeling in harsh environments.

Another common approximate deterministic modeling method is Ray-tracing or ray-launching, where rays are launched from the transmitter and their respective paths to the receiver determined from geometric optics including all fundamental propagation mechanisms. This method shows good agreements with physically exiting results (site-specific). However, there are many problems which makes deterministic model hard to be implemented in reality. The problems are: selected environments need not be representative, large data bases are required, model is expensive to produce and parameters cannot be changed easily. Furthermore, the deterministic model is not very accurate to be used in mobile channel (GSM, LTE, etc.). Because that, for simplicity and easy computations, most of the deterministic models just consider LOS and reflections phenomena which is under the assumption that the transmitting signal is optical wave and the wavelength of the optical wave is much shorter than the objects' surface dimension in the channel. However, the wavelength of mobile signal is much longer than optical wave and there are a lot of buildings in the city which can produce huge number of diffracted and scattered multipaths. If these phenomena are neglected in the deterministic model, big errors will occur in the channel predictions.

2-2-2 Pure Statistical Model

This method is usually implemented in the following procedure: on one hand, measuring the wireless channel to gain the measured data; on the other hand, proposing mathematic wireless channel model and finally utilizing the statistical methods to analyze the data to validate the developed model. Therefore, multidimensional (such as delay, position, azimuth/elevation angle and etc.) probability density functions of channel impulse response are used in this model. The main merit of this method is developing the model in a fast way and the disadvantages are difficulty to parameterize the channel over large areas. In Figure 2.7 and 2.8 are the main two models of this method.

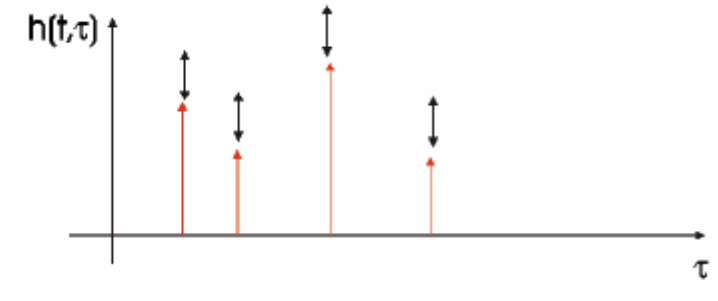

Figure 2.7: Pure stochastic model [9]

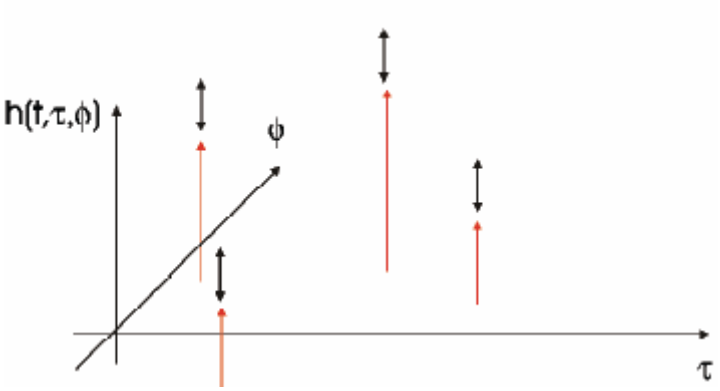

Figure 2.8: Generalization to spatial dimension [9]

2-2-3 Geometry-based Stochastic Channel Model (GSCM)

Comparing to pure stochastic model, GSCM assigns positions and properties to scatters in statistic model, such as prescribing probability density function of scatters, increasing of temporal and angular dispersion by group scatters fixed in space and etc. The merit of this method is that GSCM has the ability to capture non-stationary effects, because GSCM method considers both the locations of TX, RX and the motion of terminals in the channel modeling. However, there are many issues which should be studied in detail in this method, such as time variance, interference, spatial correlation, interfering between mobiles and etc. Figure 2.9 is the general scenario for this model.

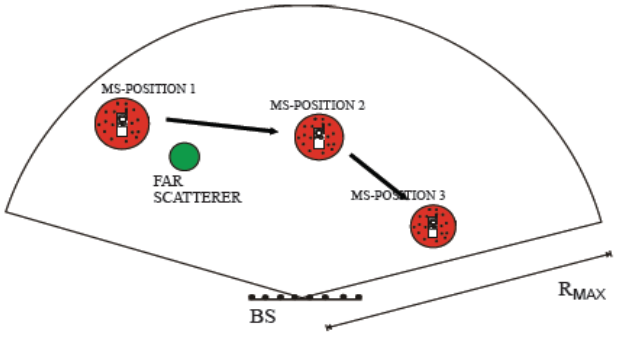

Figure 2.9: General Scenario for geometry-based stochastic channel model [1]

Considering the availability of measurement equipments in our research lab and a large number of researches about statistical channel modeling, in this Msc. thesis project, the pure statistical method is chosen as the way to model the wireless channel. In the following section, the mathematical modeling of wireless channel based on statistical method is discussed.

2-2-4 Mathematical Wireless Channel Modeling

- **Time Domain Modeling**

The wideband channel can be characterized as a linear time-varying filter with the following impulse response [5]:

$$h(t,\tau) = \sum_{n=0}^{N(t)-1} a_n(t)\delta(\tau - \tau_n(t))e^{j\theta_n(t)} \tag{2.7}$$

where τ is the excess delay, t refers to the channel impulse response at instant t and $\delta(\cdot)$ is the Dirac delta function transmitted at $\tau = 0$. The parameters a_n, τ_n, θ_n is the n^{th} path's amplitude, delay, phase, respectively and N represents the total number of multipath components. Thus, for wideband channel, the channel model parameters, such as fading statistics, delay statistics can be determined by measurements.

The bandwidth of narrowband signal is small, which leads to very low resolution in time domain and therefore the multipath components cannot be separated and seen as a superposed single path. The narrowband channel can be described as:

$$re^{j\theta} = a' \sum_{i=0}^{N-1} e^{j\theta_i} \tag{2.8}$$

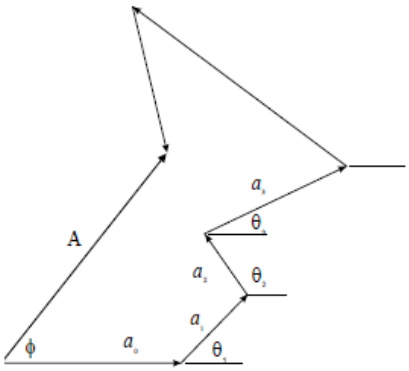

Figure 2.10: Superposing multipath

where r and θ are the amplitude and phase of the received signal. Since the narrow

bandwidth, only the fading statistics can be studied and there is no information about the delay statistics according to the model (2.8).

2-3 Modeling of Channel Parameters

(1) Amplitude Fading Modeling

For the wireless channel propagation, the signal amplitude experiences fading phenomenon and there are several types of distribution candidates to describe the statistics of the amplitude fading for different environment conditions.

- **Rayleigh distribution**

Rayleigh distribution is the most accepted model in mobile radio channel. If the LOS component is absence and the other multipath does not have dominant contribution on the received power, the superposed amplitude envelop will have Rayleigh distribution:

$$f(r) = \frac{r}{\sigma^2} e^{-\frac{r^2}{2\sigma^2}} u(r) \tag{2.9}$$

where $\sigma^2 = \sum a_i^2 \ (i = 0, 1, 2, \dots, N-1)$, u $(\cdot)$ is the unit step function. Mean of Rayleigh distribution is $\sqrt{(\pi/2)\sigma}$ and variance of Rayleigh distribution is $(2 * \pi/2)\sigma^2$.

- **Lognormal distribution**

This distribution describes the large-scale variations of the signal amplitude in fading environments with obstructions. The probability density function is [6]:

$$f(r) = \frac{1}{\sigma\sqrt{2\pi}} \exp\left(-\frac{(\ln r - u)^2}{2\sigma^2}\right) u(r) \tag{2.10}$$

where lnr has a normal (Gaussian) distribution and the parameters μ and σ are the mean and variance in dB, respectively.

- **Rician distribution**

Compared to Rayleigh distribution, if the LOS component is present, the fading satisfies Rician distribution. The probability density function is [8]:

$$f(r) = \frac{r}{\sigma^2} \exp\left(-\frac{r^2 + A^2}{2\sigma^2}\right) I_0\left(\frac{Ax}{\sigma^2}\right) u(r) \tag{2.11}$$

which is called Rician distribution. *A* is the LOS component amplitude and I_0 is the zero-order modified Bessel function of the first expressed as:

$$I_0(x) = \frac{1}{2\pi}\int_{-\pi}^{+\pi} e^{x\cos\phi} d\phi \tag{2.12}$$

Usually, a parameter called K factor is introduced to describe how important the LOS path in the distribution, which is defined as:

$$K = \frac{A^2}{2\sigma} \tag{2.13}$$

If $K = 0$, the Rician distribution becomes a Rayleigh distribution.

- **Nakagami distribution**

In the Rayleigh distribution, the amplitude of each multipath component is nearly equal and their phases are random. However in Nakagami distribution, the amplitude of each multipath component is kept random. Therefore, this distribution is more realistic than Rayleigh distribution [13].

$$f(r) = \frac{2m^m r^{2m-1}}{\Gamma(m)\Omega^m}\exp(-\frac{mr^2}{\Omega^2}) \tag{2.14}$$

where $\Omega = E[r^2]$, $\mathrm{m} = [E[r^2]]^2/var(r^2) \geq 0.5$, and $\Gamma(\cdot)$ is Gamma function defined as:

$$\Gamma(m) = \int_0^{\infty} t^{m-1}\exp(-t)\,dt \tag{2.15}$$

The Nakagami distribution reduces to the Rayleigh distribution for *m*=1.

- **Weibull distribution**

The probability density function of this distribution is [8]:

$$f(r) = \frac{\beta}{\lambda}\left(\frac{r}{\lambda}\right)^{\beta-1}\exp\left[-\left(\frac{r}{\lambda}\right)^{\beta}\right] \tag{2.16}$$

Where β and λ are the shape and scale factors, respectively. The distribution reduces to the exponential distribution for $\beta = 1$, and to the Rayleigh distribution for $\beta = 2$.

(2) Time Delay Modeling

- **Distribution of Arrival Times**

Channel multipath travels through different distance, so that multipath arrives at the receiver with different time delays. Distribution of the arrival time sequence has been investigated. As a first model, Poisson distribution for the sequence of path arrival times may be considered (2.17). And if considering the cluster factors, the Δ-k modified Poisson distribution is used.

$$P(I = i) = \frac{u^i e^{-u}}{i!} \tag{2.17}$$

I denotes the number of paths occurring in a given time interval T, $\mu = \int_0^T \lambda(t)dt$, where $\lambda(t)$ is the mean arrival rate at time t. For a stationary process, $\lambda(t)$ is constant and both the mean and variance of I are equal to λ. TheΔ-k modified Poisson distribution is shown in Figure 2.11, which considers clusters in the model.

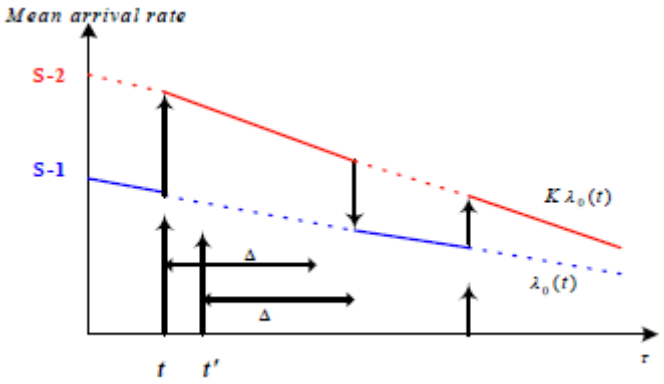

Figure 2.11: TheΔ-k modified Poisson distribution [7]

- ***RMS* Delay Spread**

The channel impulse response profile can be defined as an one-number parameter, which is *rms* delay spread.

$$\tau_{rms} = \sqrt{\overline{\tau^2} - (\bar{\tau})^2} \tag{2.18}$$

where $\bar{\tau}$ and $\overline{\tau^2}$ are the first and second moments of the power delay profile respectively. They are defined as:

$$\overline{\tau^\beta} = \frac{\sum_n a_n^2 \tau_n^\beta}{\sum_n a_n^2} \tag{2.19}$$

where a_n and τ_n are the amplitude and delay characteristics, respectively. *rms* delay

spread is a good measure of the channel's multipath components distribution on the time domain and it is also an important indicator reflecting the performance of the communication system. According to some previous researches, it has been indicated that the *rms* delay spread is an important parameter to determine the mobile system's maximum data transmission rate. In [20], the authors discussed if there is no frequency/space diversity or equalization used in system, the *rms* delay spread is inversely proportional to the maximum usable data rate R_{max} of the channel where

$$R_{max} = \frac{1}{\upsilon \tau_{rms}} \tag{2.20}$$

and $\upsilon \approx 4$ as extracted from [20].

(3) Distribution of Phase

The multipath component's phase is critically sensitive to path length and changes by a factor of 2π as the path length changes by a wavelength. Considering the geometry of the paths, moderate changes (in order of meters) in the position of portable results in a great change in phase. For narrowband channel, the phase is seen as superposition value of all multipath components, which is reasonable to be considered as an uniform distribution in [0, 2π).

(4) Power Delay Profile

According to the channel impulse response, the received signal power can be obtained as:

$$P(\tau_n) = E\{|h(t)|^2 = \sum_{n=0}^{N-1} \overline{a_n^2} \delta(t - \tau_n) \tag{2.21}$$

Usually the later paths of the power delay profile experience more attenuation and accordingly the power delay profiles are generally decreasing function of the excess delay. A good model is exponential decrease of the received power as in (2.22):

$$P(\tau_n) = P(0) \sum_{n=0}^{N-1} e^{-\alpha \tau_n} \delta(t - \tau_n) \tag{2.22}$$

where *P(0)* is the received power at delay τ_0 and α is a parameter that controls the decreasing shape of the power delay profile.

(5) Coherence Bandwidth

Coherence bandwidth is a statistical measurement of the range of frequencies over which the channel can be considered "flat", or in other words the approximate maximum bandwidth or frequency interval over which two frequencies of a signal are likely to experience comparable or correlated amplitude fading. Let $H(f)$ denotes

the frequency transform of the channel impulse response $h(t)$. The coherence bandwidth is related to the frequency correlation function as [2]:

$$R_H(\Delta f) = \frac{E\{H^*(f)H(f+\Delta f)\}}{E\{|H(f)|^2\}} \tag{2.23}$$

The coherence bandwidth B_c of level k is the smallest number so that $|R_H(B_c)| < k$. The frequency correlation function is actually the Fourier transform of the normalized power delay profile $\tilde{P}(\tau) = P(\tau)/\int_{-\infty}^{\infty} P(\tau)d\tau$ as:

$$R_H(\Delta f) = \int_{-\infty}^{\infty} \tilde{P}(\tau)e^{-j2\pi\Delta f\tau}d\tau \tag{2.24}$$

For the exponential power delay profiles, Jakes [25] has shown the following relation between the rms delay spread and the coherence bandwidth:

$$R_H(\Delta f) = \frac{1}{1 + (2\pi\Delta f\tau_{rms})^2} \tag{2.25}$$

From this it can be seen that

$$B_{0.5} = \frac{1}{2\pi\tau_{rms}} \tag{2.26}$$

(6) Angular Spread (AS)

For typical wireless channel propagation, radio waves arrive at a receiver from azimuthal directions about the horizon. This distribution of multipath power is conveniently described by the function, $p(\varphi)$, where φ is the azimuthal angle. Angular spread, Λ, is an important propagation parameter which determines how spread out multipath power is about the horizon. However, the definition of angular spread Λ is not as simple as that of delay spread, since angle is a type of circular data. There are several ways to define angular spread, such as Fleury's definition [63], Fisher's definition [64] and Winprop's definition [65]. In [24], the author compared the above mentioned three AS definitions and the result showed that the AS is similar.

- Fleury definition

The AS is defined as the square root of the *circular variance* $V = 1 - R$:

$$\Lambda = \sqrt{V} = \sqrt{1 - R} \tag{2.27}$$

$$R = \left| \sum_{n=1}^{N} \exp(\mathrm{j}\varphi_n) \cdot P_n \right| \Big/ \sum_{n=1}^{N} P_n$$

where φ_n and P_n are the azimuth angle of arrival and power of path *n*, respectively.

- Fisher definition

The AS is defined as the *circular standard deviation*:

$$\Lambda = \sqrt{-2\log(R)} \tag{2.28}$$

- Definition Winprop:

The AS is defined as follows:

$$\Lambda = \sqrt{\frac{\sum_{n=1}^{N}(\varphi_n - \bar{\varphi})^2 \cdot p_n}{\sum_{n=1}^{N} p_n}} \tag{2.29}$$

$$\bar{\theta} = \angle R = \angle \left[\sum_{n=1}^{N} exp\,(j\varphi_n) \cdot p_n \Big/ \sum_{n=1}^{N} p_n \right]$$

where φ_n and p_n are the *n*th multipath's arrival angle and power, respectively. The '$\angle(\cdot)$' denotes the angle and $\bar{\theta}$ denotes the average angle.

Angular spread, Λ, ranges from 0 to 1, with 0 denoting the case of a signal multipath component from a single direction and 1 denoting no clear bias in the angular distribution of received power, which means the signal's arrival angle coming at any direction has the same probability.

Furthermore, some researches show that the multipath arrival angles can be grouped into clusters [33]. These clusters can be associated with objects in the environment. A cluster is defined as a group of waves whose delay, azimuth or elevation angles at receiver are very similar. The angular clustered channel impulse response can be represented as in (2.30). Additionally, all waves inside a cluster must stem from the same propagation mechanism. The definition of clusters always involves a certain amount of arbitrariness. Even for mathematically 'exact' definitions, arbitrary parameters (e.g. thresholds or numbers of components) must be defined. Clustering identification by visual inspection of maps of environment can be a good way to improve the accuracy.

$$h(\varphi) = \sum_{m=1}^{\infty} \sum_{n=1}^{\infty} a_{mn} \delta(\varphi - \Phi_m - \omega_{mn}) \tag{2.30}$$

where a_{mn} is the amplitude of the n^{th} arrival in the m^{th} cluster, Φ_m is the mean azimuth AoA of the m^{th} cluster and ω_{mn} represents the azimuth AoA of the n^{th} arrival in the m^{th}cluster relative to Φ_m.

Not only this, in [62], the author classifies the clusters and each cluster is assigned to one of three different classes in the outdoor scenario.

Class 1. Street-guided propagation: waves arrive at the receiver from the street level after traveling through street canyons.
Class 2. Direct propagation-over the rooftop: Waves arrive at the BS from the rooftop level by diffraction at the edges of roofs, either directly or after reflection from buildings surrounding the MS. The azimuth mostly points to the direction of the transmitter, with some spread in azimuth and delay.
Class 3.Reflection from high-rise objects-over the rooftop: The elevation angles are near the horizon, pointing at or above the rooftop. The waves undergo a reflection at an object rising above the average building height before reaching the BS. The azimuth shows the direction of the reflecting building, the delay is typically larger than for Class 1 or Class2.

2-4 Summary

In this chapter, we introduced the basic theory of wireless channel propagation and then discussed several available methods of channel modeling. Finally, a detailed discussion on mathematical modeling of wireless channel and related parameters modeling was given.

Chapter 3

Measurement System Design and Channel Measurements

In this thesis project, the main task can be generally divided into two parallel parts. One is channel modelling and the other one is channel measurements, which are used for validating the developed channel model. In the end, the measured data is utilized to validate the proposed channel model. Therefore, we need to design a measurement system which can help us to study the frequency dependency and spatial modelling of wireless channel. In this project, we focus on the modelling of channel parameters, such as power/amplitude fading, *rms* delay spread and arrival angle spread.

Furthermore, this project is cooperating with KPN Telecom company and we require the designed measurement system can be utilized in the same environment as the real LTE scenario. Therefore, the measurement set-up design, such as Tx, Rx antenna selection, receiving antenna array, movable power supply, measurement routes, etc., should match the real LTE outdoor scenario. However, because of some technical and practical problems such as the maximum transmitting distance of the UWB pulse generator is below 70m and the insurance issues for all measurement equipments using at outdoor scenario, finally we have given up the outdoor channel measurement plan and only performed the indoor scenario measurements at power lab, canteen and library of EWI building, TU Delft. Because the measurement system is designed for outdoor measurements, there are some limitations or mismatches for the indoor measurements. The details of the measurement system design and indoor measurements will be discussed in this chapter.

3-1 Measurement Sounding Techniques

In one sense or another, all channel modeling methods rely on channel measurements. For statistical channel modeling, model parameters need to be extracted from measured data, but also postulated scattering models or ray tracing models need to be verified against reality. Measurements of the wireless channel propagation is also known as channel sounding, a name stemming from a transmitter that "sounds" (or excites) the channel, whereas the receiver records the channel output. While early channel sounders in the 1960s were only required to measure strength, their complexity has increased drastically since then. The introduction of wideband wireless systems requires measurements of the multipath components with time delay information, whereas the research on multiple antenna systems has rendered an interest in directional or spatial channel properties. Furthermore, up until the 1990s, channel measurements were mostly focused on macro cells. Many recent campaigns, however, have been aiming at characterizing indoor scenarios, which puts higher demands on the required delay resolution of a channel sounder. Finally, recent wireless applications such as vehicle-to-vehicle communications systems imply that current channel sounders are required to store the fast fluctuations of the time-varying, wideband, double-directional propagation channel [4].

According to the up-to-now developed channel measurement systems, although different measurement system has its own characters, they can be generally divided into two types: Frequency domain measurement technique and time domain measurement technique.

- **Time domain (TD) measurement technique**

Time-domain measurements obtain the channel impulse response $\mathrm{h}(t)$ by exciting the channel with pulses or pseudo-noise sequences. Therefore, the received signal is the convolution of the sounding pulse with the channel impulse response. The main parts of such measurement system are oscilloscope controlled by a PC, pulse generator and Tx/Rx antenna. The principle of this TD measurement technology is, at transmitting side, the signal pulse is sent frequently with a constant interval time through transmitting antenna. At receiving side, antenna connected to the oscilloscope to sample the received signal. The sampling rate should satisfy Nyquist criterion. Figure 3.1 shows one example of channel measurement system in time domain [22].

- **Frequency domain (FD) measurement technique**

Frequency domain measurements, on the other hand, typically use a chirp-like or other multitone signal to sound the channel. In this technique, a Vector Network Analyzer (VNA) controlled by a PC (personal computer) conducts the measurements. VNA sounds the channel by sweeping the frequency range of interest and estimating the transfer function between its two ports. Since the antennas are not a part of the VNA calibration procedure, obtaining the "pure" channel from VNA measurements thus requires a separate calibration of the antennas, whose influence only can be completely removed if the directions of all multipath components are known (in elevation as well as azimuth).

The principle of this FD technique is through transmitting a sine-wave signal at each frequency, the magnitude and phase of the received signal constitute that frequency's complex channel frequency response $H(f)$. The channel frequency response can be transferred to channel impulse response by inverse fast Fourier transform. Figure 3.2 shows the frequency domain channel measurement system [4].

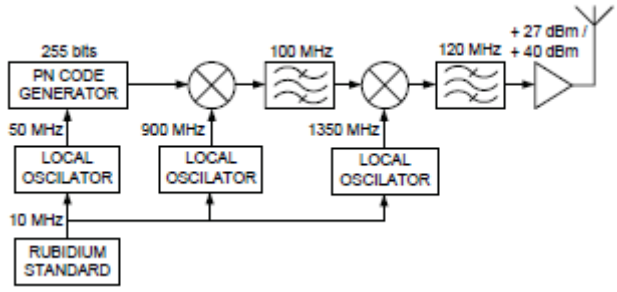

(a)

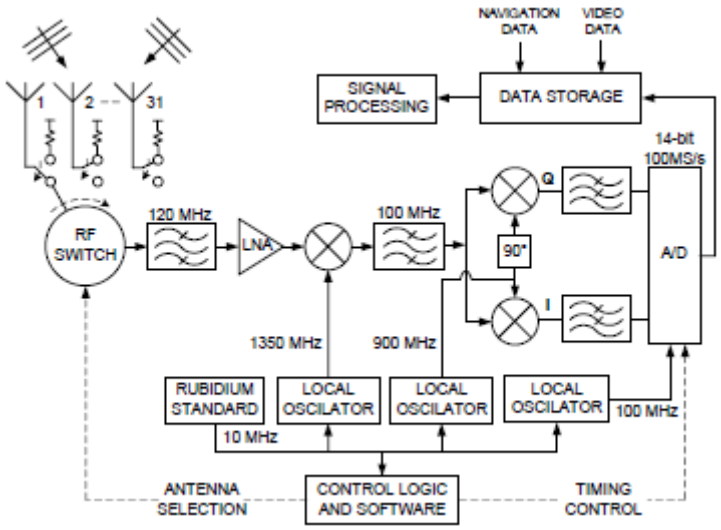

(b)

Figure 3.1: One example of channel measurement system in time domain [22]

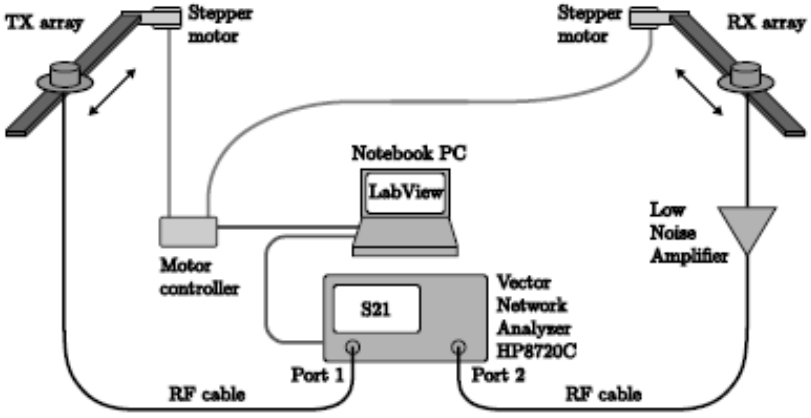

Figure 3.2: Vector Network Analyzer measurement system in frequency domain [4]

As shown in Figure 3.2, the FD technique requires that both Tx and Rx antenna should be connected to the VNA when doing the channel measurements. Thus, this method is not fit for long distance channel measurements such as outdoor mobile channel measurement. The reason is if the distance between the Tx and Rx antenna is as long as several hundred meters, it is not very easy to find such long cables that connect antenna with VNA. Therefore, the TD measurement technique is chosen for our channel measurement.

According to the measurement systems introduced in references, their measurement systems are usually designed for their specific research purposes. If we copy their designs and directly apply it for our project, the measurement system may not satisfy our measurement requirements. Thus, most of the proposed measurement systems have more or less limitations being considered for our project. For example, in [14], [17], [18], [22] and [19], they developed Single Input Multiple Output (SIMO) or Multiple Input Multiple Output (MIMO) measurement systems with high resolution in angular domain and their antenna arrays were designed as circular or rectangular shape for azimuth angle estimation and even 3 D shape, such as cubic or tilted cross, for both azimuth and elevation angle estimation. However, all of these systems are applied for narrowband or wideband channel (around 100 MHz) measurements and our thinking is to design an UWB measurement system which can cover several wideband channels by transmitting signal only once. And in [50] and [51], they both introduced the UWB SIMO measurement systems, but these two systems measured the wireless channel in frequency domain by using VNA. Because of the synchronization and cable connection problems, these designs cannot be applied for long distance measurements. Thus, a new measurement system, which fits our

requirements, should be designed.

3-2 Measurement Set-up Design

- **UWB Pulse Generator**

To investigate the frequency dependency studies, we need to measure the wireless channel on several different frequency bands. In our case, we select an UWB pulse generator having a large bandwidth. The reason is UWB signal has ultra wide frequency bandwidth, which can be considered as a constitution of many small frequency bands, for example, of 100 MHz bandwidth. Therefore, transmitting UWB signal can provide a series of frequency bands' signals simultaneously by implementing different digital band-pass filter on the received UWB signal. Thus, this way could combine several different frequency bands measurements into an integrated one, which decrease the channel measurement time. The frequency band of the generated UWB signal is at [0.1, 4] GHz and its pulse shape can be both triangle and rectangular.

- **Oscilloscope**

In this project, TD technique is chosen to measure the wireless channel. Therefore, an oscilloscope is required to connect the Rx antenna at the receiver side to sample and collect the received signal. And then after de-convolution with reference pulse, the channel impulse response can be obtained. The sampling oscilloscope we used can measure four channels simultaneously and has maximum sampling rate of 40 GHz. In our measurements, only two channels are used (one is for reference antenna, the other one is for receiving antenna). Therefore, the highest sampling rate is 20 GHz per channel. In the following, some parameters designed for the channel measurements are given.

(1) Measurement range

The pulse repetition rate of this UWB pulse generator is set as 100 KHz, which means that the unambiguous range $\mathrm{R_{un}}$ is equal to:

$$\mathrm{R_{un}} = c * \frac{1}{PRF} = 3 \text{ km} \tag{3.1}$$

Through studying many reference materials, the maximum excess delays for propagation environments are reported to be less than 500 ns (indoor) and 10 us (outdoor). Therefore, the ambiguous range of 3 km is more than enough to record all

multipath in either indoor or outdoor environment.

(2) Sampling time

Since the maximum frequency to be measured is 4 GHz. As we know, the Nyquist criterion requires the minimum sampling frequency f_s to be:

$$f_s = 2f_{max} = 8 \text{ GHz} \tag{3.2}$$

This corresponds to a minimum sampling time t_s of

$$t_s = \frac{1}{f_s} = 125 \text{ ps} \tag{3.3}$$

In order to get high time resolution, a sampling time of 50 ps (oversampling of 2.5 times) was considered for the measurements.

(3) Time window

The total delay due to RF cables and propagation between the transmitting and receiving antennas (free space propagation) is important for the determination of the time window. Through studying the related reference materials, the time window is usually set as 2 μs for indoor and 20 μs for outdoor environment. Furthermore, in order to increase the received signal's SNR (signal to noise ratio), the number of average is set to 512. Therefore, the total estimated time to measure one channel impulse response is about 30 sec.

- **Synchronization Problem**

Since the virtual antenna array is implemented at the Rx side and when the Rx antenna measures the channel at each element of the array, the time delay information is very important for the angle of arrival estimation. Therefore, all the channel measurements on the antenna array should be synchronized. However, for long distance measurement, using one cable to connect both Tx and Rx side for synchronization is not applicable, and thus, using an extra antenna as a reference to connect the triggered channel would be a good method for synchronization. At each measurement location, when the receiving antenna shifts from one element to another on the array, the reference or triggering antenna doesn't move its position. In this way, the time delay information is remained in the channel impulse response of every element. Through testing this reference antenna method, it works well and the measured signal contains the extra delay information resulting from antenna array structure.

- **Tx and Rx Antenna Selection**

Since the UWB sounder is used in the measurements, the transmitting and receiving antenna should have flat antenna gain inside the frequency band 1-4 GHz. Otherwise, the antenna will reshape the transmitting pulse. For the Tx antenna, there are two possible choices of directional ultra wideband antennas in IRCTR lab. One is double wedged antenna (DWA) and the other one is IRK horn antenna. The reason why to use directional antenna is its high antenna gain (~10 dB) compared to omni-directional antenna (~1 dB) and therefore the long distance measurements can be lunched. And another important reason to use directional Tx antenna is for the real mobile communication system, such as LTE, the Tx antenna at base station is usually a directional antenna and our measurement set-up design simulates such design. For the Rx antenna, omni-directional Biconic antenna is selected, since we want to study the multipath components' angular spread and the Rx antenna should be able to receive the signal coming from whole 360 degrees. Figure 3.3 and Figure 3.4 show the antenna gain of DWA and IRK horn antennas separately. We can see that the DWA antenna has almost flat gain from 1 GHz to 5 GHz, but for IRK horn antenna, the antenna gain at frequency band 1-5 GHz is not flat and there are deep notches around 3 GHz and 5 GHz. Thus, the DWA antenna is selected as the Tx antenna for our measurement system.

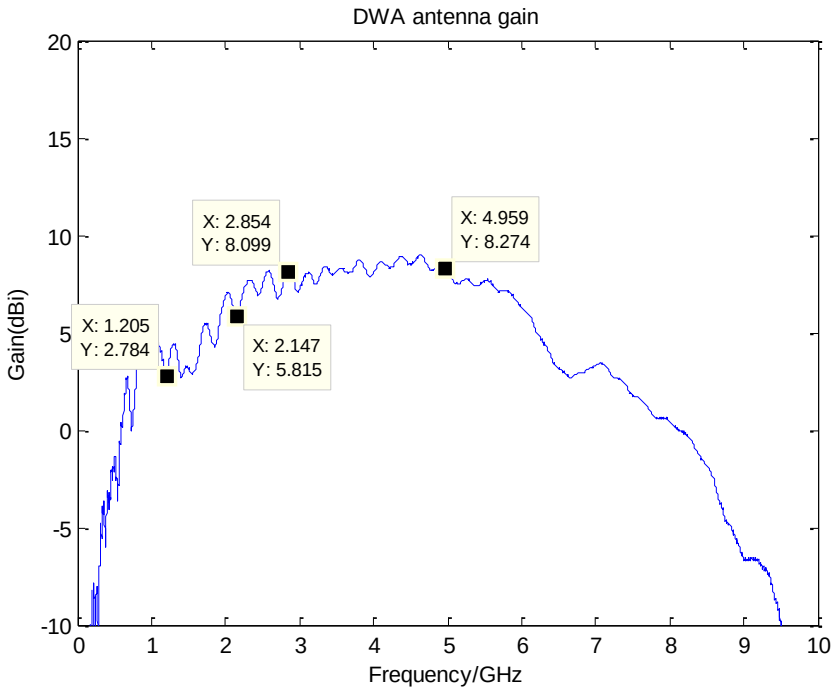

Figure 3.3: DWA antenna gain

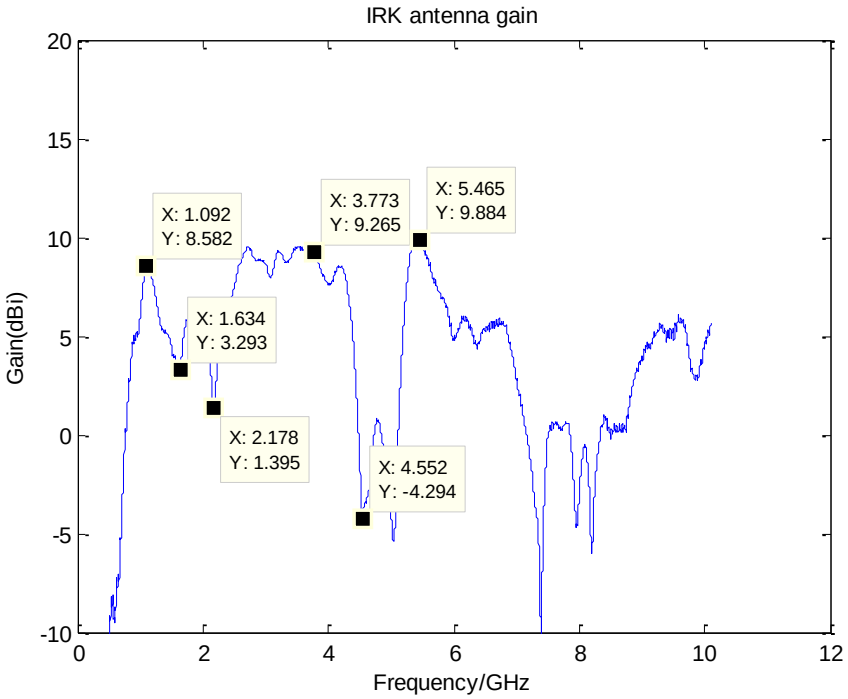

Figure 3.4: IRK horn antenna gain

- **Multiple Antenna Reflection Problem**

Since there are mismatches between the pulse generator and transmitting antenna, then part of the generated pulse will experience reflection bouncing between the transmitting antenna input and the pulse generator output before being transmitted out to the wireless channel and it can also arouse several faked multipath which cannot be separated from real channel multipath. Additionally, the antenna multiple reflection problem can lead to measuring a substantially larger maximum excess delay which results in overestimation of the *rms* delay spread of the channel and it will also seriously influence the statistics of the channel model parameters, such as cluster arrival rate. This is called antenna multiple reflection problem. Thus, before doing the real measurement, the antenna reflection problem should be checked and find method to avoid such problem. Otherwise, the measured channel impulse response is not the real one according to the environment.

Using the cables with different length between the transmit antenna and pulse generator is the way to check whether the DWA antenna has the antenna multiple reflection problem. The testing on the Tx antenna (DWA) multiple reflection problem is done at a lab room. Tx antenna is DWA antenna, Rx antenna is Bionic antenna and the distance between two antennas is 1 m. The height of two antennas is ~1 m. The

channel is measured by with or without connecting a 1m cable before Tx antenna and the received signals are compared in Figure 3.5. In this figure, we find that when 1m cable is added before Tx antenna, the whole channel impulse response shifts 4.3 ns (from 2.991 ns to 7.387 ns). However there is one path shifts 13.2 ns instead of 4.3 ns. Therefore, we can prove it is not real channel multipath but antenna multiple reflection path, since the extra ~9 ns time shift is equal to the time signal travels 2 meters and this is resulted from the Tx antenna multiple reflection (double reflections inside the Tx antenna).

There are many ways to solve such problem. However, in our measurement, the attenuator is added before the Tx DWA antenna to remove the antenna multiple reflection pulses. The received signal with and without adding 6 dB attenuator is compared in Figure 3.6. It is easy to see that at around 43.35 ns, the antenna multiple reflection pulse is disappeared, because of the 6 dB attenuation at transmitting side.

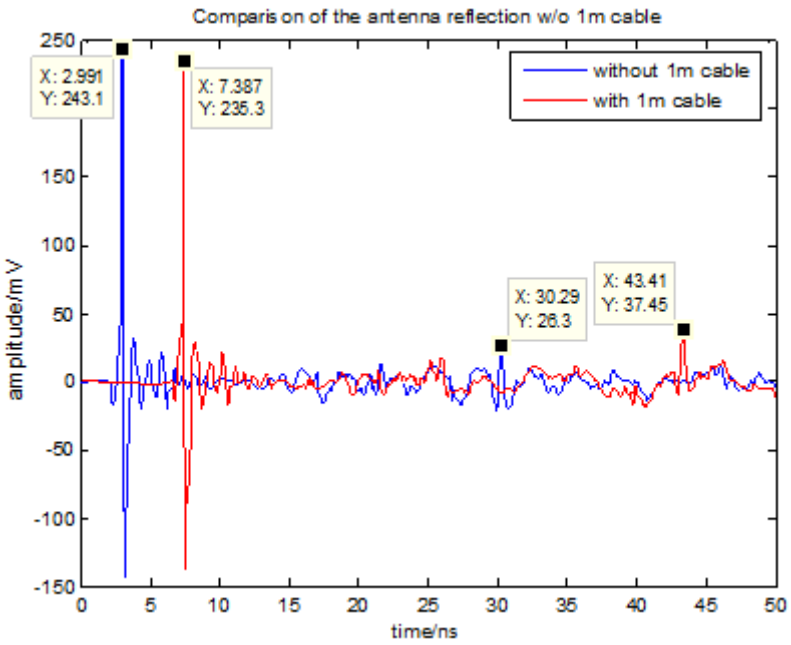

Figure 3.5: Comparison of the antenna reflection w/o 1m cable

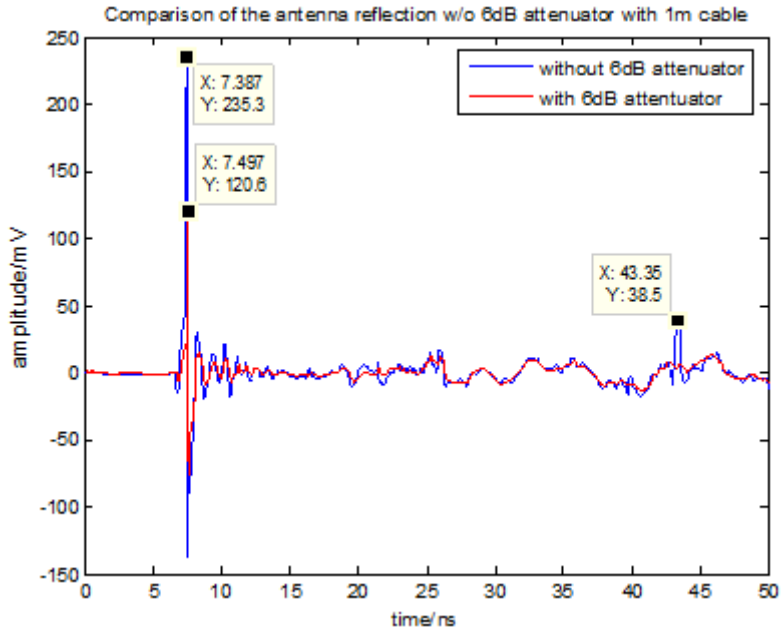

Figure 3.6: Comparison of the antenna reflection w/o 6dB attenuation

- **Jitter Problem**

As we know, usually there is a jitter problem induced by the oscilloscope and if doing the sampling average, the jitter problem is cancelled in the averaged samples. However, for the angle of arrival estimation, the delay information on each antenna element is very important and should not be influenced by the jitter. Thus, we want to know how the oscilloscope works for the sampling average and keep sure that the averaging process inside the oscilloscope can still remain the exact delay information. Therefore, two averaging methods: (1) direct summing all 1024 CIR samples and divide by 1024, (2) shifting all 1024 CIR samples with same delay firstly and then doing the same as (1) do, are compared with the averaging process used by oscilloscope itself, which are showed in Figure 3.7 and Figure 3.8, separately.

As shown in the below two figures, there is no much difference for the two methods compared to the oscilloscope average, which means the jitter for our used oscilloscope is not very serious and therefore the jitter problem for our channel measurement can be neglected during the measurement.

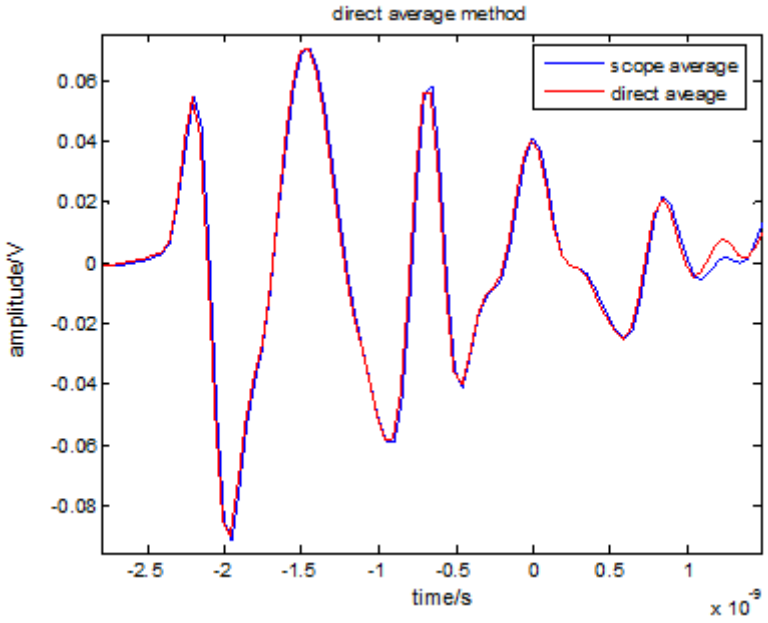

Figure 3.7: The comparison between direct average and scope's average method

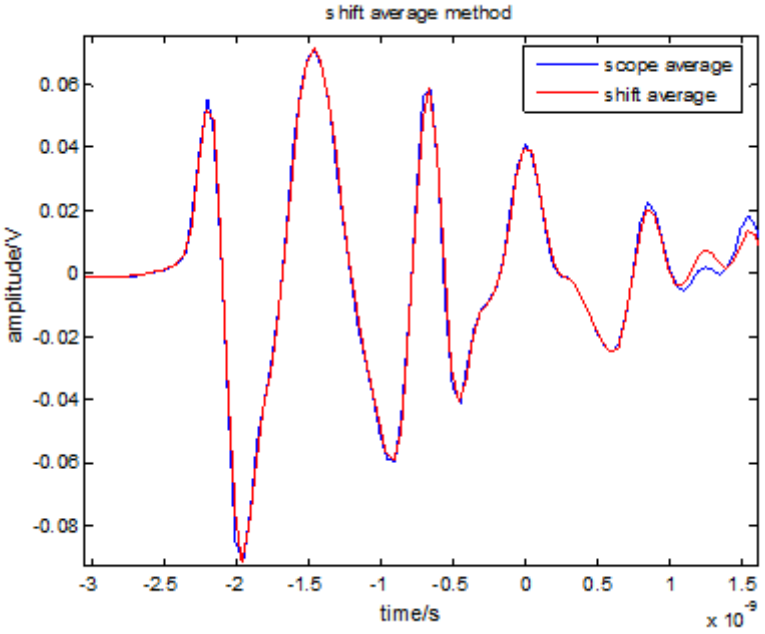

Figure 3.8: The comparison between shift average and scope's average method

- **Link Budget Issue**

In this section, the maximum measured distance of the designed system is tested in a corridor scenario inside the EWI building, TU Delft. The environment is shown in Figure 3.9. The received signals are measured at different Tx-Rx distances, staring from 25 m to 125 m with 25 m per step. A 10 dB LNA is used at Rx side to increase the receiving signal's SNR. The received signals at 25 m and 125 m are showed in Figure 3.10. And the received maximum peak to peak voltage at different distances is showed in Table 3.1

Figure 3.9: Measurement environment of corridor scenario (left), Tx side (middle) and Rx side (right)

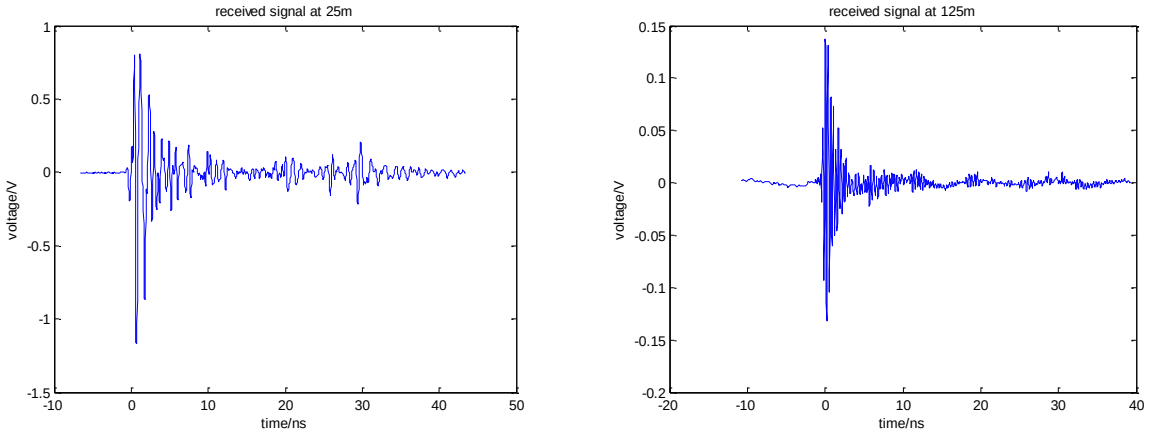

Figure 3.10: Received signal at 25m (left) and 125m (right)

Table3.1: Received signal's Vp-p

Distance	Vp-p	Power
25m	2V	6.02dBW
50m	670mV	-3.48dBW
75m	520mV	-5.68dBW
100m	275mV	-11.2dBW
125m	170mV	-15.4dBW

The measured indoor noise floor is around -25 dBm. Therefore, for 125 m, the received signal's power is around 40 dB above the noise floor, which is a very good SNR. However, at real indoor and outdoor environments, there will be very serious narrowband interference from GSM, UMTS, WIFI, etc., the noise floor would be higher than this measured noise floor. By doing outdoor pilot measurement, we find the maximum distance is less than 70 meters in outdoor scenario, which limits our

designed system for outdoor channel measurements.

- **Narrowband Signal Interference**

Many wireless communication systems, such as GSM, WiFi, UMTS, etc., are operated simultaneously. Therefore, our world is full of signals with different frequency bands. If our measuring UWB signal's frequency band is overlapped with the wireless communication services, such service signals will make serious narrowband interferences on our measuring signals, especially at outdoor scenario.

The pilot outdoor measurement has done near the car parking of EWI building, TU Delft on 20th, Jan. 2011. And the distance between Tx and Rx is around 70m. The height of both Tx and Rx is 1m. Figure 3.11 shows the measuring environment. The received time domain signal and its frequency spectrum are showed in Figure 3.12 and 3.13, respectively.

Figure 3.11: Outdoor pilot measurement Tx side (left) and Rx side (right)

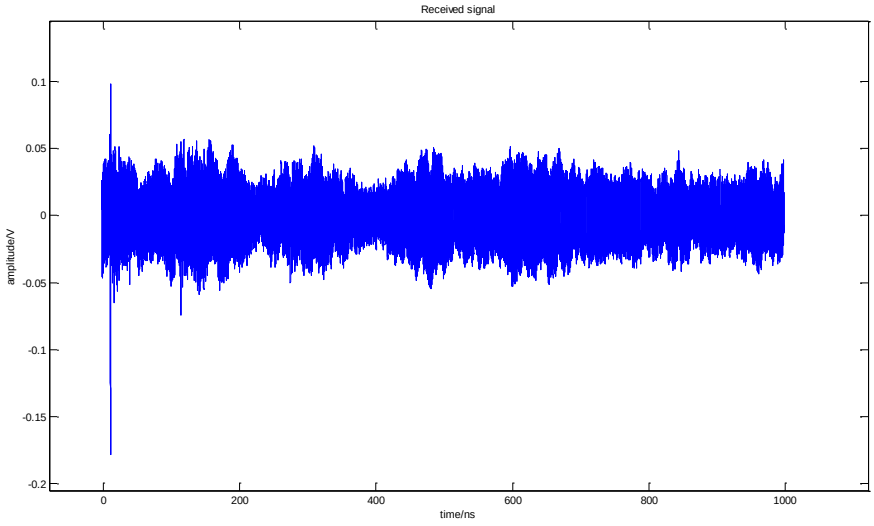

Figure 3.12: Received UWB signal at 70m

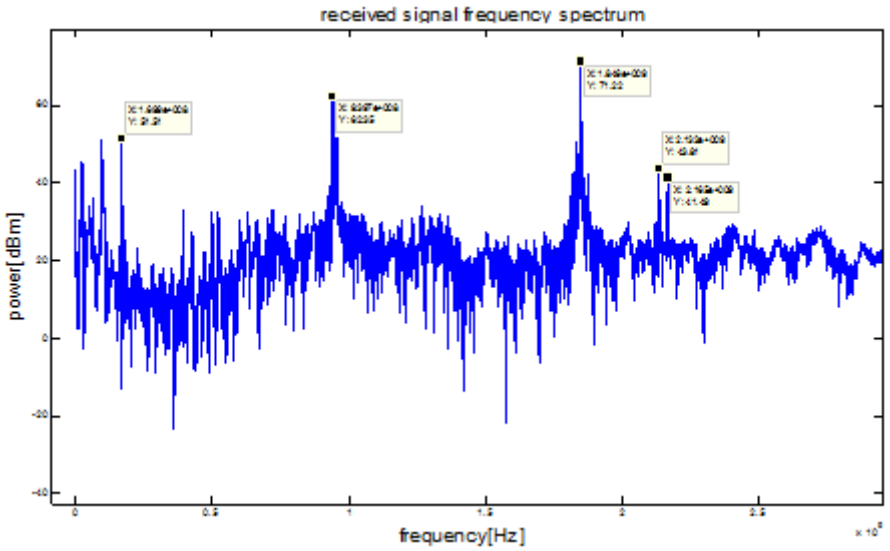

Figure 3.13: Frequency spectrum of received signal

From Figure 3.12, we can see that the UWB signal is mostly hidden in noise and narrowband interference signals and except the LOS path, all other multipath are submerged inside the interference signals. Looking at the received signal's frequency spectrum in Figure 3.13, there are several high peaks on the frequency spectrum, which are related to GSM (around 950 MHz), DCS-1800 (around 1800 MHz), WiFi (around 2.1 GHz) and UMTS (around 2.2 GHz) signals. Such narrowband signals will influence our measurement data and also for the later channel modeling. According to this problem, there are five possible solutions, which are given in the following:

(1) Use several narrowband antennas as receiver antenna groups to collect the signal at certain frequency bands which are not influenced by narrowband interference signals.

(2) Use several notch filters and cascading them to filtering the narrowband interference signals. Such as Cellular Band Fixed Notch Filter - Cellular Band Fixed Notch Filter (806-960 MHz), 3DRPN-1710.2/U3-N/N - DCS/PCS Band Fixed Notch Filter (DCS 1710-1880, PCS 1850-1990 MHz) and WSN-00084 - UMTS Notch Filters (DC-1800 & 2260-2340 MHz), etc.

(3) Use sampling oscilloscope (wireless trigging) to measure the signals. Since for the present measurement set-up, the scope receives both the UWB signal and interference signals. Therefore, the UWB signal is submerged in the interference signals. However, if the sampling oscilloscope is used, the scope is only triggered by the UWB signal and the interference signals are considered as random signals which will not highly interferes the UWB signals. And for long distance

measurement, it is better to use wireless triggering to synchronize both Tx and Rx sides.

(4) Use digital filter to filter the influence signals, because the UWB signal is ultra wide band and the influence signals are narrowband signals. And for the reference antenna, we should make sure that it is triggered by UWB signal, therefore, using some directional horn antenna to aim at Tx antenna which can remove the influence from narrowband signal coming at other direction.

(5) Instead of using ultra wide band sounder, we can use narrowband or wideband sounders to transmit signal at some frequency band without interference from narrowband signals. However, if the frequency dependency should be studied, the channel measurement should be repeated several times for different frequency bands.

- **Receiving Antenna Array**

In order to study the multipath components' angular spread, the measurement set-up should be a Single Input Multiple Output (SIMO) system. Thus an antenna array is designed to be used at Rx side. Since for normal outdoor wireless communication, the angular spread of multipath components' elevation angles are small and most of multipath components' elevation angle is between -15 deg and +15 deg, we focus on studying the angular spread of azimuth angle. In this case, a 2-D planer antenna array should be designed. There are many types of 2-D antenna array designs, such as linear array, circular array, rectangular array, 'X' shape array, 'Y' shape array, etc. Figure 3.14 shows linear array and circular array type. And each kind of antenna array has its advantages and disadvantages comparing to others. For example, the linear array has very high angle resolution, but it has angular ambiguity that can only estimate from 0 deg to 180 deg. The uniform circular array (UCA) has drawn much attention due to its perfectly uniform performance in azimuth angle domain. After comparing these several types of antenna arrays, the circular antenna array is selected as in our array design. However, the two parameters, number of antenna elements and circular array radius, also decide the array's angular resolution and angular ambiguity.

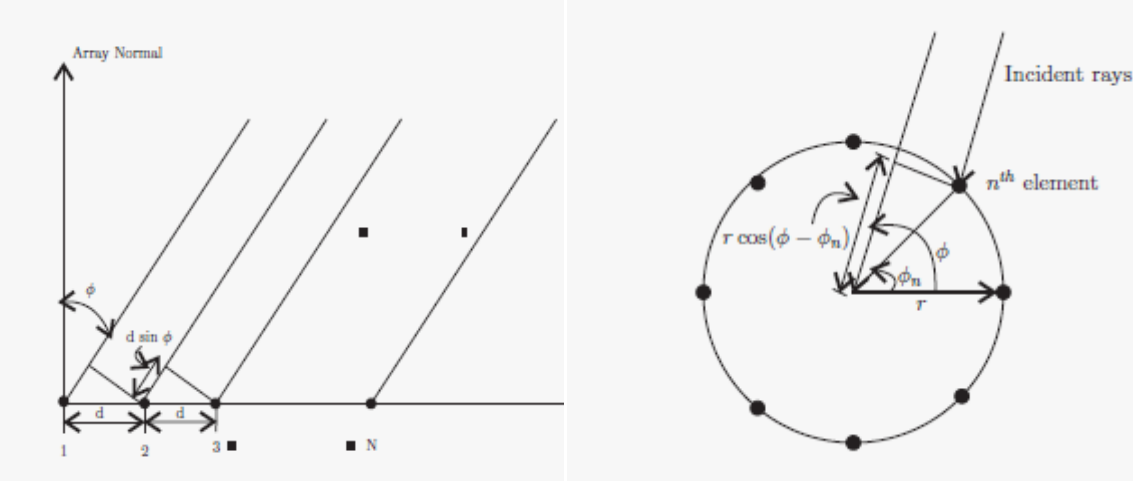

Figure 3.14: Linear antenna array (left) and circular antenna array (right)

For circular array, more elements can increase the resolution of the DoA estimation. The beamformings of circular array with different number of antenna elements are simulated in Matlab and shown in Figure 3.15. However, there is saturation that above some threshold, the resolution can't increase anymore. The antenna spacing should be smaller than $1/2\lambda$. Otherwise, the angular ambiguity occurs (there are several values of θ bringing to the same estimated angle ϕ). After considering the implementing factors, such as the Rx antenna physical size, sufficient number of elements for statistic fading studies, etc, finally the number of antenna elements is 72 and the circular array radius is 0.3m. Since the number of Biconic antenna is limited in our research lab, the physical size of Biconic antenna is much larger than the designed antenna spacing and there are just four channels for the oscilloscope, the virtual antenna array is designed for the measurement set-up, which is showed in Figure 3.16. The definition of virtual array is only one antenna element is available at each side of the link and MIMO measurements are performed by moving the elements to predefined positions before each sounding of the channel. The advantage of virtual array is its simplicity. However, the main shortcoming of this type is the limitation on the temporal variations of the channel which means the channel should be static during the whole measurement run.

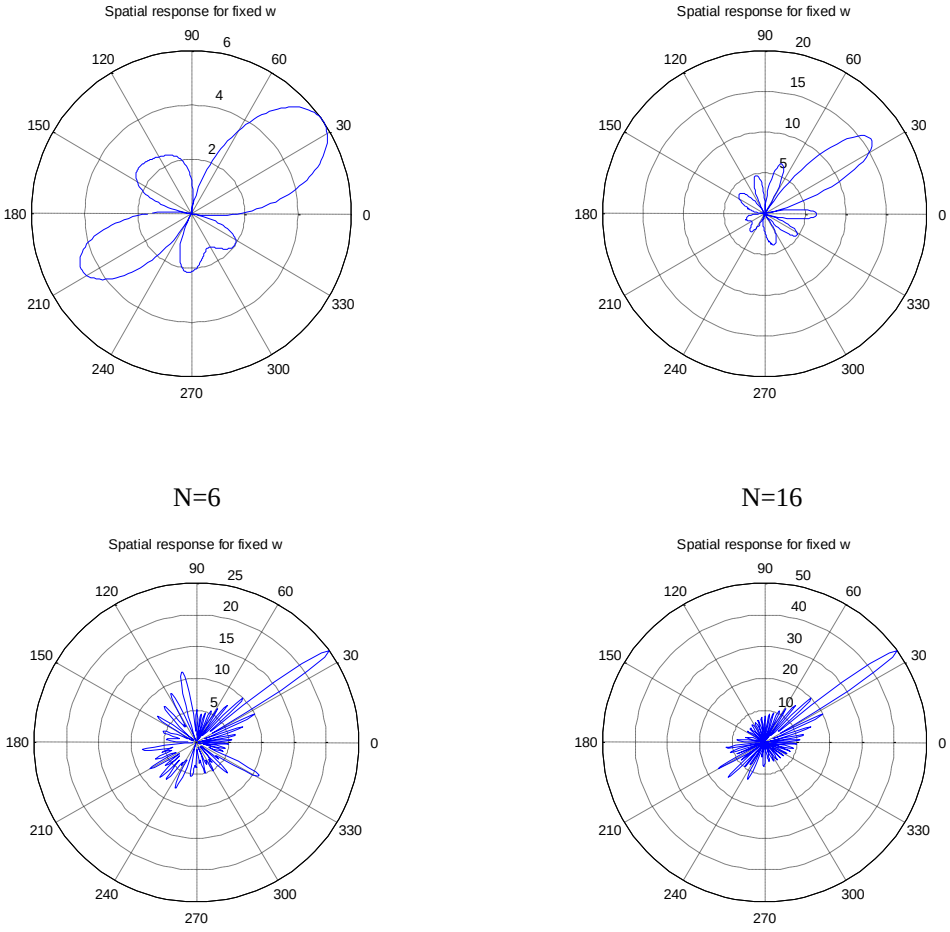

N=6 N=16

N=25 N=50

Figure 3.15: The simulated beamforming of circular array with different number antenna elements

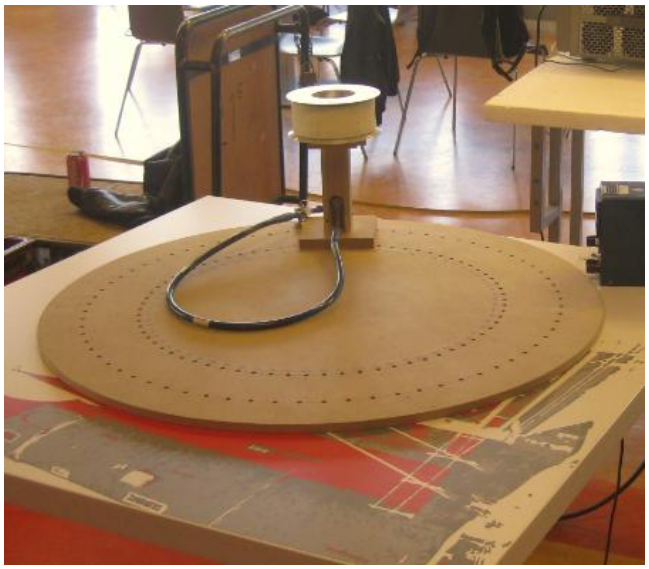

Figure 3.16: The designed circular antenna array

- **Measurement Set-up**

The whole measurement set-up design is showed in Figure 3.17.

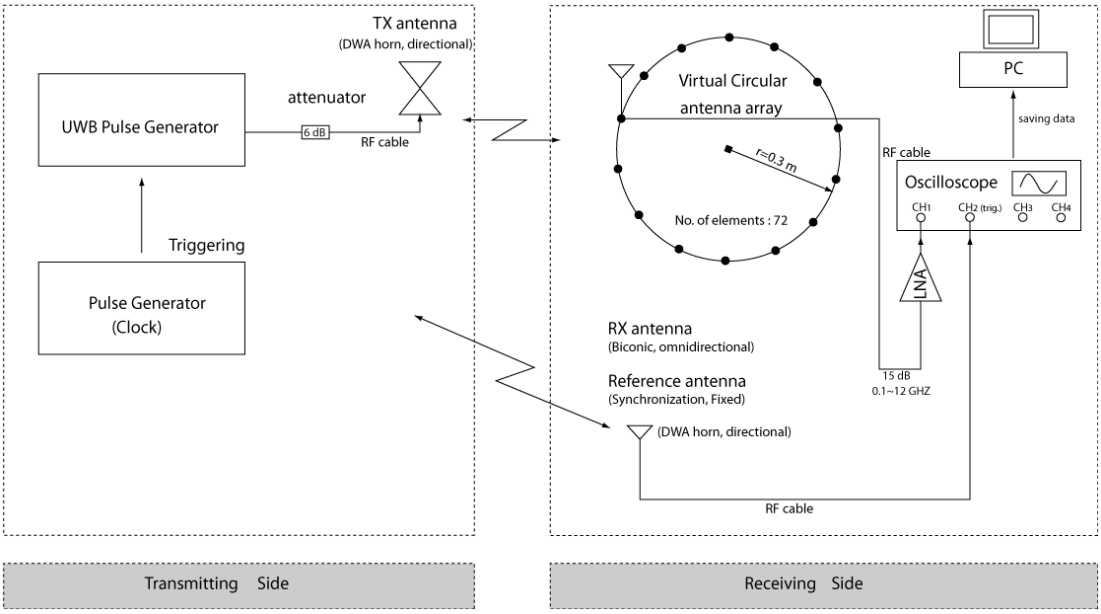

Figure 3.17: The structure of measurement system set-up

- **Outdoor Scenario Measurement Plan**

The measurement system is originally designed for outdoor case and the measurement scenario is similar to real LTE scenario. Therefore, we make plan and measurement for the outdoor measurement. Following are the details of the plan.

(1) The equipments used in the real scenario measurement

➢ **Tx side:**

1. UWB pulse generator
2. Long Cables
3. Tx antenna (DWA, directional)
4. Pulse generator for clock triggering
5. Long distance electric wires for connecting power supply
6. Some matched connectors for cables, antenna's connection

➢ **Rx side:**

1. Oscilloscope
2. Circular wooden plate
3. Rx antenna (Biconic, omni-directional)
4. Long cables
5. Movable power supply
6. Long distance electric wires for connecting power
7. Some matched connectors for cables, antenna's connection
8. Trolley or movable table to carry all Rx equipments
9. Reference antenna

(2) Real outdoor scenario map

The measurement place is selected around the TU Delft EWI building. The Tx is installed on the roof of low building and the route of the Rx is around the parking place behind EWI building. The real scenario pictures and maps are showed in Figure 3.17.

➢ **LOS**

The LOS route (**Route 1+ Route 2**) has the total length of 200 m. The measurement starts at 50 m and adds 25 m for every next position. Therefore the total number of positions is 7. However considering the height of the Tx antenna is ~17 m. The real distance for each position is measured from the wall of EWI low building, which is showed in Table 3.2.

Figure 3.20: Real outdoor scenario map (marked on Google map)

Table 3.2: The real distance for each LOS measuring position (Route 1+2)

	Real value	Theoretical value
1	50m	47m
2	75m	73m
3	100m	99m
4	125m	124m
5	150m	149m
6	175m	174m
7	200m	199m

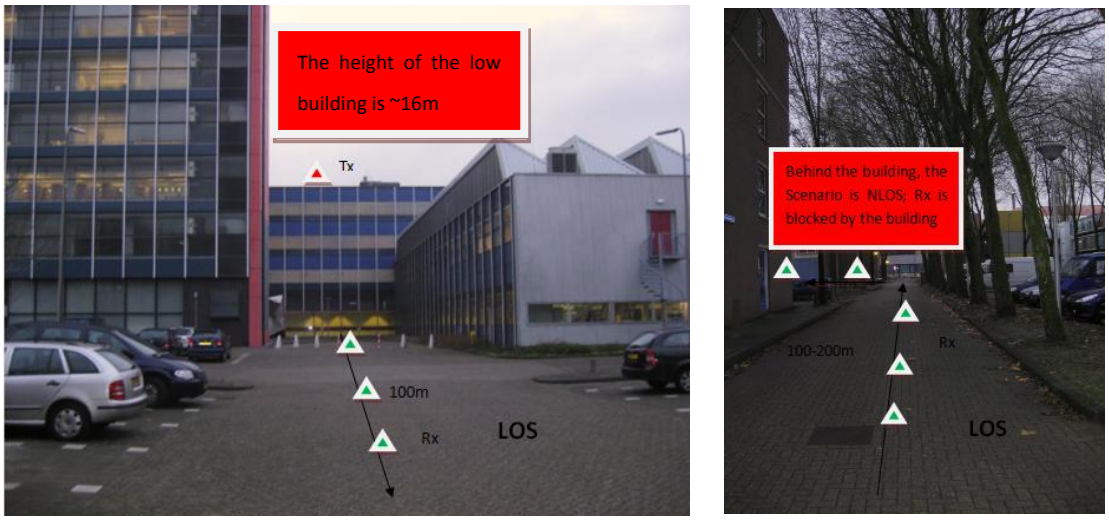

Figure 3.21: LOS scenario measurement of part 1 (left) and part 2 (right)

- **LOS to NLOS**

The length of LOS to NLOS route (**Route 3+ Route 4**) is 74 m (**Route 3**) and 127 m (**Route 4**). The measurement starts at the center of the crossroad and adds 25 m for every next position. Therefore the total number of positions is 4 for **Route 3** and 6 for **Route 4**. However considering the height of the Tx antenna is ~17 m. The real distance for each position is (the following distance are measured from the wall of EWI low building, which are showed in Table 3.3 and 3.4.

Table 3.3: The measured distance from the center of crossroad (Route 3)

	Real value	Theoretical value
1	86.5m	0m
2	89m	20m
3	95.5m	40m
4	105m	60m

Table 3.4: The measured distance from the center of crossroad (Route 4)

	Real value	Theoretical value
1	86.5m	0m
2	89m	20m
3	95.5m	40m
4	105m	60m
5	118m	80m
6	132m	100m

Figure 3.22: LOS scenario measurement route of part 1 (left) and part 2 (right)

➢ **NLOS**

The length of NLOS route (**Route 5**) is 40 m and the distance step is 10 m, therefore there are 5 positions. However considering the height of the Tx antenna is ~17 m. The real distance for each position is showed in Table 3.5.

Table 3.5: The measured distance from the center of crossroad (Route 5)

	Real value	Theoretical value
1	120.0m	0m
2	120.5m	10m
3	121.5m	30m
4	123.5m	40m
5	126.5m	50m

- **Indoor Measurement Description**

The Msc. project is originally planned to implement outdoor scenario measurement. However, as discussed in the above that the transmitting power of the UWB pulse generator is not enough for long distance transmission (>100 m) and also the equipments' insurance problem, the channel measurement is finally taken at indoor scenario. The detail of the measurement report is attached in the Appendix C.

3-3 Summary

In this chapter, we discussed our channel measurement set-up design and also gave the solution for all the technical and practical problems which we met during the system development. And then the wireless channels were measured at power lab, canteen and library, three different indoor environments. For each scenario, we

implemented the channel measurements at 10 different locations (5 LOS and 5 NLOS) and at each location, 72 positions on the circular array were measured. Therefore, the total number of measured channel impulse response profiles is about 2016.

Chapter 4

Spatial Modeling Of Wideband Channel

The performance of any communication system is determined by the characteristics of the radio channel on which it operates. Thus, developing an accurate channel model which can reflect real characteristics of the wireless channel is necessary and helpful for communication system designs. As discussed in Chapter 2, there are several methods to model the wireless channel, such as deterministic model, statistical model, and geometric based model, but in this thesis, we only focus on the statistical modeling method. The main idea of the statistical modeling is that first a mathematic model describing the wireless channel is proposed and then a large number of real channel measurements are performed to validate such proposed model. Furthermore, since the Multiple Input Multiple Output (MIMO) technique is popularly utilized in modern communication systems, the spatial information can be studied and it has close relation to the MIMO system capacity. Through implementing high resolution DoA algorithms on the antenna array, signals' angle of arrival can be estimated, which can provide additional information of the wireless channel and therefore improve the performance of communication system.

At beginning of this chapter, we discuss the spatial modeling of wideband channel and then explain the method to get the wideband channel's Channel Impulse Response (CIR) from our measured Ultra Wideband (UWB) signals. In the second section, we discuss the channel parameters, such as multipath component's amplitude, time of arrival and angle of arrival. For estimating channel parameters, several useful methods and models are introduced and especially, the high resolution MUSIC for

ToA, DoA and Joint ToA and DoA estimation (JADE) algorithms are discussed. At the end of this chapter, we present the modeling of channel parameters: *rms* delay spread (RDS), amplitude fading distribution and angular spread (AS).

4-1 Modeling of Wideband Channel

4-1-1 Spatial Modeling of Wideband Channel

For wideband channel, the signal's bandwidth is wide and therefore the resolution of the channel on time domain is relatively high, which makes the multipath components be separated on time domain. Thus, the wideband channel can be modeled as:

$$h(t,\tau) = \sum_{n=0}^{L_p(t)-1} a_n(t)\delta(\tau - \tau_n(t)) \tag{4.1}$$

where τ is the excess delay, t refers to the impulse response at instant t and $\delta(\cdot)$ is the Dirac delta function. The parameters a_n, τ_n, is the n^{th} path's amplitude, delay, respectively and L_p represents the total number of multipath components. However, if the channel is time invariant, the channel impulse response can be simplified to:

$$h(\tau) = \sum_{n=0}^{L_p-1} a_n\delta(\tau - \tau_n) \tag{4.2}$$

Because of the inventions of antenna array and high resolution AoA estimation algorithms, the multipath component's AoA information can be estimated. Therefore, if the multipath components are separated by their arrival angles rather than their time delays, the CIR can be represented in angular domain, as (4.3):

$$h(\varphi) = \sum_{n=0}^{L_p-1} a_n\delta(\varphi - \varphi_n) \tag{4.3}$$

where a_n and φ_n is the n^{th} multipath component's amplitude and arrival azimuth or elevation angle, respectively. The signal's AoA adds the spatial dimension into the channel modeling and the channel's angular spread (AS) indicates how abundant the channel propagation mechanisms of scattering, reflection, diffraction are. For example, in MIMO system, both the multipath angular spread and antenna spacing determine the spatial correlation of the antenna array and therefore influence the MIMO system capacity. Furthermore, the principle of smart antenna technology is through estimating the AoA of the strongest signal path and then rotating the main beam to that direction to receive it by using digital beamforming method, which can increase the system's

performance.

Since the importance of the angular information, through combining (4.2) and (4.3), a wideband spatial model can be expressed as (4.4):

$$h(\tau,\varphi)=\sum_{n=0}^{L_p-1} a_n\cdot\delta(\tau-\tau_n)\cdot\delta(\varphi-\varphi_n) \tag{4.4}$$

This spatial channel model evolves the channel modeling from 2D (amplitude, time delay) to 3D version (amplitude, time delay and arrival angle).

4-1-2 Studying Wideband Channel through UWB Signal

In Chapter 3, it has been mentioned that our measurement system is actually a UWB system. At the transmitting side, an ultra wideband signal with bandwidth from 0.1 to 4 GHz is sent out to excite the wireless channel. This bandwidth can lead to a high resolution of 250 ps. However, our purpose of this project is to study the frequency dependency of channel modeling. Therefore, we divide the whole UWB into many wideband bins (sub-bands) having different centre frequency and then the frequency dependency can be studied among these different frequency bands. The signal filtering method can be generally divided into two types: analog filtering and digital filtering. For the analog filtering, it is directly applied on the analog signal. Through installing the analog filter component in the measurement system, only the part of signal inside the analog filter's passing band can go through the analog filter. Therefore, the finally received signal is only with certain filtered frequency band. For the channel frequency dependency study, many analog band-pass filters having different passing frequencies are needed. However, the digital filtering method performs signal filtering after the process of receiving UWB signal. The procedures are firstly choosing some window function with predetermined starting point (lowest frequency) and window width (bandwidth) and then adding it on the received signal's frequency spectrum. Therefore, the UWB signal is filtered to the certain band-passed signal. Since we want to collect several wideband signals with different centre frequencies by measuring the channel only once, it is better to use digital filter rather than analog filter.

In our case, a digital filter is implemented and applied on the received UWB signal. The bandwidth of the filtered signal is chosen to be 100 MHz, The reason for such chosen is that 100 MHz bandwidth will result in 10 ns time resolution and the related

time delay difference between any two multipath component is usually longer than 10 ns in mobile communication scenario, which makes sure that most of the multipath can be separated in the channel impulse response. Figure 4.1 shows the received UWB signal at power lab scenario And Figure 4.2 shows the signal after digital filtering for the frequency band [1.5, 1.6] GHz and its power frequency spectrum.

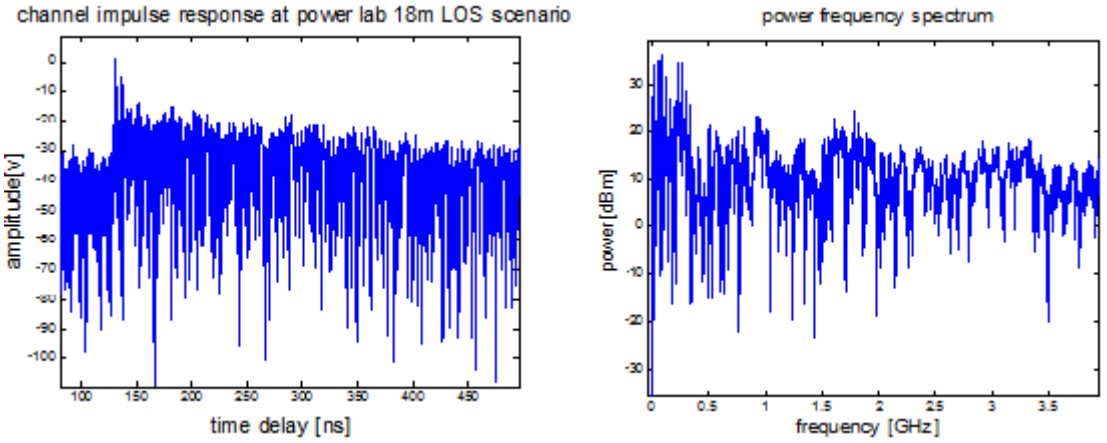

Figure 4.1: CIR of UWB signal (left) and its power spectrum (right)

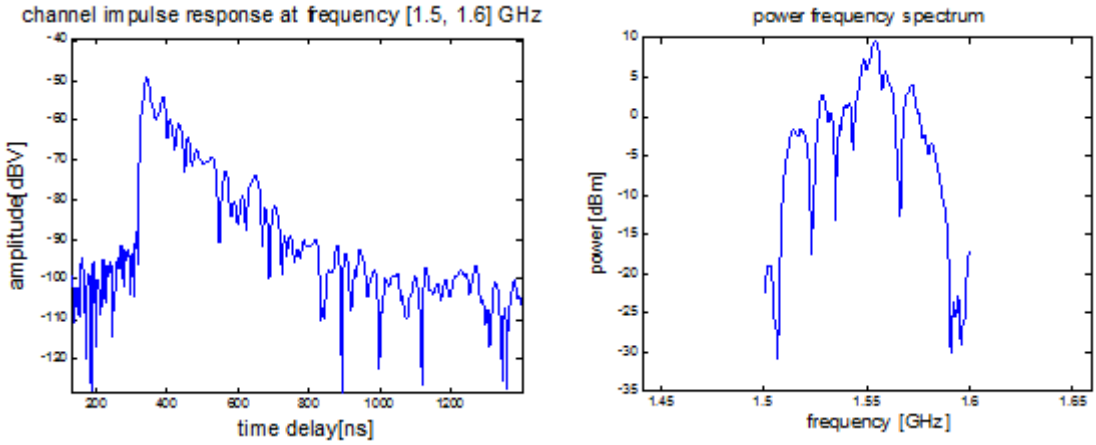

Figure 4.2: CIR of UWB signal after digital filtering (left) and its power spectrum (right)

For the further studying on frequency dependency of wireless channel, we can firstly decide several frequency bands we want to study and then apply related digital band-pass filters on the received UWB signal's frequency spectrum to obtain those frequency bands' signals. The details of the frequency dependency studies will be discussed in Chapter 5.

4-2 Estimation of Channel Parameters

4-2-1 Amplitude Estimation

As shown in section 4.1, the amplitude a_n in (4.1) represents the strength of each multipath component. There are several methods to estimate the multipath amplitude [7]. Here we only introduce two methods to evaluate this parameter, which are discrete channel impulse response (D-CIR) and maximum detection (MD).

- **D-CIR method**

In [26], the *IEEE* discrete channel impulse response model (D-CIR) is introduced to estimate each multipath component. In this method, the temporal axis of the CIR is divided into adjacent time bins and each bin is assumed to contain either one resolvable path or no path. The width of each bin is determined by the signal bandwidth. Since the signal bandwidth is 100 MHz, the width of time bin is equal to 10 ns (1/100 MHz). According [26], the time window (maximum multipath time delays) for indoor and outdoor scenario is usually smaller than 500 ns and 2 μs, respectively. Therefore, the temporal axis is divided into 50 time bins for indoor scenario and 200 time bins for outdoor scenario. And in each bin, the represented path amplitude is the averaged amplitude of all points in that bin.

- **Maximum Detection method**

Another way to estimate the multipath amplitude is through the Maximum Detection (MD) method [7]. For the MD method, the multipath components are detected by finding the local maxima in the channel impulse response. Figure 4.3 shows the detected multipath by red '+' on the channel impulse response and the power threshold level is set to 30 dB below the strongest path, which is enough to receive nearly 97% of the total power.

In Chapter 5, the bandwidth influence on *rms* delay spread by using these two methods is discussed and for wideband channel (100 MHz), the two methods have similar result. Therefore, both MD and D-CIR method can be used to estimate the multipath amplitude for wideband channel.

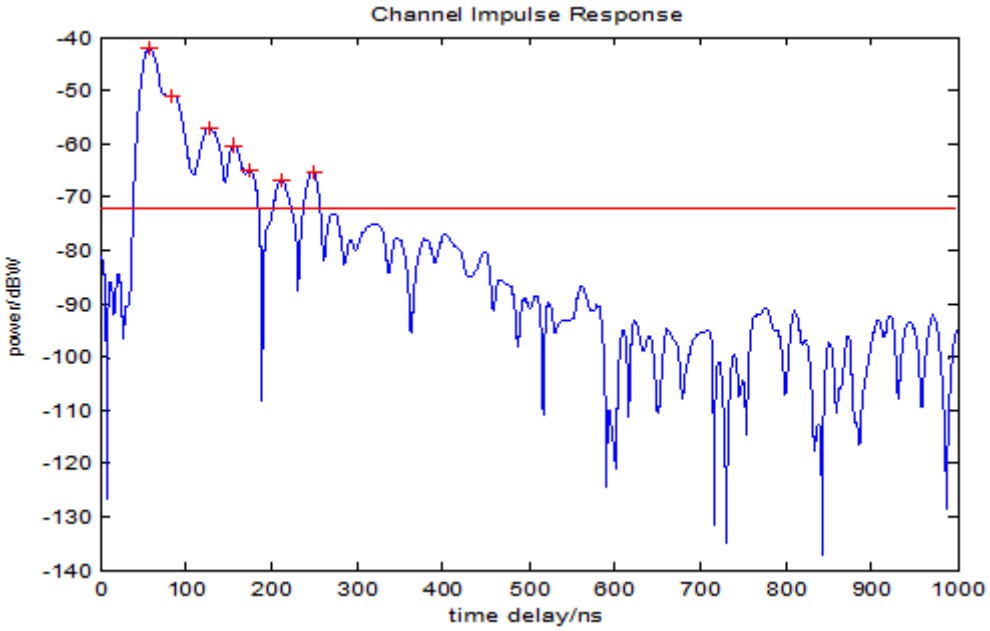

Figure 4.3: The maximum detection (MD) method

4-2-2 Time of Arrival (ToA) Estimation

The arrival time of each multipath component is a parameter to indicate how long of each multipath travels in the wireless channel. Furthermore, using Time of Arrival (ToA) as ranging metric is the most popular technique for accurate indoor positioning. The accuracy of measuring distance by using ToA is sensitive to the bandwidth of the system and the multipath condition between the wireless terminal and the access point.

The time resolution determines the accuracy of the channel model. As we know, the increasing of the signal bandwidth can also enhance the signal's resolution on time domain and therefore improve the ToA estimation. However, if the bandwidth is fixed, there is also other way to improve the accuracy of ToA estimation by applying some better signal processing algorithms on the measured data. In the following, two ToA estimation methods are introduced.

- **Inverse Filtering (IF) method**

IF is the simplest and conventional ToA estimation algorithm. Through Fast Fourier Transforming (FFT), the channel impulse response can be obtained from the frequency domain data. The flow chart of the IF algorithm is showed in Figure 4.4. As shown in this figure, a Hanning Window is used to filter the signal to certain frequency band, which also avoids leakage and false peaks by reducing the side-lobes of the time domain response at the cost of reduced resolution. After the IFFT block,

the peak detection algorithm selects the local maxima and their related times indicate the detected multipath ToAs.

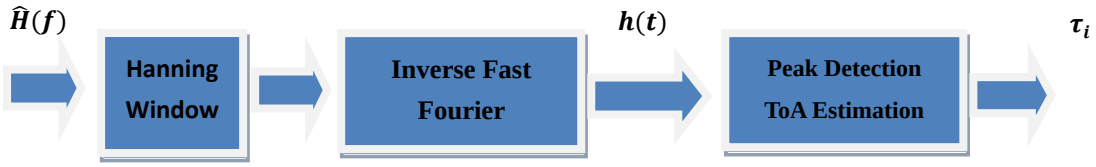

Figure 4.4: The flow chart of Maximum Detection algorithm

- **MUSIC Algorithm**

MUltiple Signal Classification (MUSIC) is one of the high-resolution spectral estimation techniques applied to the channel frequency response to detect the multipath delay information. And it detects the multipath signals' ToAs by eigen-decomposition method.

The wireless radio channel suffers from multipath propagation phenomenon and then the channel impulse response can be written as:

$$h(\tau) = \sum_{k=0}^{L_p-1} a_k \delta(\tau - \tau_k) \tag{4.5}$$

where L_p is the number of multipath components, $a_k = |a_k|e^{j\theta_k}$ and τ_k are the amplitude and propagation delay of the k^{th} path, respectively. For example, τ_0 in the above equation is the line of sight (LOS) path's time delay. The multipath ToAs should be detected for building channel model. The Fourier transform of (4.5) is the channel frequency response which is given by

$$H(f) = \sum_{k=0}^{L_p-1} a_k e^{-j2\pi f \tau_k} \tag{4.6}$$

The phase of the complex amplitude θ_k is assumed random with an uniform probability density function (PDF) ~$U[0, 2\pi)$. Usually these parameters are frequency dependent. And a harmonic signal model (channel frequency response) can be created by exchanging the role of time and frequency variables in (4.6) which yields,

$$H(\tau) = \sum_{k=0}^{L_p-1} a_k e^{-j2\pi f_k \tau} \tag{4.7}$$

This model is well known in spectral estimation field and any spectral estimation

techniques that are suitable for the harmonic model can be applied to the frequency response of multipath radio channel to perform time-domain analysis.

The actual channel frequency response $H(l)$ should get rid of the influence from the Tx/Rx antennas, signal pulse shape, which can be obtained by dividing the FFT of the received signal $s(t)$ by the FFT of the LOS signal $s_{LOS}(t)$ shown in (4.8):

$$H(l) = \frac{\text{FFT}(s(t),\ L)}{\text{FFT}\ (s_{LOS}(t),\ L)} \tag{4.8}$$

of L equally spaced frequency components. Considering the additive white noise in the measurements, the sampled discrete channel frequency response is given by [40]:

$$X(l) = H(f_l) + w(l) = \sum_{k=0}^{L_p-1} a_k e^{-j2\pi(f_0+l\Delta f)\tau_k} + w(l) \tag{4.9}$$

where $l = 0,1,\dots,L-1$ and $w(l)$ denotes additive white measurement noise with zero mean and variance σ_w^2. The signal model in vector form is [44]:

$$\boldsymbol{X} = \boldsymbol{H} + \boldsymbol{W} = \boldsymbol{V\alpha} + \boldsymbol{W} \tag{4.10}$$

where

$$\boldsymbol{X} = [X(0)\ \ X(1)\ \dots X(L-1)]^T \tag{4.11}$$

$$\boldsymbol{H} = [H(f_0)\ \ H(f_1)\ \dots H(f_{L-1})]^T \tag{4.12}$$

$$\boldsymbol{W} = [W(0)\ \ W(1)\ \dots W(L-1)]^T \tag{4.13}$$

$$\boldsymbol{V} = [\boldsymbol{v}(\tau_0)\ \ \boldsymbol{v}(\tau_1)\ \dots \boldsymbol{v}\left(\tau_{L_p-1}\right)] \tag{4.14}$$

where

$$\boldsymbol{v}(\tau_k) = [1\ \ e^{-j2\pi\Delta f\tau_k}\ \dots e^{-j2\pi(L-1)\Delta f\tau_k}]^T \tag{4.15}$$

$$\boldsymbol{\alpha} = [\alpha_0'\ \ \alpha_1'\ \ \dots \alpha_{L_p-1}'\ ]^T \tag{4.16}$$

where

$$a_k' = a_k e^{-j2\pi f_0\tau_k} \tag{4.17}$$

MUSIC algorithm is based on eigen-decomposition of the autocorrelation matrix, derived from (4.7). The autocorrelation matrix is given by [40]:

$$\boldsymbol{R_{XX}} = E\{\boldsymbol{XX}^H\} = \boldsymbol{VAV}^H + \boldsymbol{\sigma_w^2 I} \tag{4.18}$$

where $\boldsymbol{A} = \boldsymbol{E}\{\boldsymbol{aa^H}\}$ and superscript '*H*' means the Hermitian, conjugate transpose of a matrix. Since the propagation delays τ_k in (4.5) can be theoretically assumed to be different among each other, the matrix $\boldsymbol{V}$ has full column rank which means the column vectors of $\boldsymbol{v}$ are linearly independent. The $L_p \times L_p$ covariance matrix $\boldsymbol{A}$ is non-singular since that $|a_k|$ is assumed as constant and the phase is usually considered as a uniform random variable between 0 and 2π. Therefore, as we learned from the theory of linear algebra, if the dimension L is larger than L_p, then the rank of the matrix $\boldsymbol{VAV}^H$ is L_p and it also means that the $L - L_p$ smallest eigenvalues of $\boldsymbol{R_{XX}}$ are equal to σ_w^2 [21]. The eigenvectors corresponding to L_p largest eigenvalues are called signal eigenvectors. Therefore, the *L*-dimensional space can be split into two orthogonal subspaces, known as signal subspace and noise subspace, which are represented as the signal eigenvectors and noise eigenvectors, respectively. The projection matrix of the noise subspace is then given by [40]:

$$\boldsymbol{P_w} = \boldsymbol{Q_w}(\boldsymbol{Q_w^H Q_w})^{-1}\boldsymbol{Q_w^H} = \boldsymbol{Q_w Q_w^H} \tag{4.19}$$

Where $\boldsymbol{Q_w} = [\boldsymbol{q_{Lp}}\ \boldsymbol{q_{Lp+1}} \ldots \boldsymbol{q_{L-1}}]$ and $\boldsymbol{q_k}(L_p \le k \le L-1)$, are noise eigenvectors. Since the vector $\boldsymbol{v}(\tau_k)$, $0 \le k \le L_p - 1$, must lie in the signal subspace, we have

$$\boldsymbol{P_w v}(\tau_k) = 0 \tag{4.20}$$

Thus, the multipath delays τ_k, $0 \le k \le L_p - 1$, can be determined by finding the delay values where the following MUSIC pseudo-spectrum achieves maximum value.

$$S_{music}(\tau) = \frac{1}{\|\boldsymbol{P_w v}(\tau)\|^2} = \frac{1}{\boldsymbol{v}(\tau)^H \boldsymbol{P_w v}(\tau)} = \frac{1}{\|\boldsymbol{Q_w^2 v}(\tau)\|^2} = \frac{1}{\sum_{k=Lp}^{L-1} |\boldsymbol{q_k^H v}(\tau)|^2} \tag{4.21}$$

In the above analysis [44], the theoretical correlation matrix $\boldsymbol{R_{xx}}$ is considered. However, in real case, the correlation matrix must be estimated from the measurement data samples.

Figure 4.5 shows the flow chart of MUSIC algorithm used in ToA estimation. The autocorrelation matrix is estimated from the measurement data followed by an eigen-decomposition where the L_p parameters are estimated. Then the pesudospectrum is computed from the L_p parameters, the eigenvectors and the eigenvalues. Once the pseudospectrum is obtained, the peak detection algorithm is applied to select all multipath components' ToAs.

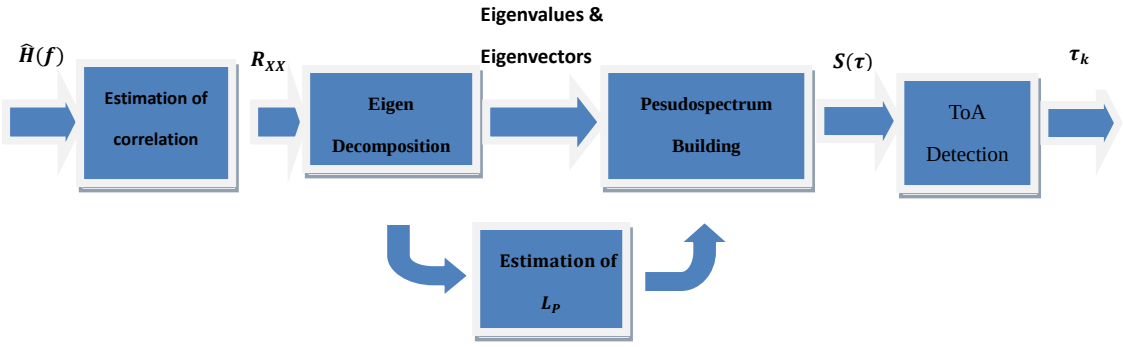

Figure 4.5: Block diagram of MUSIC super-resolution TOA estimation algorithm

In the real case, the autocorrelation matrix must be estimated from a limited set of data. As a result with P snapshots of measurement data, estimating the correlation matrix can be obtained from [40]:

$$\widehat{\boldsymbol{R}}_{\boldsymbol{xx}} = \frac{1}{P}\sum_{k=1}^{P} \boldsymbol{X_k}\,\boldsymbol{X_k^H} \tag{4.22}$$

$$= \frac{1}{P}\begin{bmatrix} X_1(0) & \dots & X_p(0) & \dots & X_P(0) \\ \vdots & & \vdots & & \vdots \\ X_1(l) & & X_p(l) & & X_P(l) \\ \vdots & & \vdots & & \vdots \\ X_1(L-1) & \dots & X_p(L-1) & \dots & X_P(L-1) \end{bmatrix} \times \begin{bmatrix} X_1(0) & \dots & X_p(0) & \dots & X_P(0) \\ \vdots & & \vdots & & \vdots \\ X_1(l) & & X_p(l) & & X_P(l) \\ \vdots & & \vdots & & \vdots \\ X_1(L-1) & \dots & X_p(L-1) & \dots & X_P(L-1) \end{bmatrix}^H$$

However, if only one snapshot of length N is available, then the data sequence is divided into M consecutive segments of length L and then the correlation matrix is estimated as $(M = N - L + 1)$

$$\widehat{\boldsymbol{R}}_{\boldsymbol{xx}} = \frac{1}{M}\sum_{k=0}^{M-1} \boldsymbol{X_k}\,\boldsymbol{X_k^H}$$

$$= \frac{1}{M}\begin{bmatrix} X(0) & X(1) & \dots & X(M-1) \\ X(1) & X(2) & & X(M) \\ \vdots & \vdots & & \vdots \\ X(L-1) & X(L) & & X(M+L-2) \end{bmatrix} \times \begin{bmatrix} X(0) & X(1) & \dots & X(M-1) \\ X(1) & X(2) & & X(M) \\ \vdots & \vdots & & \vdots \\ X(L-1) & X(L) & & X(M+L-2) \end{bmatrix}^H \tag{4.23}$$

For super-resolution ToA estimation techniques, the measurement data vector $\boldsymbol{X}$ is obtained by $\boldsymbol{X} = \frac{\mathrm{FFT}(s(t),\ N)}{\mathrm{FFT}\,(s_{LOS}(t),\ N)}$ or sampling the channel frequency response

uniformly over a certain frequency band. By selecting the frequency domain sampling interval Δf to satisfy the condition $\frac{1}{\Delta f} \geq 2\tau_{max}$, where τ_{max} is the maximum delay of the measured multipath, it is possible to avoid aliasing in the time domain which is similar to the time domain Nyquist sampling theorem.

4-2-3 Direction of Arrival (DoA) Estimation

Multipath AoA adds spatial information in channel modeling. After knowing each path's angle of departure and angle of arrival and then according to the environment's geometry structure, we are able to estimate each multipath signal's propagation route, which help us better understand the wireless channel.

Generally speaking, the ways to estimate AoA can be divided into two categories: analog beamforming and digital beamforming.

- **Analog Beamforming**

For the analog beamforming method, in reference [45], they use narrow beam-width directional antenna as a receiving antenna and install a motor under the Rx antenna to rotate the directional antenna with small step angle to receive the arriving waves coming from different angles. The angular resolution depends on the receiving antenna beam width, which is a critical factor to determine the accuracy of angular spread model. For example, in [47], the receiving antenna during the rotational measurement is selected as a directional antenna with beamwidth of 4 degree and at an azimuth step of 4 degree. These 90 CIRs are associated to 90 directions and the azimuth angle resolution is also 4 degree.

The channel impulse response at Rx antenna's angular direction, φ (0~360deg) can be represented as [45]:

$$h(\tau, \varphi) = \sum_{n=1}^{L_p} a_n(\varphi)\delta(\tau - \tau_n(\varphi)) \cdot e^{j\theta_n} \tag{4.24}$$

The related signal power at direction φ can be defined as [45]:

$$p(\varphi) = w_{cal} \int_{\tau_{min}}^{\tau_{max}} |h(\tau, \varphi)|^2 dt \tag{4.25}$$

where w_{cal} is the measurement system calibration value, τ_{min} and τ_{max} are the

minimum and maximum time threshold considered in power estimation.

- **Digital Beamforming**

Digital beamforming method becomes popular due to the use of antenna array. The basic idea of digital beamforming is utilizing the antenna array's geometric structure and applying the high resolution DoA estimation algorithms on it to detect each arrival signal's angle. There are several types of high resolution DoA algorithms, such as ESPRIT [37], MUSIC [30] and etc. In this section, MUSIC based on circular array azimuth DoA estimation algorithm is discussed.

The idea of DoA MUSIC [30] is similar to ToA MUSIC, which is also based on the eigen-decomposition of the autocorrelation matrix $\boldsymbol{R_{XX}}$ and through orthogonally separating it into signal subspace and noise subspace to estimate the multipath components' arrival of angles. In the circular antenna array case, the channel impulse response for m^{th} antenna element is [17]:

$$h_m(\tau) = \sum_{k=0}^{L_p-1} a_{m,k}\delta\left(\tau - \tau_k - \tau_{m,k}\right), for\ n \in (1,2 \dots M) \qquad (4.26)$$

where L_p is the number of multipath and τ_k is multipath delay and the extra delay $\tau_{m,k}$ for the k^{th} multipath on the m^{th} antenna element results from both the circular array structure (compared to the centre point of the circular array) and the arrival angle of the k^{th} multipath component. Therefore, we can utilize all the extra time delay information $\tau_{m,k}$ for DoA estimation. Seeing the following circular array structure showed in Figure 4.6, the antenna array manifold can be represented as [29]:

$$\boldsymbol{\alpha}(\phi) = \begin{bmatrix} exp(j2\pi\Delta cos(\phi - \phi_1)) \\ \vdots \\ exp(j2\pi\Delta cos(\phi - \phi_m)) \\ \vdots \\ exp(j2\pi\Delta cos(\phi - \phi_M)) \end{bmatrix} \qquad (4.27)$$

where $\Delta = radius/wavelength$, ϕ is the angle of arrival of an incident signal, $\phi_m = \frac{2\pi(m-1)}{M}$ and assuming that the elevation angle $\beta = 90$ deg.

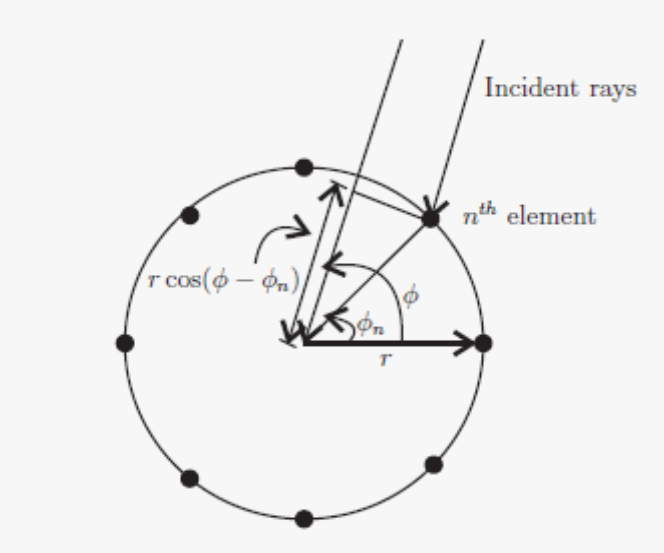

Figure 4.6: Circular antenna array

And then the data model can be written as [30]:

$$\boldsymbol{X} = \boldsymbol{AS} + \boldsymbol{N} \tag{4.28}$$

$$\begin{bmatrix} \boldsymbol{x_1} \\ \boldsymbol{x_2} \\ \vdots \\ \boldsymbol{x_M} \end{bmatrix}_{\boldsymbol{M\times N}} = [\boldsymbol{a(\theta_1)}\ \boldsymbol{a(\theta_2)} \dots\ \boldsymbol{a(\theta_{L_p})}]_{\boldsymbol{M\times L_p}} \times \begin{bmatrix} \boldsymbol{s_1} \\ \boldsymbol{s_2} \\ \vdots \\ \boldsymbol{s_{L_p}} \end{bmatrix}_{\boldsymbol{L_p\times N}} + \begin{bmatrix} \boldsymbol{n_1} \\ \boldsymbol{n_2} \\ \vdots \\ \boldsymbol{n_M} \end{bmatrix}_{\boldsymbol{M\times N}} \tag{4.29}$$

where the vector $\boldsymbol{x_m}$ is the channel frequency response of received signal on m^{th} antenna element, the vector $\boldsymbol{a(\theta_i)}$ is the antenna manifold directed to i^{th} multipath component's arrival angle and the vector $\boldsymbol{s_i}$ and $\boldsymbol{n_m}$ represent i^{th} multipath component and the added noise at m^{th} antenna element, respectively. Then the MUSIC algorithm can be described in the following three main steps [30]:

Step 1: building the autocorrelation matrix $\widehat{\boldsymbol{R}}_{\boldsymbol{xx}} = \frac{1}{N}\boldsymbol{XX^H}$

Step2: building antenna array manifold $\boldsymbol{a(\theta)} = \begin{bmatrix} exp(j2\pi\Delta cos(\theta - \phi_1)) \\ \vdots \\ exp(j2\pi\Delta cos(\theta - \phi_m)) \\ \vdots \\ exp(j2\pi\Delta cos(\theta - \phi_M)) \end{bmatrix}$

Step3: searching θ for whole azimuth angular intervals to find L_p highest local maxima of cost function $\boldsymbol{J_{music}(\theta)} = \frac{\boldsymbol{a(\theta)^H a(\theta)}}{\boldsymbol{a(\theta)^H \widehat{U}_n \widehat{U}_n^H a(\theta)}}$ (4.30)

where $\widehat{\boldsymbol{U}}_{\boldsymbol{n}}$ is the noise subspace. The angle of each local maxima is the related multipath component's azimuth angle of arrival

- **Wideband MUSIC DoA Estimation Method**

The MUSIC DoA estimation algorithm introduced above is applied for narrowband signal ($BW \lesssim 0.1f_c$). But it cannot be directly utilized for wideband signal, since the antenna array manifold is relative to signal's frequency/wavelength, seen in (4.27) and for wideband signal ($f \in F = [f_c - BW/2, f_c + BW/2]$), we cannot directly approximate any frequency f in the wideband is equal to the centre frequency f_c. Therefore, the antenna manifold will be different for different frequency f, which produces errors in MUSIC DoA estimations for wideband signals. According to this problem, in [66], [67] and [68], they introduced several frequency focusing methods, such as Incoherent Average, Steered Covariance Matrix (STCM) and Array Manifold Interpolation (AMI) to modify the autocorrelation matrix $\boldsymbol{R_{XX}}$ that the M (the number of narrowband frequency components) autocorrelation matrixes can be combined into one focused one at centre frequency f_c and then apply the narrowband MUSIC algorithm for DoA estimation.

However, in [68], the narrowband signal definition is $BW \lesssim 0.1f_c$. For our case, although the signal bandwidth is 100 MHz, the signal centre frequency is between 1 and 4 GHz. Therefore, the used signal still satisfies the narrowband definition and the MUSIC algorithm can be used directly. The related algorithm testing is showed in the following section.

- **Joint DoA and ToA estimation**

As discussed in the above two sections, the MUSIC algorithm can be applied on ToA and DoA estimation, separately. However, there is no direct pairing between each angle and delay, which means we can't know each multipath component's related arrival angle and time delay directly. Since the correlation matrix $\widehat{\boldsymbol{R}}_{\boldsymbol{xx}}$ contains both delay and angle information. Therefore, through some matrix transforming, MUSIC can implement double searching on both time domain and angular domain, which can estimate both multipath components' time delays and arrival angles simultaneously [46].

For the m^{th} antenna element, the received channel impulse response can be written as:

$$h_m(\tau) = \sum_{k=0}^{L_p-1} a_{m,k}\delta\left(\tau - \tau_k - \tau_{m,k}\right), for\ n \in (1,2 \dots M) \tag{4.31}$$

Seeing above formula, the channel impulse response contains both multipath delay information τ_k and multipath arrival angle information $\tau_{m,k}$. Therefore, through combing the ToA and DoA correlation matrixes discussed in the above two section, a modified correlation matrix can be build and the matrix contains both delay or angle information, $\{(a_i, \tau_i)\}$. And then JADE algorithm can be implemented on it to realize both DoA and ToA estimations simultaneously [46].

The antenna array is assumed as a circular array consisting of *M* omni-directional antennas with circular array radius r [46].

$$\boldsymbol{H} = \boldsymbol{AS} \tag{4.32}$$

where $\boldsymbol{A} = \boldsymbol{A_\theta}$

$$\boldsymbol{A_\theta} = \begin{bmatrix} \theta_{1,1} & \dots & \theta_{L_{p,1}} \\ \theta_{1,2} & \ddots & \theta_{L_{p,2}} \\ \vdots & & \vdots \\ \theta_{1,M} & \dots & \theta_{L_{p,M}} \end{bmatrix} \tag{4.33}$$

where

$$\theta_{i,m} = exp\left(j2\pi \frac{r * cos(\theta_i - \phi_m)}{\lambda}\right) = \exp\left(j2\pi \Delta cos(\theta_i - \phi_m)\right) \tag{4.34}$$

and

$$\boldsymbol{\Theta} = diag\left[\theta_1 \dots \theta_{L_p}\right] \tag{4.35}$$

In analogy, we can define (for some *K*)

$$\boldsymbol{\Phi} = diag\left[\psi_1 \dots \psi_{L_p}\right] \tag{4.36}$$

$$\boldsymbol{A_\psi} = \begin{bmatrix} 1 & \dots & 1 \\ \psi_1 & \ddots & \psi_{L_p} \\ \vdots & & \vdots \\ \psi_1^{K-1} & \dots & \psi_{L_p}^{K-1} \end{bmatrix} \tag{4.37}$$

where

$$\psi_i = exp(j2\pi \Delta f \tau_i) \tag{4.38}$$

Because that there is only one snapshot for each antenna element. From $\boldsymbol{H}$, we can construct a Hankel matrix $\boldsymbol{\mathcal{H}}$ by left shifting and stacking *K* copies of $\boldsymbol{H}$. In particular, for $1 \leq i \leq K$, define the left-shifted matrix $\bar{\boldsymbol{H}}^{(i)} := \bar{\boldsymbol{H}}_{\blacksquare, i \dots \boldsymbol{L-1+i}}$. (The notation $\blacksquare, i \dots j$ indicates taking columns i through j of a matrix.) Then, we can define $\boldsymbol{\mathcal{H}}$ by

$$\boldsymbol{\mathcal{H}} = \begin{bmatrix} \bar{\boldsymbol{H}}^{(1)} \\ \vdots \\ \bar{\boldsymbol{H}}^{(K)} \end{bmatrix}_{(\boldsymbol{KM \times L})} \tag{4.39}$$

The motivation for this step is $\boldsymbol{\mathcal{H}}$ has a factorization as:

$$\boldsymbol{\mathcal{H}} = \boldsymbol{BS} \tag{4.40}$$

$$\boldsymbol{B} = \begin{bmatrix} \boldsymbol{A_\theta} \\ \boldsymbol{A_\theta \Phi} \\ \vdots \\ \boldsymbol{A_\theta \Phi^{K-1}} \end{bmatrix} \tag{4.41}$$

Hence, if the parameter K is selected to be large enough, such that both $KM \geq L_p$ and $L \geq L_p$ and if all factors are full rank, then $\boldsymbol{\mathcal{H}}$ has rank L_p, which means we can estimate $\boldsymbol{B}$ up to an $L_p \times L_p$ factor at the right. Then MUSIC JADE algorithm is applied to estimate both DOA and TOA of received signals.

The MUSIC JADE algorithm can be described into following four steps [46]:

Step1: build correlation matrix: $\widehat{\boldsymbol{R}}_{\boldsymbol{xx}} = \frac{1}{M}\boldsymbol{\mathcal{H}}\boldsymbol{\mathcal{H}}^{\boldsymbol{H}}$

Step2: build antenna array manifold

$$\boldsymbol{b}(\boldsymbol{\theta_i}, \boldsymbol{\tau_i})_{KM\times 1} = [\boldsymbol{a_i} \quad \psi_i \boldsymbol{a_i} \quad \ldots \quad \psi_i^{K-1}\boldsymbol{a_i}]^T \tag{4.42}$$

where

$\boldsymbol{a_i} = [exp(j2\pi\Delta cos(\theta_i - \phi_1)) \quad exp(j2\pi\Delta cos(\theta_i - \phi_2)) \quad \ldots \quad exp(j2\pi\Delta cos(\theta_i - \phi_M))]$

Step3: build JADE cost function: $\boldsymbol{J_{music}}(\boldsymbol{\theta_i}, \boldsymbol{\tau_i}) = \frac{\boldsymbol{b}(\boldsymbol{\theta_i},\boldsymbol{\tau_i})\widehat{\boldsymbol{U}}_{\boldsymbol{n}}\widehat{\boldsymbol{U}}_{\boldsymbol{n}}^{\boldsymbol{H}}\boldsymbol{b}(\boldsymbol{\theta_i},\boldsymbol{\tau_i})}{\boldsymbol{b}(\boldsymbol{\theta_i},\boldsymbol{\tau_i})^{\boldsymbol{H}}\boldsymbol{b}(\boldsymbol{\theta_i},\boldsymbol{\tau_i})}$

Step4: find the peaks on the 3D plotted figure and each peak's coordinate value on the time and angle axis indicate each multipath component's time delay and arrival angle, respectively.

In this section, the MUSIC JADE algorithm is tested on a real channel measurement data, which is measured in a lab room with LOS scenario. The data is collected from a circular antenna array with radius of 0.05 m and there is one element on the centre of the antenna array and four elements on the circular with 90 deg spacing. The real LOS path's time delay and its azimuth angle of arrival can be known by using both Tx and Rx antennas' coordinates to calculate, which is about 82 ns and 69 degree, respectively. After digital filtering, the received signal has 100 MHz bandwidth from 1.5 to 1.6 GHz. The centre element's channel impulse response is showed in Figure 4.7 by using IFT method.

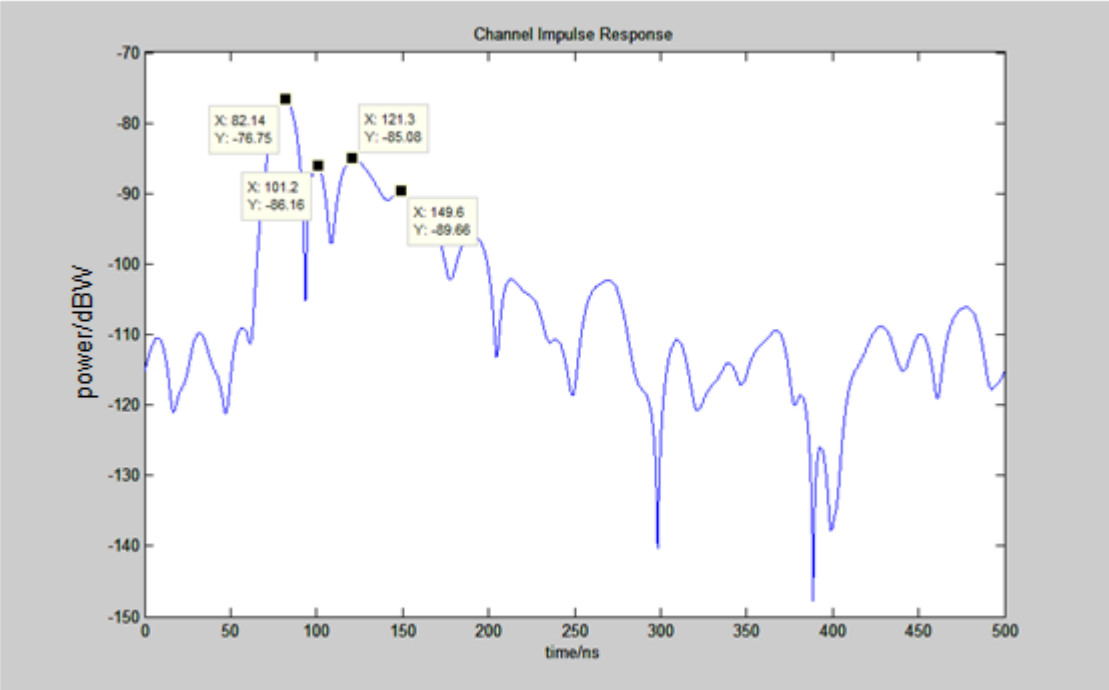

Figure 4.7: Channel impulse response of centre element

MUSIC JADE algorithm is implemented on this measured data and the estimation result is showed in Figure 4.8. Through peak detection on the 3 D estimation graph, seven multipath components are estimated and the related DoAs and ToAs are showed in Table 4.1. Through reading Figure 4.8, we can find the LOS path is coming around 82 ns with an arrival angle of 68 degree, which matches the real LOS path's both ToA and DoA very well, with only 1 degree angle error. Furthermore, since the signal bandwidth is 100 MHz, the time resolution is 10 ns. From the result shown in Table 4.1, we can find MUSIC JADE algorithm estimates three paths with different arrival angles between 104 ns and 114 ns (10 ns is the time resolution), which proves MUSIC JADE's high resolution on both ToA and DoA estimations and it increase the channel resolution that the extra angle dimension can separate multipath components which are irresoluble by only according to the time domain of using MD method. Furthermore, the angle information makes the 3D spatial channel modeling become possible and also help us have further understanding of the wireless channel propagation and therefore design better communication systems.

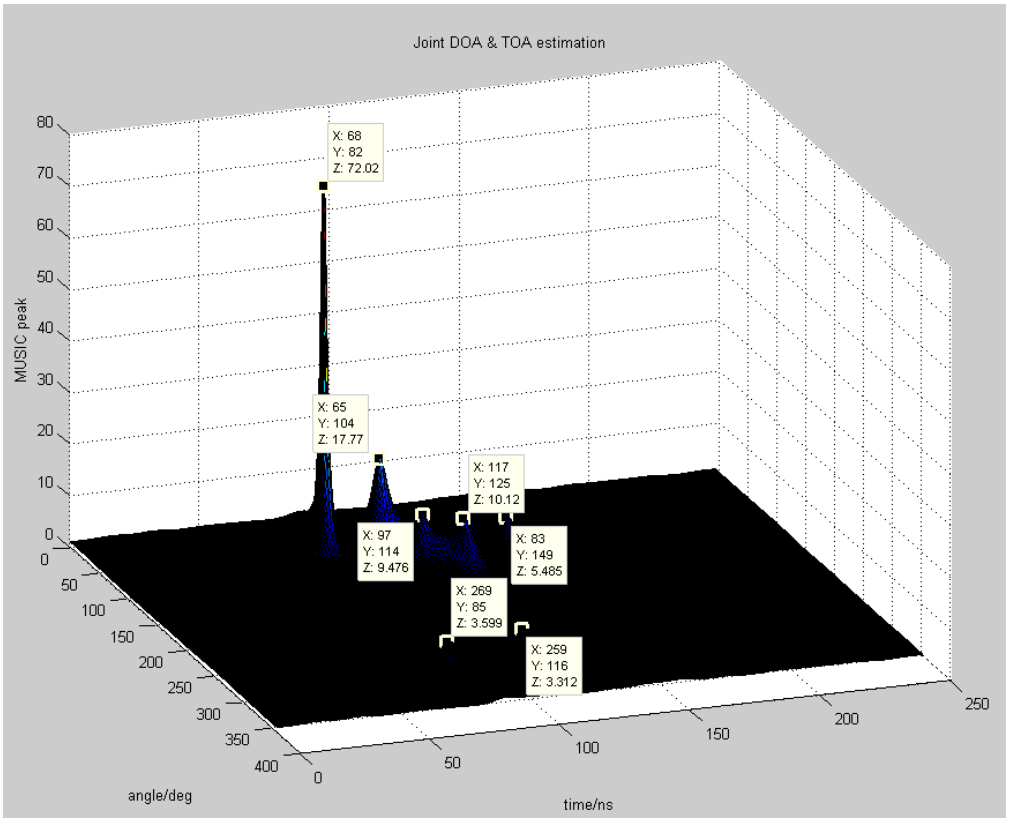

Figure 4.8: MUSIC JADE estimation result

Table 4.1 Estimated multipath components

MUSIC JADE estimation result		
Multipath	**Time delay (ns)**	**Arrival angle (deg)**
1	82	68
2	85	269
3	104	65
4	114	97
5	116	259
6	125	117
7	149	83

4-3 Modeling of Wideband Channel Parameters

4-3-1 Modeling of Multipath Amplitude Fading

Small-scale fading refers to the dramatic changes in signal amplitude and phase that can be experienced as a result of small changes (as small as half wavelength) in the spatial position of transmitter and/or receiver. Small-scale fading really influences the

wireless communication quality.

According to [1] and [2], the way to model fading is studying its statistical distribution. Since for wideband signals, the resolution is high that multipath components can be separated on the time delay profile. Therefore using either maximum detection (MD) or discrete channel impulse response (D-CIR) introduced in the above section is applicable to decide the multipath component's amplitude or power.

The statistical distribution of fading can be extracted from a group of measurement data within small-scale area. Therefore, all the measurement positions should be close and the distance of the measuring antenna shifting from one position to the next should be very small (less than half wavelength). The reason of only measuring the signal in small area is to exclude the effects from pathloss and shadowing. The size of the data pool for calculating the fading distribution is the larger the better, which is determined as 72 for our case. And then the K-S test can be utilized to find the best matched statistical fading distribution to the amplitude fading data.

4-3-2 Modeling of Multipath *RMS* Delay Spread (RDS)

As discussed in Chapter 2, RDS is an important channel parameter, which decides the coherence bandwidth of the channel. In [42], the author shows that the coherence bandwidth is in general inversely proportional to RDS. If the signal's bandwidth is smaller than the coherence bandwidth, the channel experiences frequency flat fading, otherwise, the channel experiences frequency selective fading. For example, in OFDM system, the larger delay spread means smaller coherence bandwidth and therefore the better performance, since the possibility of a large number of subcarriers being deeply faded at the same time becomes lower [57] [43]. However, when the RDS becomes so large that the maximum multipath delay exceeds the cyclic prefix (CP) duration, the communication system's performance suddenly degrades seriously since the excessive delay introduces inter-symbol interference (ISI).

The definition of RDS is given in (2.23) and in order to determine the RDS of each channel, the multipath components' amplitudes and time delays should be firstly estimated. For wideband channel, since the relative high resolution in time domain, the RDS estimation is usually based on MD or D-CIR channel model. For the MD model, each multipath component's amplitude and time of arrival is derived from each local maxima. And for D-CIR model, the amplitude and time of arrival are

calculated from each time bin's averaged amplitude and centre time delay.

4-3-3 Modeling of Multipath Angular Spread (AS)

The AS of a radio channel, denoted as Λ, is caused by different angles of arrival (AoAs) or angles of departure (AoDs) of multipath propagation. Similar to how RDS determines the coherence bandwidth, AS determines the coherence distance in the spatial domain [42] and it indicates that the larger the AS is, the smaller the coherence distance of the antenna array is. Here the coherence distance is defined as the maximum spatial separation between MIMO antenna elements over which the channel response can be assumed correlated. The coherence distance and the antenna spacing jointly determine the spatial correlation between the channel elements. When the antenna spacing is larger than the coherence distance, the spatial correlation between the two channel elements is relatively small and thus spatial diversity is obtained. In general, the more spatial diversity, the better the performance of the MIMO system is. Spatial correlation among MIMO channel elements is reduced by objects in the propagation environments that scatter the radio signal, such as rough building surfaces, vegetation, lampposts and etc. The wideness of AoAs or AoDs is proportional to the richness of scattering and it can be characterized in terms of AS. Thus AS is a key channel modeling parameter to characterize the spatial behavior of a channel environment. A larger AS generally leads to better MIMO system performance [58]. Furthermore, knowing the arrival multipath signals' angles can increase the received signal power of the antenna array system. Since after scanning the whole angular domain, the digital beamforming technology can build the antenna manifold of shifting the antenna main beams to direct to these several strong arrival signals, the summation of these signals coming at different angles largely increase the system's performance.

The definition of AS is given by (2.30), (2.31) or (2.32). For wideband channel, the digital beamforming can be applied on antenna array to estimate the multipath DoAs. According to each multipath component's power and angle of arrival, the AS for each location can be calculated. Because the channel measurements are performed at different locations and scenarios, we can estimate the AS for each position and then statistically study the AS for the indoor scenarios, which is an important indicator to determine the MIMO system's capacity.

In this thesis project, the MUSIC DoA algorithm is chosen and applied on circular antenna array to study AS.

4-4 Summary

In this chapter, the spatial modeling of wideband channel was discussed. Methods to estimate the channel parameters, such as multipath component's amplitude fading, ToA and DoA, were given. Furthermore, the modeling of the fading, RDS and AS was provided. These will be applied on the frequency dependency studies of wireless channel in Chapter 5.

Chapter 5

Frequency Dependency Study Of Wireless Channel

The free space pathloss is proportional to the square of the transmitting signal's carrier frequency and also the channel propagation mechanisms such as diffraction, scattering, are also having close relationship to the frequency as discussed in Chapter 2. Furthermore, the signal bandwidth determines its time resolution. Therefore, the frequency dependency including both centre frequency and bandwidth would influence the shape of channel impulse response and finally determine the performance of communication systems. In order to make the developed channel model match the real channel, the frequency dependency factor should be considered into the channel modeling. Thus, in this chapter, we study the effects of frequency dependency on the channel modeling.

At beginning of this chapter, an introduction to channel frequency dependency study is given. In the second section, a power fading margin model in frequency domain is given and followed by a discussion of the bandwidth effect on the power fading. Through analyzing the measured data, the frequency correlation of the power fading is also studied. In the third section, we continue to discuss the bandwidth's influence on *rms* delay spread (RDS) model derived by both Discrete Channel Impulse Response (D-CIR) method and Maximum Detection (MD) method. Through comparison of these two methods, it can be concluded that for narrowband channel, it is better to use D-CIR method rather than MD method to calculate the RDS, since the MD model gives large errors on RDS for such case. In the fourth section, a frequency dependent channel model is given. Through analyzing the measured data in four

different frequency bands, we study the frequency dependency of the channel parameters, such as multipath amplitude fading, *rms* delay spread and azimuth angular spread. Finally, the related issue discussions and future work suggestions are given at the end of this chapter.

5-1 Introduction to Frequency Dependency Study

5-1-1 Principle of Wireless Channel Frequency Dependency

Multipath propagation is the main challenge for the wideband wireless communication system. The received signal usually arrives via different multipath due to direct transmission, reflection, diffraction and scattering. As we know, the wireless channel propagation mechanisms are frequency dependent and therefore the wireless channel is also frequency dependent. In [59]-[61], the authors incorporate the multipath frequency dependency into the channel model and study insight into the frequency effects on individual multipath signals although such frequency dependence produces a relatively small impact on the channel frequency response function. However, for wireless communication systems, it is not just the channel frequency response provides important information for system design. The information of individual path signals, such as the path delay for RAKE receiver and the AoA for smart antenna, is also significant for wideband wireless system. This motivates the deeper study of multipath signals.

According to [1], [2], [6] and [7], most of the channel models are developed only for one individual frequency band. These channel models do not consider the frequency dependency effects on different signal propagation mechanisms and therefore the developed model would have mismatches or errors compared to the real wireless channel. However, a frequency dependent channel frequency response model is proposed in [61]. For this new model, a frequency dependency component $(\frac{w}{w_0})^{\beta_l}$ is added into the modeling, where w_0 and β_l are the lowest angular frequency and frequency dependency factor, respectively. The frequency dependency factor β_l has different value for different signal propagation scenario, such as -0.5 for signal diffracted by edge, +1 for signal diffracted by broadside of cylinder and etc. This research quantitatively reveals the frequency effects on each individual multipath. Furthermore, the signal bandwidth determines the time resolution and hence it influences the shape of the received signal. In Chapter 2, it is shown that the channel modeling for wideband channel is different than narrowband channel, since the wireless channel modeling is serious affected by the signal bandwidth.

5-1-2 Meaning of Channel Frequency Dependency Study

Understanding the frequency dependency of wireless channels is important for designing future communication system. Because the available frequency bands are limited, they are fully occupied by different types of wireless communication applications, such as GSM, WiFi, UMTS and etc. If different communication systems use the same frequency band, there will be serious interference among these communication systems when they are working simultaneously. If considering the frequency influence on channel modeling, it incurs the doubts like, can we directly apply the developed channel model of known frequency band (such as GSM band) on new frequency band (such as LTE band)? Is there any frequency correlation among these different frequency bands? Or if the frequency correlations are known, can we utilize it to deduce the new frequency band's channel model by only modifying the channel model of known frequency bands without complex channel modeling work? Furthermore, the frequency diversity technologies, such as Multiband OFDM, cognitive frequency hopping, are promising choice for next generation communication systems and the transmitted data on different sub-carriers (sub-frequency band) experience different channel responses. Therefore, knowing the channel characteristic in each individual frequency sub-carrier and also obtaining their frequency correlations are significant and helpful for designing such systems.

Besides considering the centre frequency effect on channel modeling, the signal bandwidth influence should also be noticed. Since the signal bandwidth would determines the channel time resolution and hence affects the accuracy of the developed channel models. Therefore, studying the bandwidth effect on channel modeling is helpful for us to choose the best matched channel modeling method for different bandwidth situation.

Therefore, to answer all these questions or solve the issues mentioned above attracts our interests on studying the frequency dependency of wireless channel. Finding the frequency correlations among each frequency bands and also developing a frequency dependent channel model can simplify our future channel modeling works at different frequency bands.

5-1-3 Method of Investigating Frequency Dependency

Because the purpose of this project is to study the frequency dependency of wireless channel, the wireless channels of different frequency bands will be investigated and compared. The UWB measurement system provides us a very convenient way to

study wireless channels in different frequency bands. When the UWB signal is transmitted through the channel, the wireless channel with frequency from 0.1 GHz to 4 GHz is excited by such signal. Therefore, the received signal covers a large frequency bands' wireless channel information. In order to study the frequency dependency of wireless channel, we can consider such UWB as a series of adjacent small wideband bins and then utilize the digital filtering method of adding window function, such as Hanning window, on the UWB frequency spectrum to only select out the interested frequency bands for studies, which is shown in Figure 5.1. Through adding the window on several different frequency bands, the wireless channel information of different frequency bands will be known. Finally, the frequency dependency of wireless channel can be studied by comparing the characteristics of these wireless channels in different frequency bands. The advantage of this method is its convenience and efficiency. We only need to transmit the UWB signal and measure the wireless channel once, all several wideband channel information can be collected. However, if we use wideband measurement system, the channel measurement should be delivered separately for each frequency band, which requires several channel measurements at the same measuring position and also the measuring environment may change during these several different frequency bands' channel measurements. Therefore, the wireless channel may vary for different time.

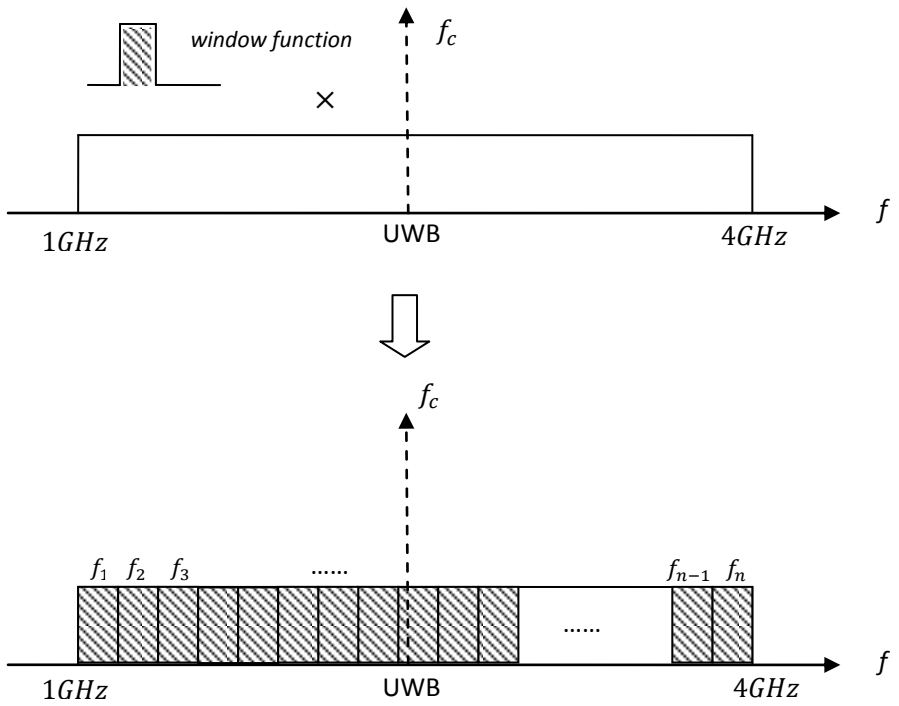

Figure 5.1: The method to investigate the frequency dependency study: before digital filtering (up) and after digital filtering (down)

5-2 Frequency Dependency of Power Fading

In wireless communications, fading is the attenuation of the power that a carrier-modulated signal experiences over certain propagation media. The fading may vary with time, geographical position and/or radio frequency, and is often modulated as random process. In wireless systems, fading can be generally classified by movements scale. Here, we focus on small-scale fading due to the multipath propagation. The presence of reflectors in environment surrounding the transmitter and receiver create multiple paths. However, the amplitude, phase, time delay for each multipath component is different. Therefore, the superposition of all these multipath components can result in either constructive or destructive interference on signal power at the receiver. Strong destructive interference is frequently referred as a deep fade and may result in temporary failure of communication due to a severe drop of the signal-to-noise ratio (SNR).

5-2-1 Power Fading Margin Model

The received signal's power spectrum is not flat in the frequency domain. Due to the small scale fading phenomenon, the received power is attenuated at some frequencies, but also amplified at other frequencies. Such phenomenon is called frequency selective fading. Therefore, in this section, how frequency bandwidth influences the power fading phenomenon is studied and to investigate this effect, the power fading margin parameter γ_{FM} is defined as [5]:

$$\gamma_{FM}=\frac{\gamma_{FM_m}}{\overline{\gamma_{FM}}} \tag{5.1}$$

where

$$\gamma_{FM_m} = \int_{fc-\frac{B_w}{2}}^{fc+\frac{B_w}{2}} |R_m(f)|^2 df \tag{5.2}$$

is the fading margin at location m within the circular antenna grid, $\overline{\gamma_{FM}}$ is the fading margin averaged over all grid elements, $R_m(f)$ is the Fourier Transform (FT) of the received signal $r_m(t)$ and B_w and f_c are the bandwidth and the center frequency, respectively. This parameter gives a measure of robustness of a signal against small-scale fading. The fading margin in our case is normalized to the mean value of all measured grid elements in order to combine all data collected in different positions as the effects of pathloss and shadowing are excluded. The fading margin can be considered as observations in a stochastic process.

Figure 5.2 shows the (Cumulative Density Function) CDFs of the fading margin with different bandwidths for both LOS and NLOS scenario. From these figures it can be observed that for both LOS and NLOS scenario, the fading margin increases when the bandwidth is decreasing, For example the fading margin at LOS scenario is about 18.8 dB and 2.9 dB for a bandwidth of 10 MHz and 2 GHz, respectively. The results also indicate that the variation in the fading margin with a bandwidths of 1 GHz and higher is almost the same which means that a bandwidth of 1 GHz is enough to receive all power and hence mitigate the multipath fading effect for such indoor environment. Moreover, Figure 5.2 shows a similar significant increment of robustness observed for both LOS and NLOS scenario when the bandwidth is increasing and it means that no matter for LOS or NLOS scenario, the multipath components contribute remarkably to the fading margin.

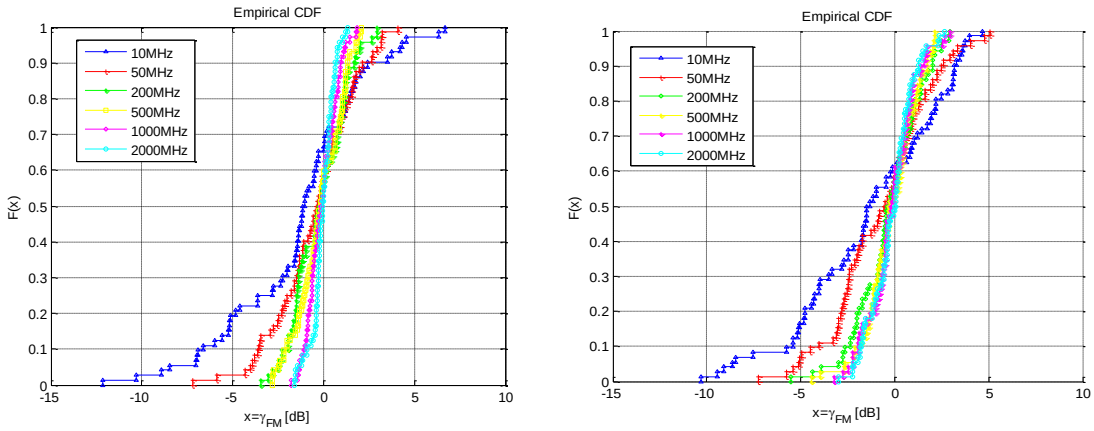

Figure 5.2: *CDF* of the fading margin γ_{FM} for LOS scenario (left) and NLOS scenario (right) at EWI power lab with Tx and Rx distance 18m

The statistics of the fading margin using different bandwidth for LOS and NLOS scenario are given in Table 5.1 and Table 5.2. From the tables, we can observe that when the bandwidth is increasing, both the maximum fading difference and fading standard deviation are decreasing. The reason why it has such trend is that the fading phenomenon is not happened in all frequency simultaneously. At some frequency, the multipath may have destructive effects which will attenuate the signal power, but at other frequency, the multipath may has constructive effects which will amplify the signal power. Therefore, when the bandwidth is increased, the signal will cover more frequencies and then there will be more chance that the received power at constructive frequencies can compensate it at destructive frequencies. This can lead to the decrease of the fading phenomenon and therefore the received power will be less

influenced by fading.

Table 5.1: Fading margin statistics for LOS scenario

B_w [MHz]	Min(γ_{FM}) [dB]	Max(γ_{FM}) [dB]	Std.(γ_{FM}) [dB]
10MHz	-12.1574	6.6896	6.6963
50MHz	-7.1829	4.0909	2.2378
200MHz	-3.4341	2.9446	1.4854
500MHz	-2.8397	2.1078	1.2830
1000MHz	-1.7904	1.8620	0.8070
2000MHz	-1.6300	1.3267	0.6198

Table 5.2: Fading margin statistics for NLOS scenario

B_w [MHz]	Min(γ_{FM}) [dB]	Max(γ_{FM}) [dB]	Std.(γ_{FM}) [dB]
10MHz	-10.3035	4.6902	3.7036
50MHz	-7.2299	5.0767	2.5877
200MHz	-5.5155	2.9148	1.7275
500MHz	-4.4532	2.1422	1.4036
1000MHz	-3.2242	2.9701	1.2786
2000MHz	-2.9690	2.6612	1.1623

Furthermore, to model the fading margin the distribution of its amplitude $\sqrt{\gamma_{\mathrm{FM}}}$ is tested for all used bandwidths. The result shows that the Nakagami distribution gives the best fit to all measured data as can be seen from Figure 5.3. Through using the least square method, the parameters of the Nakagami distribution are estimated for each signal bandwidth. The corresponding estimates are given in Table 5.3 and Table 5.4 for LOS and NLOS scenario, respectively.

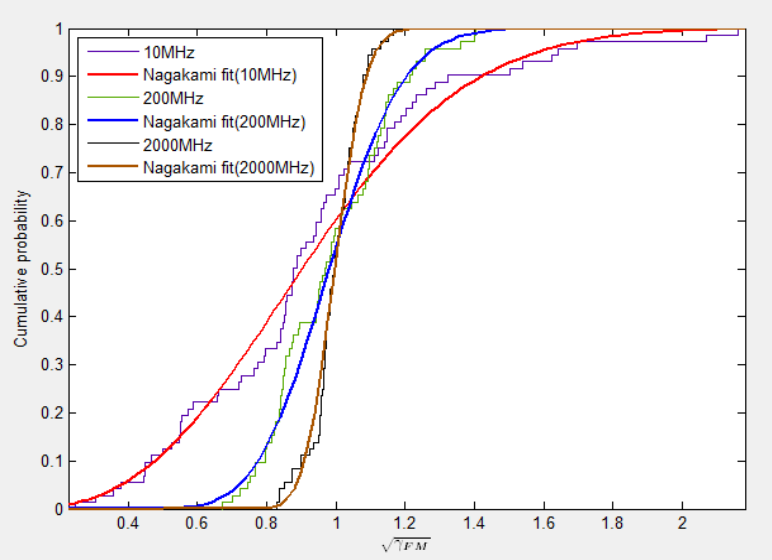

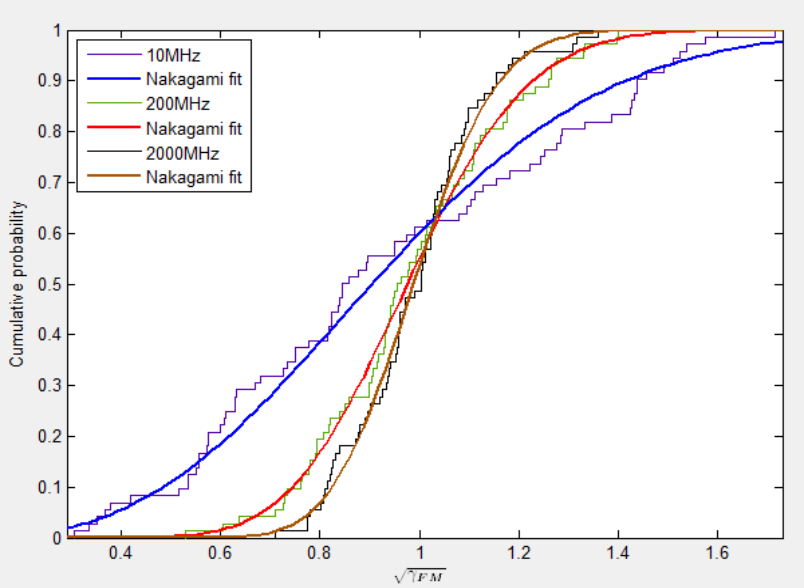

Figure 5.3: CDF of the square root of fading margin $\sqrt{\gamma_{FM}}$ for LOS scenario (up) and NLOS scenario (down) at EWI power lab with Tx and Rx distance 18m

Table 5.3: Estimated Nakagami fit parameters for LOS scenario

Nakagami fit	10MHz	50MHz	200MHz	500MHz	1000MHz	2000MHz
μ	1.72229	4.23752	8.8164	12.1205	29.156	51.0197
Ω	1	1	1	1	1	1

Table 5.4: Estimated Nakagami fit parameters for NLOS scenario

Nakagami fit	10MHz	50MHz	200MHz	500MHz	1000MHz	2000MHz
μ	1.77033	3.07106	6.92932	10.3925	11.8493	14.3671
Ω	1	1	1	1	1	1

5-2-2 Frequency Dependency Study On Power Fading

Continuing the fading margin model, in order to study the frequency dependency on small-scale fading, the same fading model is statistically studied on several different frequency bands. The statistics of small-scale fading, such as standard deviation, maximum fading difference, are compared among different frequency bands. Such method is explained before.

The general process steps:

Step1: Selecting four centre frequencies f_i at 1.3 GHz, 2.0 GHz, 2.7 GHz and 3.2 GHz with bandwidth 100MHz by utilizing Hanning window to filter the UWB signal, which is shown in Figure 5.4.

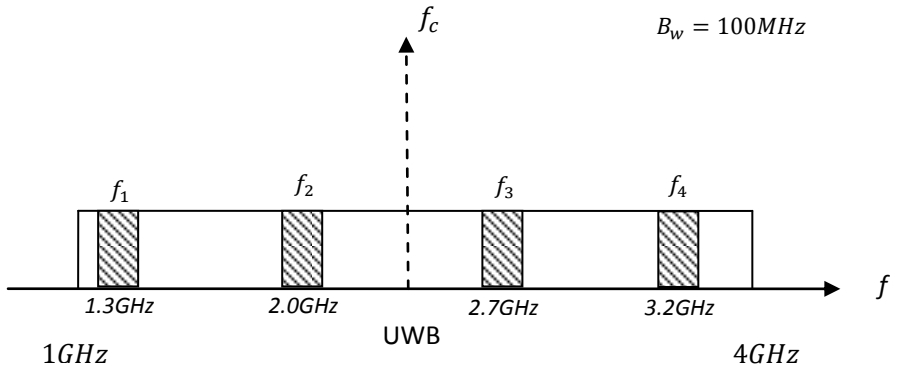

Figure 5.4: The selected four wide frequency bands

Step2: At frequency band f_i, the received power for the m^{th} antenna element can be represented as:

$$\gamma_{FM_{m,f_i}} = \int_{f_i-\frac{B_w}{2}}^{f_i+\frac{B_w}{2}} |R_m(f)|^2 df \tag{5.3}$$

where m is from 1 to 72 and $R_m(f)$ is the channel frequency response of m^{th} antenna element.

Step3: Normalizing each antenna element's received power by the average power of all 72 antenna elements, $\gamma_{FM'_{m,f_i}} = \frac{\gamma_{FM_{m,f_i}}}{\overline{\gamma_{FM_{f_i}}}}$

Step4: Calculating the standard deviation and maximum fading difference for each position at each frequency band.

The statistic studies are implemented on three different environments (power lab, school canteen and library) for both LOS and NLOS scenario. And in each environment, five positions with different Tx-Rx distance are measured. The averaged results are shown in Table 5.5. The results of the small-scale fading standard deviations and fading margin are similar for these four frequency bands, which are in the range of [0.4, 0.6] for standard deviation and [11.5, 16.6] dB for maximum fading difference at both LOS and NLOS scenarios, which means that the fading characteristics are similar in this four frequency bands. The standard deviation and fading margin at high frequency band (like around 3.2 GHz) is slightly larger than low frequency band (like around 1.3 GHz), which maybe is resulted from the frequency dependency of propagation mechanisms.

Table 5.5: Statistics studies on small scale fading under different frequency bands

Fading						
Location		*Frequency band*				
		$f_i - {}^{B_w}/_2$, $f_i + {}^{B_w}/_2$	*1.25GHz -1.35GHz* f_1	*1.95GHz -2.05GHz* f_2	*2.65GHz -2.75GHz* f_3	*3.15GHz -3.25GHz* f_4
LOS	Power lab	σ	0.3904	0.4996	0.4123	0.6352
		Max.-Min.[dB]	11.1610	11.6911	11.7769	13.2671
	Canteen	σ	0.4799	0.4397	0.4699	0.5024
		Max.-Min.[dB]	11.4203	11.4003	10.3387	15.8530
	Library	σ	0.4331	0.5201	0.5358	0.5849
		Max.-Min.[dB]	8.8471	12.7247	12.2306	13.5400
	total	$\boldsymbol{\sigma}$	**0.4345**	**0.4865**	**0.4727**	**0.5742**
		Max.-Min.[dB]	**11.4203**	**12.7247**	**12.2306**	**15.8530**
NLOS	Power lab	σ	0.3694	0.3852	0.5305	0.5642
		Max.-Min.[dB]	9.2392	9.4865	11.3502	12.9587
	Canteen	σ	0.4219	0.4456	0.4112	0.4675
		Max.-Min.[dB]	9.9278	10.1413	10.9194	11.2116
	Library	σ	0.5351	0.6389	0.7422	0.8114
		Max.-Min.[dB]	11.9956	14.5961	13.9568	16.6363
	total	$\boldsymbol{\sigma}$	**0.4221**	**0.4899**	**0.5613**	**0.6144**
		Max.-Min.[dB]	**11.9956**	**14.5961**	**13.9568**	**16.6363**

5-2-3 Frequency Correlations Studies on Power Fading

The frequency correlation on power fading is also studied for these separated four frequency bands. However the correlation coefficient seems no constant trend (sometimes, it is high, but also sometimes the value is low, which I cannot make a conclusion on the trend). The reason for this is the central frequency difference of any two frequency bands is bigger than the channel's coherence bandwidth. Therefore, we re-study the frequency correlation among neighboring frequency bands.

The starting frequency band is at [2.000, 2.100] GHz and then 20MHz per step increasing the center frequency. Therefore, the last frequency band is at [2.180, 2.280] GHz. The frequency correlations for power lab scenario are presented in the Table 5.6. And the frequency correlation tables for both canteen and library scenarios are attached in the Appendix D. The results show that, when the frequency difference is increasing, the power fading's frequency correlation becomes lower. The reason is, when the frequency difference between frequency bands is increasing, the overlapped frequency bandwidth between these two bands will be less. Therefore, the related power fading's frequency correlation will also be less. Figure 5.5 shows the frequency correlation trend when the bandwidth is increasing at the power lab Tx-5m-Rx scenario. Furthermore, The same study is also done at other frequency bands, such as from [1.20, 1.30] GHz to [1.38, 1.48] GHz. The results show that the frequency correlation has the similar trend as in Figure 5.5. The details of this statistical study are showed in the table of Appendix D.

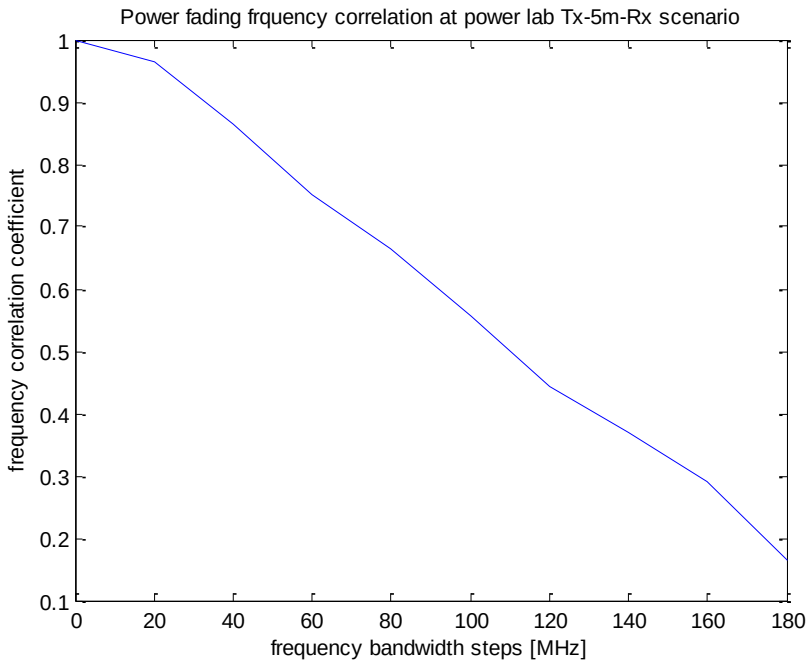

Figure 5.5: Power fading's frequency correlation at power lab Tx-5m-Rx scenario

Table 5.6: Power fading frequency correlation for power lab scenario

Power fading frequency correlation											
Location											
Power lab		$C_{1,1}$	$C_{1,2}$	$C_{1,3}$	$C_{1,4}$	$C_{1,5}$	$C_{1,6}$	$C_{1,7}$	$C_{1,8}$	$C_{1,9}$	$C_{1,10}$
LOS	23m	1.0000	0.9723	0.9267	0.8278	0.7294	0.5106	0.2440	0.0371	-0.0708	-0.0683
	18m	1.0000	0.9353	0.5820	0.3626	0.2590	0.1170	-0.0833	-0.0987	-0.1808	-0.1415
	13m	1.0000	0.8785	0.7039	0.4089	0.2698	0.2323	0.4754	0.6012	0.6094	0.6050
	8m	1.0000	0.9661	0.8475	0.7229	0.4926	0.2331	0.1084	0.0400	0.0108	-0.1001
	5m	1.0000	0.9633	0.8639	0.7518	0.6656	0.5565	0.4425	0.3693	0.2915	0.1648
NLOS	23m	1.0000	0.8557	0.6985	0.3435	0.0704	0.0262	-0.0715	-0.0732	-0.1460	-0.2155
	18m	1.0000	0.9397	0.6415	0.3038	0.1131	-0.0203	-0.0153	-0.0053	0.0300	0.1091
	13m	1.0000	0.9422	0.7080	0.4520	0.4116	0.3550	0.1740	0.0051	-0.1322	-0.1674
	8m	1.0000	0.9097	0.8150	0.6032	0.5114	0.3204	0.4134	0.4063	0.5776	0.5079
	5m	1.0000	0.9801	0.9397	0.8564	0.8547	0.8183	0.7715	0.6472	0.5892	0.4166

5-3 Bandwidth effects on *RMS* Delay Spread (RDS)

The multipath delay spread is a measure of the multipath abundance of a channel. In general, it can be interpreted as the difference between the time of arrival of the first significant multipath component (typically the line-of-sight path) and the time of arrival of the last multipath component. The time delay parameters directly affect the performance of high speed wireless systems. For instance, the mean excess delay can be used to estimate the searching range of RAKE receivers and the *rms* delay spread can be used to determine the maximum transmission data rate in the channel without equalization. The time jittering and standard deviation parameters can be used to determine the update rate for a RAKE receiver or an equalizer.

As discussed in Chapter 4, the *rms* delay spread estimation is based on Maximum Detection (MD) or Discrete Channel Impulse Response (D-CIR) model. However the estimation's accuracy really depends on the frequency bandwidth. In the following, we study the bandwidth effects on the MD or D-CIR based *rms* delay spread model.

The resolution on time domain depends on the signal bandwidth, which is equal to $1/B_w$. And the resolution on time domain will heavily influence the multipath detection by MD method and therefore make big error on the related RDS estimation. In this section, the RDS is estimated under different bandwidth for both LOS and NLOS scenario, separately. Figure 5.6 plots the CDF of normalized RDS with different bandwidth for LOS scenario and it shows that as the frequency bandwidth increases from 30 MHz, 100 MHz to 2000 MHz, the slope of the CDF curve becomes

larger and at 90% level, the related normalized RDS of 2000 MHz (1.1) is smaller than that of 30 MHz (1.4) and 100 MHz (1.3), which indicates that the estimated RDS for the measured signal samples are more close to the mean RDS value and the variance of RDS becomes smaller when the bandwidth is increasing.

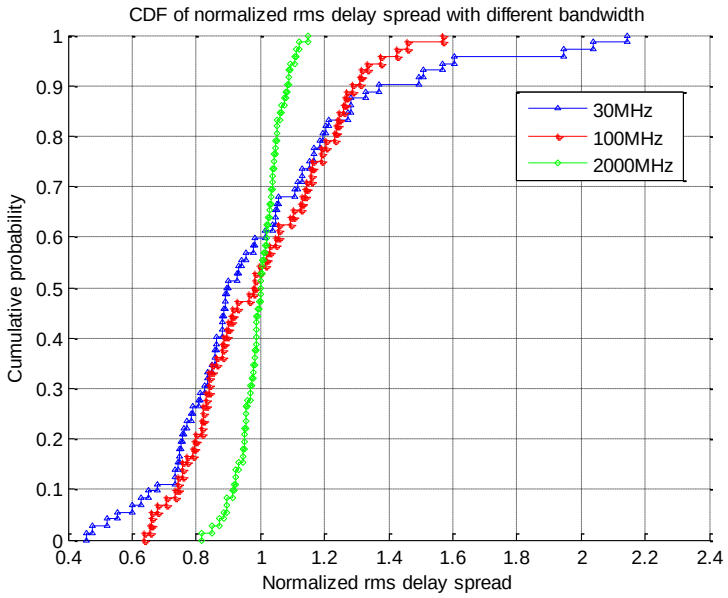

Figure 5.6: CDF of the *rms* delay spread for LOS scenario

Table 5.7 also shows the *rms* delay spread statistics for both LOS and NLOS scenarios. As the results showed in this table, for both LOS and NLOS scenario, when the bandwidth is increasing, the mean, the maximum difference (max.-min.) and the standard deviation of *rms* delay spread become smaller, simultaneously. The reason why it has such trend is when the bandwidth is decreasing; the multipath resolution on time domain becomes lower. And at narrow bandwidth case, because of the low resolution, the channel impulse response is presented as the superposition of many multipath components, which cannot be separated and lead to the amplitude fading phenomenon. Therefore, the estimated *rms* delay spread will vary intensively. For instance, Seeing Table 5.7, at 10 MHz bandwidth case, there is just one peak detected on the channel impulse response and it results in the *rms* delay spread estimation value is zero. This means the system can transmit data with infinite rate, which does not match the reality and the estimated *rms* delay spread cannot describe the wireless channel well. However, for wide bandwidth case, the multipath resolution on time domain is high that each multipath can be separated very accurately and then the amplitude fading phenomenon or multipath superposition is not obvious. In Figure 5.7 and 5.8, the channel impulse response related to maximum and minimum *rms* delay spread estimation for 20 MHz and 1000 MHz bandwidth are showed separately. Through comparisons, we can conclude that the accuracy of multipath detection is

better when the frequency bandwidth is also higher. And for narrow band channel case, the MD can make big errors on *rms* delay spread estimation. And then we also studied the bandwidth effects on D-CIR based method and we found it is more accurate to use D-CIR method rather than MD method, when it is narrowband channel ($B_w \leq$ 10 MHz). Since in each time bin, the averaged signal power is represented as a multipath component's power in that time bin and therefore the situation of only one multipath detected, discussed in MD method, will not happen in D-CIR method. However, for wideband or super wide band channel, both the MD and D-CIR model have the similar *rms* delay spread estimation. The details of the D-CIR method will be discussed in following sections.

Table 5.7: *rms delay spread* statistics for both LOS and NLOS scenario

RMS delay spread						
Centre frequency: 2GHz						
location		*bandwidth* [MHz]	*mean* [ns]	*std dev.* [ns]	*min* [ns]	*max* [ns]
LOS	power lab 18m	10	50.1706	33.5167	0.0000	137.8733
		50	42.3169	9.6437	25.5316	75.4807
		200	36.1249	6.7775	25.5831	54.3016
		500	30.6192	5.7935	19.3566	44.7363
		1000	28.0141	4.0357	20.4380	36.6149
		2000	24.8657	1.6226	20.2704	28.5729
NLOS	power lab 18m	10	19.8521	27.9416	0.0000	116.4108
		50	32.3172	9.5725	13.5646	54.2102
		200	31.9964	7.6388	158206	47.0821
		500	29.2659	4.8658	19.7307	43.3720
		1000	26.5964	4.8899	17.5857	36.3700
		2000	25.5067	5.0451	14.7445	36.1562

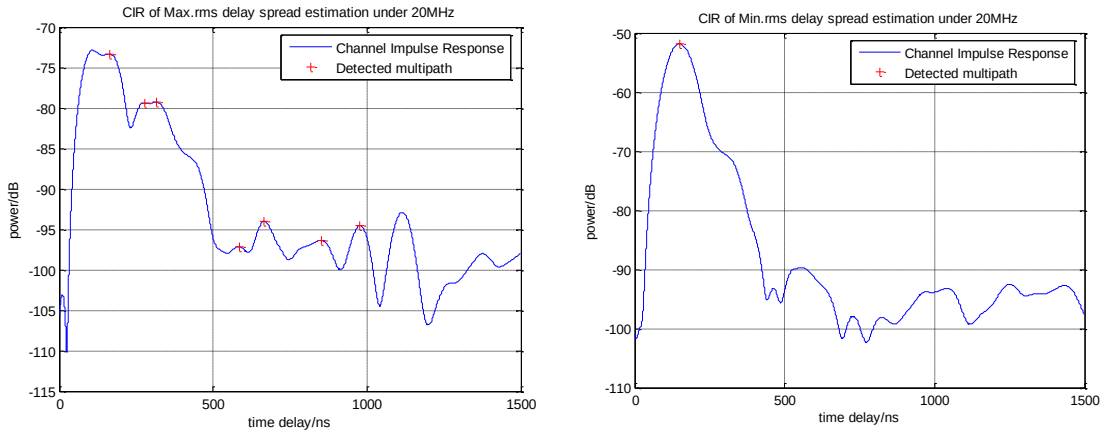

Figure 5.7: CIR related to Max. (left) & Min. (right) *rms* delay spread estimation for 20MHz bandwidth

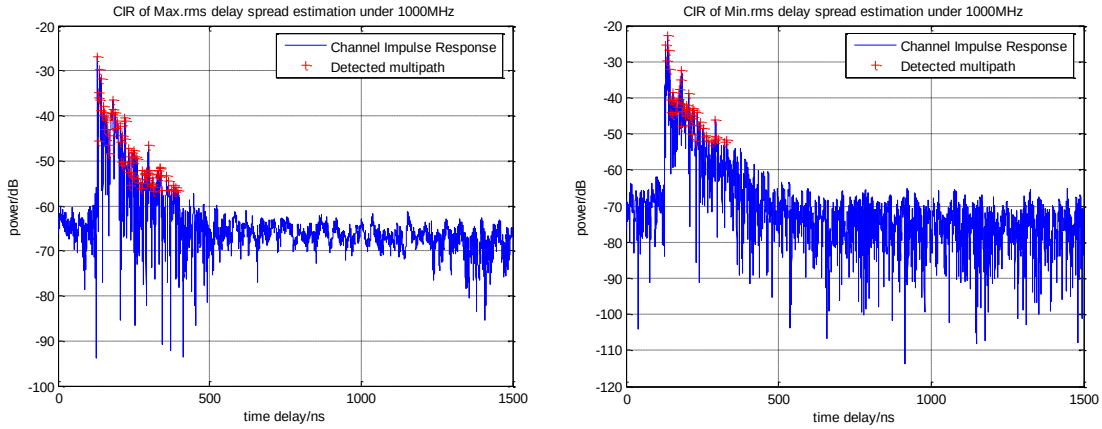

Figure 5.8: CIR related to Max. (left) & Min. (right) *rms* delay spread estimation for 1000MHz bandwidth

5-4 Frequency Dependency of Channel Parameter Modeling

5-4-1 Frequency Dependent Channel Model

As discussed at the beginning of the chapter, the wireless channel is frequency dependent. However, the channel impulse response and channel frequency response in previous researches are usually written as (4.3) and (4.4), respectively and the frequency dependencies are not considered in these two formulas. There, a new frequency dependent channel frequency response model can be expressed by taking frequency dependency factor into consideration [61] and the mathematic form can be represented in (5.4):

$$H(w) = \sum_{l=1}^{L} a_l \left(\frac{w}{w_0}\right)^{\beta_l} e^{-jw\tau_l} \tag{5.4}$$

where L indicates the total number of multipath components and $\{a_{l,}\tau_l\}$ represent the l^{th} path's amplitude and delay. And the component $\left(\frac{w}{w_0}\right)^{\beta_l}$ incorporates the frequency dependency's effect to l^{th} path. w_0 is the lowest angular frequency and β_l is the frequency dependency factor, which is different for different propagation mechanism showed in Table 5.8. However, the AoA of each multipath component is an extra dimension of explaining the multipath channel's spatial character, which is not included in the frequency dependent channel frequency response.

Table 5.8: Physical mechanism versus frequency dependence factor

Physical Mechanism	Frequency Dependence Factor β
Line of Sight	0
Reflection	0
Diffraction from smooth or flat surface	0

Diffraction by edge	-0.5
Diffraction by Corner or tip	-1
Diffraction by Axial Cylinder Face	+0.5
Diffraction by Broadside of a Cylinder	+1

The above frequency dependent model quantitatively studies the frequency effects on each individual multipath component. However, there are no many studies of frequency dependency's effects on the whole channel level and the wireless channel characteristic decides the communication systems' performance. Therefore, in the following sections, we focus on the studies of frequency dependency of channel parameters, such as amplitude fading distribution, *rms* delay spread and angular spread.

5-4-2 Frequency Dependency Studies on Amplitude Fading

The frequency dependency of amplitude fading distribution is studied in this section. To evaluate the small-scale amplitude fading statistics, the amplitudes over small-scale areas (i.e. measured over the circular grid) are used [5]. In our case, the D-CIR model is used to study the amplitude fading distribution. Thus, the whole channel impulse response is divided into time bins on time axis and then in each bin, there is a represented path, whose amplitude and time delay are the averaged amplitude and the centre time of that time bin, separately.

The frequency dependency of the amplitude fading is studied in four different frequency bands. The centre frequency of the four bands is 1.3 GHz, 2.0 GHz, 2.6 GHz and 3.2 GHz and the bandwidth is 100 MHz for these four bands. Therefore, the resolution of the channel impulse response is 10 ns. Prior to data reduction the excess delay axis was divided into small intervals of width 10 ns, called bins. Each bin contains either one component or no component. Since it is indoor scenario measurement, it was observed from the data that probability of receiving components with excess delays larger than 400 ns is negligible. The excess delay axis was therefore divided into 40 bins.

Each position contains 72 CIR profiles and there are 10 positions for each scenario. Therefore, both local and global amplitude fading distributions can be studied. For the local amplitude fading distribution, the distribution test is calculated for each 10 different positions (5 LOS and 5 NLOS in power lab scenario). Therefore at each position, there are 72 samples for each of the 40 time bins. Because the data pool is not big (72 samples), the Kolmogorov-Smirnov test (KS-test) fitting test function was

selected with confidence level of 90% to test each bin's theoretical amplitude fading distribution and the passing rates of K-S test for LOS and NLOS in power lab for different frequency bands are showed in Table 5.9, 5.10, 5.11 and 5.12.

Table 5.9: Passing rates of K-S test for local fading in power lab at [1.25, 1.35] GHz

K-S (%) for [1.25, 1.35]GHz at power lab										
Distribution	**LOS**					**NLOS**				
	5m	**8m**	**13m**	**18m**	**23m**	**5m**	**8m**	**13m**	**18m**	**23m**
Rayleigh	72.5	70	77.5	80	75	75	52.5	70	85	82.5
Rician	20	35	25	20	17.5	25	25	25	15	12.5
Lognormal	97.5	97.5	90	97.5	97.5	92.5	92.5	95	92.5	87.5
Nakagami	97.5	100	97.5	100	97.5	92.5	92.5	97.5	97.5	100
Weibull	97.5	100	97.5	100	97.5	92.5	87.5	100	97.5	100

Table 5.10: Passing rates of K-S test for local fading in power lab at [1.95, 2.05] GHz

K-S (%) for [1.95, 2.05]GHz at power lab										
Distribution	**LOS**					**NLOS**				
	5m	**8m**	**13m**	**18m**	**23m**	**5m**	**8m**	**13m**	**18m**	**23m**
Rayleigh	80	82.5	75	82.5	70	65	72.5	67.5	87.5	75
Rician	20	15	20	10	15	22.5	12.5	5	12.5	17.5
Lognormal	100	95	97.5	95	97.5	97.5	97.5	97.5	97.5	95
Nakagami	100	97.5	97.5	97.5	97.5	100	97.5	100	97.5	100
Weibull	100	100	100	100	95	100	97.5	100	100	100

Table 5.11: Passing rates of K-S test for local fading in power lab at [2.55, 2.65] GHz

K-S (%) for [2.55, 2.65]GHz at power lab										
Distribution	**LOS**					**NLOS**				
	5m	**8m**	**13m**	**18m**	**23m**	**5m**	**8m**	**13m**	**18m**	**23m**
Rayleigh	90	67.5	65	80	82.5	87.5	90	92.5	87.5	90
Rician	10	17.5	20	12.5	7.5	5	5	0	0	10
Lognormal	97.5	95	97.5	100	100	100	95	95	100	97.5
Nakagami	100	97.5	97.5	95	100	97.5	92.5	100	100	100
Weibull	100	100	97.5	97.5	100	97.5	97.5	100	100	100

Table 5.12: Passing rates of K-S test for local fading in power lab at [3.15, 3.25] GHz

K-S (%) for [3.15, 3.25]GHz at power lab										
Distribution	**LOS**					**NLOS**				
	5m	**8m**	**13m**	**18m**	**23m**	**5m**	**8m**	**13m**	**18m**	**23m**
Rayleigh	92.5	90	85	82.5	97.5	90	72.5	92.5	95	92.5
Rician	15	5	12.5	10	7.5	7.5	7.5	0	2.5	5
Lognormal	97.5	97.5	97.5	97.5	100	95	95	97.5	97.5	97.5
Nakagami	97.5	100	100	95	100	97.5	95	97.5	100	95
Weibull	97.5	100	100	100	100	97.5	97.5	97.5	100	100

Comparing the results showed in the tables, we can find that the passing rates for these five distributions are similar for all four frequency bands and in each frequency band, most of the passing rate for Rician distribution is below 15%, which is much lower than the other four distributions. It means Rician distribution is not good for modeling wideband signal amplitude fading distributions. The reason for the low passing rate is the Rican distribution assumes one of the components (a_k, θ_k) is fixed and other scatter vectors are random in amplitude and phase [2], but there are few bins containing the static strong path, such as LOS path. Furthermore, among the other four fitted fading distribution, Weibull distribution (all above 97.5%) is slightly better than Rayleigh, Lognormal and Nakagami distributions. In conclusion, for the wideband channel, no matter in what frequency band, the best distribution to describe the amplitude fading distribution is Weibull. Figure 5.9 shows the empirical normalized small-scale amplitude fading distribution at 2nd time bin and it shows that the Weibull distribution fit the data best among the three distributions. The related parameters of these three estimated distributions are showed in Table 5.13.

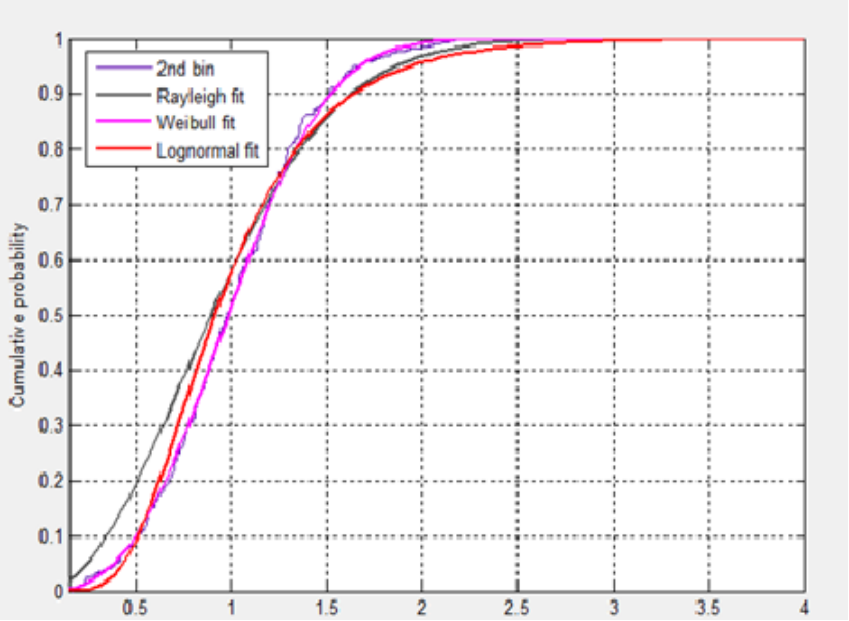

Figure 5.9: CDF of the empirical small scale amplitude fading fitted to Weibull distribution for 2nd time bin

Table 5.13: The parameters of the three estimated distributions

Rayleigh	σ	N/A
	0.758808	N/A
Lognormal	μ	σ
	-0.0897792	0.454817
Weibull	β	λ
	2.76362	1.12334

5-4-3 Frequency Dependency Studies on *RMS* Delay Spread

In this section, we focus the frequency dependency on *rms* delay spread (RDS). The RDS is statistically studied in four different frequency bands in three different scenarios by using both MD model and D-CIR model. Figure 5.10 gives the CDF of the RDS at power lab LOS scenarios. As showed in the figure, the RDS data fits the Normal distribution and the related estimated function parameter values are presented in Table 5.14. In [5], the authors found the RDS value relates to the propagation distance between Tx and Rx antennas. Usually the longer the distance, the higher the RDS value will be. However in Figure 5.10, at 90% level, the RDS of 8 m Tx-Rx distance position is larger than the RDS of 13m Tx-Rx distance position. This can be explained by the power lab environment structure. The free space at 8 m position is larger than it at 13 m position and the power machines near the 8 m position are a little further away from the received antenna array compared to the 13 m position and there is extra wall near the 8 m position, which lead to the spreader multipath distribution and therefore bigger RDS value at the 8m position.

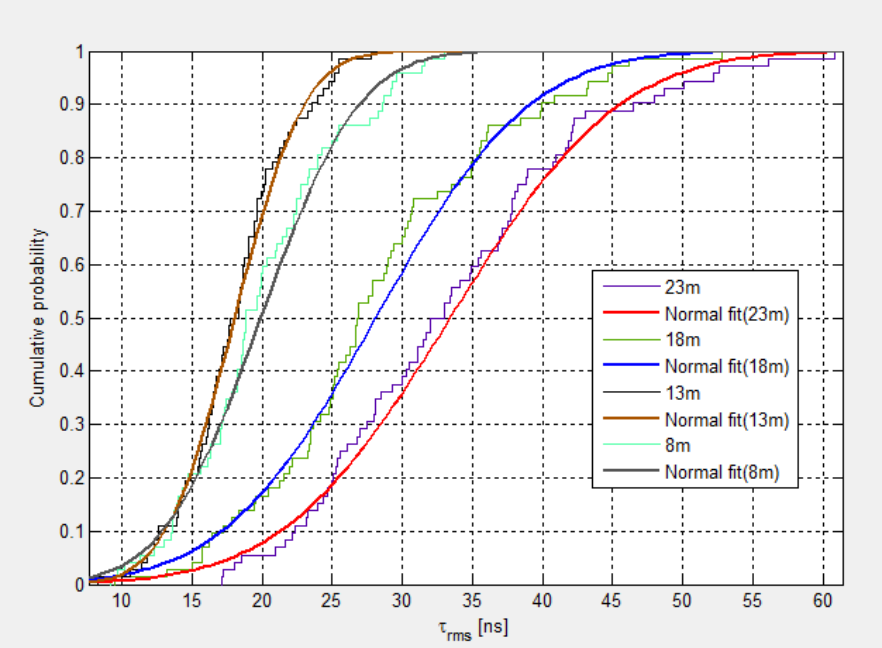

Figure 5.10: The obtained CDF of the RDS τ_{rms} for power lab LOS scenario

Table 5.14: Estimated Normal fit parameters for Power lab LOS scenario

Normal fit	23m	18m	13m	8m
μ	33.4188	28.1272	18.0492	19.91
Ω	9.4566	8.57281	3.88335	5.47661

The statistics of RDS after averaging 14 positions in three different scenarios for both LOS and NLOS case are showed in Table 5.15 (MD model) and Table 5.16 (D-CIR

model). As the results showed in tables, for all these four frequency bands, the averaged RDS for LOS case is lower than NLOS's. The reason for this issue is in our measurement, the Tx antenna is directional antenna and thus the LOS path owns much higher power than other multipath components. Therefore, the LOS path contributes much more weights than other multipath components in RDS calculation, which leads to the estimated RDS is more close to the LOS path.

Through comparing these results in tables, I found that the statistics of the RDS are similar among these four frequency bands. The reason why there is no much difference is maybe the four frequency bands are close and therefore the channel propagation mechanisms, such as scattering may express similar performance. Furthermore, since the RDS is a cumulative value which indicates how wide the multipath spread in the time domain, the frequency dependency may not show out when all multipath components' powers and time delays are combined together for RDS.

Table 5.15: The statistics of *rms* delay spread on different frequency bands (MD method)

RMS delay spread (MD model)						
			Frequency band [GHz]			
location		*Parameter*	1.25~1.35	1.95~2.05	2.55~2.65	3.15~3.25
LOS	Power lab Canteen Library	**Mean [ns]**	**21.1867**	**30.1434**	**29.8816**	**26.6525**
		Std. dev.[ns]	5.9303	9.9025	8.9733	9.4872
		Min [ns]	3.1759	4.0106	3.6414	3.4111
		Max [ns]	57.4557	94.2231	101.9284	96.3356
NLOS	Power lab Canteen Library	**Mean [ns]**	**29.2056**	**31.6208**	**37.2892**	**35.5123**
		Std. dev.[ns]	6.5619	7.4849	9.6286	8.5454
		Min [ns]	5.2364	7.6970	5.7924	6.0900
		Max [ns]	63.0298	68.1398	72.7675	73.1606

Table 5.16: The statistics of *rms* delay spread on different frequency bands (D-CIR method)

RMS delay spread (D-CIR model)						
			Frequency band [GHz]			
location		*Parameter*	1.25~1.35	1.95~2.05	2.55~2.65	3.15~3.25
LOS	Power lab Canteen Library	**Mean [ns]**	**24.7521**	**32.9415**	**32.7957**	**30.7751**
		Std. dev.[ns]	5.5494	9.2950	8.0056	8.9236
		Min [ns]	8.5011	10.9960	8.1557	8.2659
		Max [ns]	58.1712	90.2483	92.3085	75.6998
NLOS	Power lab Canteen Library	**Mean [ns]**	**31.5448**	**33.9193**	**39.3204**	**37.7018**
		Std. dev.[ns]	6.3213	6.9692	9.0370	7.8749
		Min [ns]	10.9287	11.6429	12.0187	10.9453
		Max [ns]	69.4082	67.9788	75.1483	72.2230

5-4-4 Frequency Dependency Studies on Azimuth Angular Spread

The multipath components' angle of arrival is an extra dimension to describe the wireless channel and the angular spread (AS) partly decides the MIMO system's mutual antenna spatial correlation and therefore the system capacity. And because of the scattering mechanism, the angle of reflected paths has correlation to the signal's wavelength or frequency. Thus, the AS for different frequency may express differently. In this section, the frequency dependency studies of AS is based on digital beamforming method. And the Fleury definition is used and the angular spread at power lab scenario with 10 different positions and in four different frequency bands are studied, which are showed in Table 5.17 (LOS) and Table 5.18 (NLOS). Figure 5.11 shows the DoA MUSIC azimuth angle estimation for both LOS and NLOS scenario.

Compared to the angular spread of outdoor environment in previous references [45], the angular spread for indoor environment (both LOS and NLOS scenario) are very high (>0.4), which means the multipath components come at very varied directions. The reason is that in power lab, there are walls and many machines around the receiving antenna array, therefore there will be many strong reflecting multipath components coming from different angles ranging from 0 to 360 degree. Furthermore, the angular spread for NLOS scenario is even higher than LOS scenario and most of the AS values are above 0.85, which means no clear bias in the angular distribution of received power. The reason is the Tx antenna is directional antenna and therefore, the power of the LOS path is much higher than other multipath. If the LOS path is blocked for NLOS scenario, then other multipath related power will become more important (having more weights) when calculating the angular spread value.

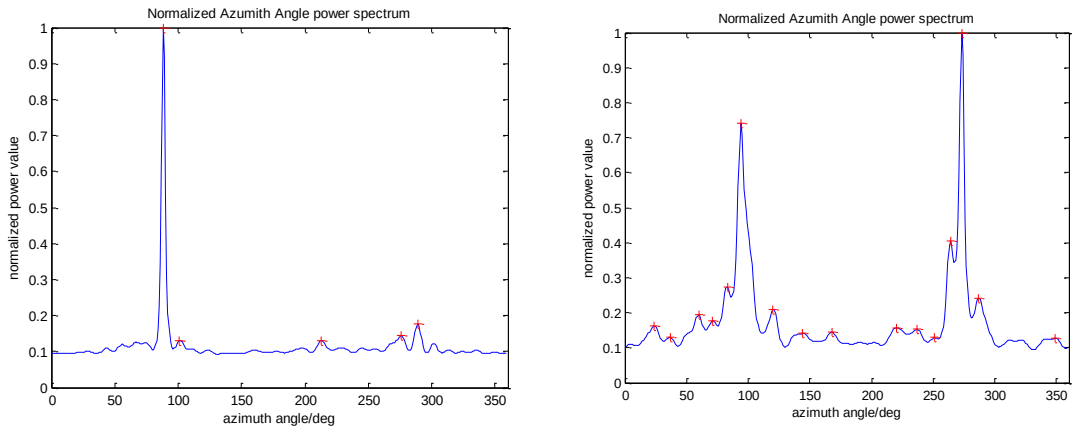

Figure 5.11: The azimuth angle estimation for LOS scenario (left) and NLOS scenario (right) at power lab 13m position (the red crosses are detected multipath)

Table 5.17: Angular spread for different frequency bands at power lab LOS scenario

Location		Angular Spread	*Frequency band*			
Power lab			*1.2GHz -1.4GHz*	*1.9GHz -2.1GHz*	*2.6GHz -2.8GHz*	*3.1GHz -3.3GHz*
LOS	23m	Λ	0.72	0.83	0.86	0.65
	18m	Λ	0.41	0.40	0.47	0.36
	13m	Λ	0.40	0.85	0.72	0.89
	8m	Λ	0.90	0.91	0.83	0.87
	5m	Λ	0.58	0.77	0.82	0.80

Table 5.18: Angular spread for different frequency bands at power lab NLOS scenario

Location		Angular Spread	*Frequency band*			
Power lab			*1.2GHz -1.4GHz*	*1.9GHz -2.1GHz*	*2.6GHz -2.8GHz*	*3.1GHz -3.3GHz*
NLOS	23m	Λ	0.80	0.92	0.84	0.90
	18m	Λ	0.80	0.93	0.87	0.97
	13m	Λ	0.86	0.94	0.97	0.95
	8m	Λ	0.77	0.86	0.70	0.84
	5m	Λ	0.78	0.85	0.84	0.92

Through comparing the angular spread for different frequency bands, we find the AS values are similar in all these four bands. The reason for the similarity is maybe these four frequency bands are close and the frequency dependency on the angular spread is not obvious among these closed frequency bands. Or since the measurements are done at indoor scenario and the surface of objects such as wall, tables, machines are flat, maybe there are less diffractions and scattering propagation mechanisms happened in such measuring environment.

- **Limitation of the measurement set-up for AS studies**

For the measurement set-up design, the circular antenna array is originally designed for outdoor scenario measurement. The diameter of the circular array is 0.6m and there are 72 antenna elements on the array. As we know, the pre-assumption of implementing DoA MUSIC algorithm on the circular array is that each antenna element receives the same multipath components (coming from same sources), but for different antenna element, the same multipath component's extra time-delay-shifting is different, which is resulted from the circular array structure [33]. Therefore, the pre-assumption requires all multipath sources are far away from the antenna array and the antenna array can be seen as a receiving point from the signal sources side. However, in our indoor scenario case, there are reflectors (or multipath sources), such

as furniture, machines, walls are close to the antenna array. Thus, the circular array cannot be considered as a point compared to these closed reflectors and then the arrival angle from the same reflector may be different for different antenna element. Therefore, under such indoor environment, the pre-assumption is broken and the MUSIC DoA estimation may not work very accurately and can only estimate several main paths.

5-5 Conclusions

In this chapter, we firstly discussed the principle, meaning and method of studying the frequency dependency of wireless channel. Secondly, in the power fading margin model part, we studied the effects of bandwidth and centre frequency on the power fading. The results showed that when the bandwidth is increasing, both the maximum fading difference and fading standard deviation are decreasing. The reason why it has such trend is that the fading phenomenon is not happened in all frequency simultaneously. At some frequency, the multipath may have destructive effects which will attenuate the signal power, but at other frequency, the multipath may has constructive effects which will amplify the signal power. Furthermore, the frequency correlation study showed that when the frequency difference is increased, the power fading's frequency correlation becomes lower. Thirdly, we studied the bandwidth effect on *rms* delay spread and concluded that for both LOS and NLOS scenarios, when the bandwidth is increased, the mean, the maximum difference (max.-min.) and the standard deviation of *rms* delay spread become smaller simultaneously. Furthermore, we found for narrowband channel, it is better to use D-CIR model rather than MD model to calculate the RDS, since the narrow bandwidth would make big error on RDS estimation for D-CIR model.

Finally, the frequency dependency study of amplitude fading, *rms* delay spread and azimuth angular spread were studied. The results showed that the channel parameters have not much difference in these four frequency bands. Through reading reference and analyzing the real measurement scenario, the reasons of the insignificant frequency dependency are concluded as following:

- The channel measurement is originally planned for outdoor scenario. However, because of some technical and practical reasons, we finally measured the wireless channel only in indoor scenario. For the indoor environment such as power lab, university canteen and library, maybe there is no many scattering or diffraction

propagation mechanisms happened. Since the surface of indoor walls, machines, and furniture is very flat, it usually causes specular reflection rather than diffuse reflection. Furthermore, for indoor scenario, there are no diffractions from building roofs, no scattering from trees, vegetables and etc., but scattering and diffraction propagation mechanisms are really frequency dependent. Thus, it is better to study the frequency dependency of wireless channel by using outdoor measurement data.

- The selected four frequency bands are all around [1, 3] GHz. And the frequency difference among each two neighboring frequency bands is around 700MHz. Therefore, maybe the reason of unobvious frequency dependencies is these four frequency bands are too close and then the channel propagations are similar in these four closed frequency bands.

- The studied targets, such as amplitude fading distribution, *rms* delays spread, maybe do not directly reflect the frequency dependency. Since we compared the channel impulse response at different frequency bands in the same measurement position, the channel impulse response of different frequency bands are different, which means the channel impulse response is frequency dependent.

- As indicated in [61], some multipath components are frequency dependent, but maybe such frequency dependency has little influence on the communication systems and the related indicators such as multipath fading distribution, RDS and AS are reflected to be less frequency dependent.

In conclusion, to better study the frequency dependency of channel models and its influence on wireless communication systems, the well developed outdoor channel measurements should be implemented. And if possible, the frequency difference among these selected frequency bands is better to be large, which may result in more remarkable frequency dependency.

Chapter 6

Conclusions and Future Work

In this thesis, we presented the studies of frequency dependency and spatial modeling of wireless channel. The statistical channel modeling method is utilized in this project. At beginning, we designed the UWB channel measurement set-up. Because the circular antenna array was utilized at the receiver side, the multipath angular information can be estimated and this makes spatial modeling of the wireless channel possible. And then the designed measurement system was utilized to measure the indoor environment wireless channels at power lab, university canteen and library, three scenarios separately. Meanwhile, the spatial channel model was proposed and then we discussed the methods to estimate and model the channel parameters, such as multipath amplitude, time delay and angular information. In the end of the thesis, the frequency dependency of the channel model parameters was studied.

6-1 Conclusions

In Chapter 3, because we wanted to study the frequency dependency of wireless channel, a UWB channel measurement set-up was designed, which allows us measuring the channel only once for each location and hence, information of several different frequency bands can be obtained. Furthermore, the circular antenna array was utilized at the receiving side and it makes the multipath AoA estimation possible. The channel measurements were originally planned to perform at outdoor environments. However, during the pilot outdoor measurement, we found there are serious narrowband interferences from GSM, WiFi, UMTS, etc., which limits our system's maximum transmitting distance to only 70 m. Therefore, we implemented the channel measurements at three different indoor scenarios in the end. We concluded that the narrowband interference issue should be taken into account for the

future channel measurement set-up design and we also gave several possible solutions to this technical problem.

At the beginning of Chapter 4, a wideband channel spatial model was given and then the analysis methods to estimate the channel multipath parameters, such as amplitude, time of arrival and angle of arrival were introduced. The MUSIC algorithm for ToA, DoA and joint ToA & DoA (JADE) estimations were specifically explained. Furthermore, the JADE algorithm was also tested on the real measurement data and the result showed JADE performs high resolution on ToA and DoA estimation. In the end, we provided the methods of modeling channel parameters such as amplitude fading distribution, *rms* delay spread and angular spread, which were also the targets for the channel frequency dependency studies in Chapter 5.

In Chapter 5, we focused on the frequency dependency study of wireless channel. Firstly, the bandwidth influence and the frequency correlations on the power fading were studied. And then we continued to discuss the bandwidth influence on *rms* delay spread model based on both MD and D-CIR method, we found for narrowband channel, it is better to use D-CIR rather than MD to estimate RDS. Furthermore, the channel frequency dependency issue was studied by analyzing and comparing the channel parameters such as multipath amplitude fading distribution, RDS and AS in four different frequency bands. Although the results showed that the frequency dependency of these channel parameters are not significant, we analyzed the possible reasons and also gave the recommendations of future works.

6-2 Future Work

- The reason for the insignificant frequency dependency results among these four different frequency bands is maybe the studied frequency bands are very close (just several hundred MHz difference). Then in the future work, we can study the frequency dependency of wireless channel in several more separated frequency bands. For example, we can study the amplitude fading distribution, *rms* delay spread and angular spread in both 2 GHz, 10 GHz and 60 GHz band and then compare them to find the frequency dependency on these channel parameters. Therefore, the frequency dependency effects would be clearer.

- Here our channel frequency dependency study is based on indoor channel measurements. Therefore, we can continue the channel frequency dependency study for outdoor environment, because the signal propagating in outdoor environment might experience different scattering, diffractions from trees, plants, rough building surface. For the outdoor scenario channel measurement, we should change to another high power pulse generator for long distance measurment and perform it around the EWI building, TU Delft. The Tx antenna is installed on the roof of low building and the Rx antenna array is moved around the EWI building to measure the wireless channel. The collected outdoor channel measurement data can be used to validate the frequency dependency channel models. Furthermore, the outdoor channel modeling and its related frequency dependency research would be helpful for the design of future mobile communication system operated on higher centre frequency and bandwidth.

- The cognitive radio is one trend for the next generation wideband communication system. Based on our AoA estimation studies, how to implement the artificial intelligence into the cognitive radio system is an interesting topic. For example, there is a cognitive radio system working on the same frequency band as another normal communication system. If the cognitive radio system transmits signal and it is received by the receiver of the normal communication system, this will bring in-band signal interference to the normal communication system. Therefore, how to make the cognitive radio system automatically detect the direction of normal communication system and avoid transmitting signal to that direction is a good way to decrease the systems' mutual signal interference. The idea is shown in Figure 6.1.

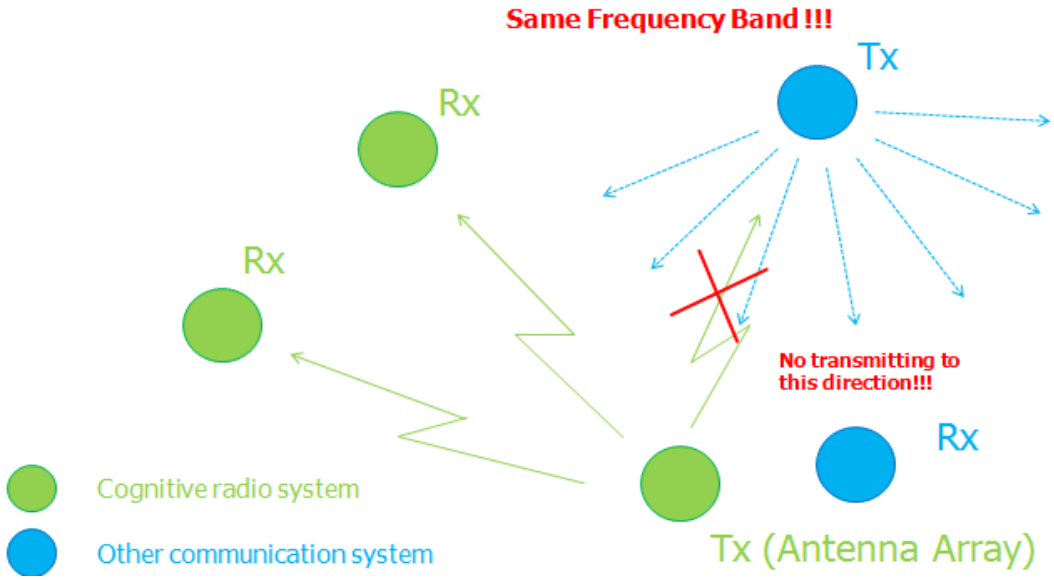

Figure 6.1: AoA estimation method used in cognitive radio system

Bibliography

[1] T. S. Rappaport, "*Wireless Communication: Principles and Practice"*. New Jersey: Prentice Hall 1996.

[2] H. Nikookar, *Advanced topics in Digital Wireless Communications*, Module ET4275 lecture notes, Delft University of Technology, 2006-2007.

[3] A. Goldsmith, Book: *Wireless Communications*, Stanford University, 2004.

[4] J. Karedal, Thesis: *Measurement-Based Modeling of Wireless Propagation Channels*, Lund University, 2009

[5] Z. Irahhauten, Thesis: *'Ultra-Wideband Wireless Channel: Measurements, Analysis and Modeling'*, Delft University of Technology, 2008

[6] H. Hashemi, "*The Indoor Radio Propagation Channel*", Processing of *IEEE*, vol.81, no.7, July 1993, pp.943-968

[7] H. Nikookar, *"Propagation of Radio Wave-Lecture Notes"*, Delft University of Technology, the Netherlands, 2004.

[8] S. O. Rice, "*Mathematical Analysis of Random Noise*", Bell syst. Tech. J., vol.23, pp.282-332, 1954, and vol.24,pp. 46-156, 1954.

[9] E. Bonek, "*On MIMO Channel Models for LTE*", Technology University of Wien and Forschungszentrum Telekommunikation Wien, Turku, 16 January 2009

[10] L. Barclay, *Propagation of Radio Waves*, IEE, 2003.

[11] L. Boithias, *Radiowave Propagation*, Mc Graw-Hill, New-York, March 1988

[12] D. A. McNamara, C. W. I. Pistotius, "*Introduction to The Uniform Geometrical*

Theory of Diffraction", Artech House, London, 1990

[13] M. Nakagami, "*The M- distribution, A General Formula of Intensity Distribution for Rapid Fading*", in Statistical Methods of Radio Wave propagation, Pergamon Press, 1960

[14] V. M. Kolmonen, J. Kivinen, "*5.3 GHz MIMO Radio Channel Sounder*", IMTC 2005 Instrumentation and Measurement Technology Conference, Ottawa, Canada, 17-19 May 2005

[15] S. S.Ghassemzadeh, R. Jana, V. Tarokh, C.W. Rice, and W. Turin, "*A Statistical Pathloss Model for In-home UWB Channels*", IEEE Conference on Ultra Wideband Systems and Technologies, Digest of Papers,pp. 59-64, May 2002.

[16] S. Howard and K. Pahlavan, "Measurement and Analysis of the Indoor Radio Channel in the Frequency Domain", *IEEE Transactions on Instrumentation and Measurement*, vol. 39, no. 5, pp. 751-755, Oct.1990.

[17] Y. L. C. D. Jong and M. H. A. J. Herben, "High-Resolution Angle-of Arrival Measurement of the Mobile Radio Channel", *IEEE Transactions on Antennas and Propagation*, Vol. 47, No. 11, November 1999

[18] M. Alatossava, L. Hentila, "*Comparison of Outdoor to Indoor and Indoor to Outdoor MIMO Propagation Characteristics at 5.25 GHz*", Vehicular Technology Conference, 2007. *IEEE 65th*, 22-25 April 2007

[19] T. Zwick, D. Hampicke, A. Richter, G. Sommerkorn, R. Thomä, "A Novel Antenna Concept for Double-Directional Channel Measurements", *IEEE Transactions on Vehicular Technology, Vol. 53, No. 2,* March 2004

[20] G. J. M. Janssen, P.A. Stigter, and R. Prasad, "Wideband Indoor Channel Measurements and BER Analysis of Frequency Selective Channels at 2.4, 4.75, and 11.5 GHz", *IEEE Transactions on Communications*, Vol. 44, no. 10, pp. 1272 – 1288, Oct. 1996

[21] N. A. Alsindi, thesis: *"Performance of TOA Estimation Algorithms in Different Indoor Multipath Conditions"*, Worcester Polytechnic Institute, Apr. 2004

[22] M. R. J. A. E. Kwakkernaat,thesis: *Angular Dispersion of Radio Waves in Mobile Channels*, Technische Universiteit Eindhoven, 2008

[23] Y. Luo and C. L. Law, "*Angle-of-arrival Estimation with Array in a Line-of-Sight Indoor UWB-IR*", Information, Communications and Signal Processing, 2009. ICICS 2009. 7th International Conference, December 2009

[24] H. Zhang, O. Mantel, "*Analysis of Wideband Radio Channel Properties for Planning of Next-Generation Wireless Networks*", TNO Information and Communication Technology, 2009

[25] W. C. Jakes, *Microwave mobile communications*, (Wiley, 1974).

[26] A. Molisch, K. Balakrishnan, D. Cassioli, C.C. Chong, S. Emami, A. Fort, J. Karedal, J. Kunisch, H. Schantz, U. Schuster, and K. Siwiak, "*IEEE* 802.15.4a Channel Model: Final Report", *IEEE P802.15.4/6620r0-SG4a*, Mar. 2003

[27] M. Haardt, M.D. Zoltowski, "*2D Unitary ESPRIT for Efficient 2D Parameter Estimation*", International Conference on Acoustics, Speech, and Signal Processing, May 1995

[28] M. Haardt and J. A. Nossek, "*3-D Unitary ESPRIT for Joint 2-D Angle and Carrier Estimation*", International Conference on Acoustics, Speech and Signal Processing, Apr. 1997

[29] C. P. Mathews and M. D. Zoltowski, "Eigenstructure Techniques for 2-D Angle Estimation with Uniform Circular Arrays", *IEEE Transactions on Signal Processing, vol. 42, issue 9*, 1994

[30] M. Pesavento and A. B. Gershman, "Unitary Root-MUSIC with A Real-Valued Eigendecomposition: A Theoretical and Experimental Performance Study", *IEEE Transactions on Signal Processing, Vol. 48, No. 5*, MAY 2000

[31] M. Haardt, and J. A. Nossek, "Unitary ESPRIT: How to Obtain Increased Estimation Accuracy with a Reduced Computational Burden", *IEEE Transactions on Signal Processing, Vol. 43, No. 5*, MAY 1995

[32] M. D. Zoltowski and C. P. Mathews, "Colosed-Form 2-D Angle Estimation with Rectangular Arrays in Element Space or Beamspace via Unitary *ESPRIT*", *IEEE Transactions on Signal Processing, Vol. 44, No. 2*, Feb. 1996

[33] Y. Zhang, A.K. Brown, W.Q. Malik, and D.J. Eswards, "High Resolution 3-D Angle of Arrival Determination for Indoor UWB Multipath Propagation", *IEEE Transactions on Wireless Communications*, VOL, 7 NO.8, August 2008

[34] P. A. Matthews and B. Mohebbi, "*Direction of Arrival Measurements at UHF*", Electron. Lett., vol. 25, no. 16, pp. 1069–1070, Aug. 3, 1989.

[35] D. E. Dudgeon and R. M. Mersereau, "*Multidimensional Digital Signal Processing"*, Englewood Cliffs, NJ: Prentice-Hall, 1984.

[36] A. Lee, "*Centrohermitian and Skew-centrohermitian Matrices*," Linear Algebra Application, vol. 29, pp. 205–210, 1980.

[37] M. Haardt and J. A. Nossek, "Unitary ESPRIT: How to Obtain an Increased Estimation Accuracy with a Reduced Computational Burden," *IEEE Trans. Signal Processing, vol. 43, pp. 1232–1242*, May 1995.

[38] D. C. Cox, "Delay Doppler Characteristics of Multipath Propagation at 910 MHz in a Suburban Mobile Radio Environment," *IEEE Trans. Antenna Propagations, vol. 20, pp. 625–635*, Sept. 1972.

[39] U. Dersch and E. Zollinger, "Physical Characteristics of Urban Micro-cellular

Propagation," *IEEE Trans. Antennas Propagat.*, vol. 42, pp. 1528–1539, Nov. 1994.

[40] X. Li and K. Pahlavan, "Super-resolution TOA Estimation with Diversity for Indoor Geolocation," *IEEE Trans. Wireless Comm.*, vol. 3, no. 1, pp. 224-234, Jan. 2004.

[41] R. J. M. Cramer, R. A. Scholtz and M.Z. Win, "Evaluation of an Ultra-Wideband Propagation Channel", *IEEE Transactions on Antennas and Propagation, vol. 5, pp. 561-570*, May 2007

[42] P. Li, H. Zhang and J. Oostveen, *"MIMO-OFDM Performance in Relation to Wideband Channel Properties"*, 21st Annual *IEEE* International Symposium on Personal, Indoor and Mobile Radio Communications, 2010

[43] K. Zhou and Y.H. Chew, "*On the Achievable Diversity Gain by the Optimal Subcarrier Allocations in Multiuser OFDM System*", in Proc. of *IEEE MILCOM 2006*, Oct. 2006.

[44] X. Li and K. Pahlavan, "Super-resolution TOA Estimation with Diversity for Indoor Geolocation", *IEEE Transactions on Wireless Communications, vol. 3, pp. 224*, Jan. 2004

[45] X. Zhao, J. Kivinen and P. Vainikainen, "Propagation Characteristics for Wideband Outdoor Mobile Communications at 5.3 GHz", *IEEE JOURNAL ON SELECTED AREAS IN COMMUNICATIONS, VOL. 20, NO. 3*, APRIL 2002

[46] A.V. D. Veen, M. C. Vanderveen and A. praulraj, "Joint Angle and Delay Estimation Using shift-Invariance Techniques", *IEEE Transactions on Signal Processing, vol. 46, No. 2*, Feb. 1998

[47] J. Kivinen, X. Zhao, and P. Vainikainen, "Empirical Characterization of Wideband Indoor Radio Channel at 5.3 GHz," *IEEE Trans. Antennas Propagation, vol. 49, pp. 1192–1203*, Aug. 2001.

[48] J. F. Lafortune and M. Lecours, "Measurement and modeling of propagation losses in a building at 900 MHz," *IEEE Trans. Veh. Technol., vol. 39, pp. 101–108*, May 1990.

[49] V. Erceg, L. J. Greenstein, S. Y. Tjandra, S. R. Parkoff, A. Gupta, B. Kulic, A. A. Julius, and R. Bianchi, "An Empirically Based Path Loss Model for Wireless Channels in Suburban Environments," *IEEE J. Select. Areas Commun., vol. 17, pp. 1205–1211*, July 1999.

[50] Y. Zhang, A.K. Brown, W.Q. Malik and D.J. Edwards, "High Resolution 3-D Angle of Arrival Determination for Indoor UWB Multipath Propagation", *IEEE Transaction on Wireless Communications, Vol. 7, No. 8*, August 2008

[51] C. Gentile, A.J. Braga, and A. Kik, "*A Comprehensive Evaluation of Joint Range and Angle Estimation in Indoor Ultra wideband Location Systems*", EURASIP

Journal on Wireless Communications and Networking, Vol. 2008

[52] Y. Karasawa and H. Iwai, "Formulation of Spatial Correlation Statistics in Nakagami-Rice Fading Environments," *IEEE Trans. Antennas Propagat.*, vol. 48, pp. 12–18, Jan. 2000.

[53] S. Y. Seidel and T. S. Rappaport, "914 MHz Path Loss Prediction Models for Indoor Wireless Communications in Multifloor Buildings," *IEEE Trans. on Antennas Propagat.*, vol. 40, no. 2, pp. 207–217, Feb. 1992.

[54] S. Gao, S. Zhong, and C. Jiang, "Path Number Distribution for Multipath Propagation in Land Mobile Communications and its Simulation" (in Chinese), *J. China Inst. Commun.*, vol. 19, pp. 66–72, Feb. 1998.

[55] H. Suzuki, "A Statistical Model for Urban Radio Propagation," *IEEE Trans. Commun.*, vol. 25, pp. 673–680, July 1977.

[56] S. Gao, "*Study of Multipath Propagation in Land Mobile Communications*", M.Sc. thesis (in Chinese), China Research Institute of Radio wave Propagation, Xinxiang, P. R. of China, 1995.

[57] P. Svedman, S.K. Wilson, L. Cimini, and B. Ottersten, *"A Simplified Opportunistic Feedback and Scheduling Scheme for OFDM,"* in Proc. of Vehicular Technology Conference 2004, May 2004.

[58] A. Intarapanich, P. L. Kafle, R. J. Davies, A. B. Sesay, and J. McRory, "*Spatial Correlation Measurements for Broadband MIMO Wireless Channels*", *IEEE* VTC'2004 Fall, pp. 52--56, 2004.

[59] R. C. Qiu and I.T. Lu, "A Novel Model of Time-dispersion Multipath Channel for Wideband CDMA Systems", *IEEE ICUPC'96*, vol. 1, pp.350 - 354 , 1996.

[60] R. C. Qiu and I. T. Lu, "Multipath Resolving with Frequency Dependence for Wide-Band Wireless Channel Modeling", *IEEE Transactions on Vehicular Technology*, Vol. 48, No. 1, Jan. 1999

[61] W. Zhang, T. D. Abhayapala and J. Zhang, "*Frequency Dependency in UWB Channel Modeling*", Scientific Commons, 2008.

[62] S.G. Glisic, "*Advanced Wireless Communications: 4G Cognitive and Cooperative Broadband Technology, 2nd Edition*", 2007 John Wiley & Sons, Ltd. ISBN: 978-0-470-05977-7

[63] N. I. Fisher, "*Statistical Analysis of Circular Data*", Cambridge, UK: Cambridge University Press, 1993.

[64] B. H. Fleury, "First- and Second-order Characterization of Direction Dispersion and Space Selectivity in the Radio Channel", *IEEE Trans. On Information Theory, vol. 46, no. 6, pp. 2027-2044*, Sept. 2000.

[65] http://www.awe-communications.com/.

[66] L. Zhou, Y. Zhao, H. Cui, "*High Resolution Wideband DoA Estimation Based on Modified MUSIC Algorithm*", Processing of the 2008 *IEEE* International Conference on Information and Automation June 20-23, 2008, Zhangjiajie, China

[67] M. R. A. Sadjadi, A. Pezeshki, L. L. Scharf and M. Hohil, " Wideband DoA Estimation Algorithms for Multiple Moving Sources using Unattended Acoustic Sensors", *IEEE Transactions on Aerospace and Electronic Systems, vol. 44, no. 4, pp. 1585-1599,* Oct. 2008

[68] T. Pham and B.M. Sadler, "*Wideband Array Processing Algorithms for Acoustic Tracking of Ground Vehicles*", J. Acoust. Soc. Am. Volume 100, Issue 4, 1996

[69] G. Janssen, *"ET4358 Wireless Communication-Lecture Notes"*, Delft University of Technology, the Netherlands, 2009.

Glossary

List of Acronyms

AS	**Angular Spread**
AoA	**Angle of Arrival**
AoD	**Angle of Departure**
CFR	**Channel Frequency Response**
CIR	**Channel Impulse Response**
D-CIR	**Discrete Channel Impulse Response**
DoA	**Direction of Angle**
DWA	**Dielectric Wedge Antenna**
ESPRIT	**Estimation of Signal Parameters via Rotational Invariance Techniques**
FD	**Frequency Domain**
FFT	**Fast Fourier Transform**
GTD	**Geometrical Theory of Diffraction**
GSM	**Global System of Mobile Communication**
GSCM	**Geometry-based Stochastic Channel Model**
IFFT	**Inverse Fast Fourier Transform**
JADE	**Joint Angle and Delay Estimation**
LTE	**Long Term Evolution**
LOS	**Line of Sight**
MUSIC	**Multiple Signal Classification**
MD	**Maximum Detection**

MIMO	**Multiple Input Multiple Output**
NLOS	**None Line of Sight**
OFDM	**Orthogonal Frequency-Division Multiplexing**
QoS	**Quality of Service**
RDS	**RMS Delay Spread**
RMS	**Root Mean Square**
SNR	**Signal to Noise Ratio**
SIMO	**Single Input Multiple Output**
ToA	**Time of Arrival**
TD	**Time Domian**
UWB	**Ultra Wide Band**
UMTS	**Universal Mobile Telecommunications System**
UCA	**Uniform Circular Array**
VNA	**Virtual Network Analyzer**
WiFi	**Wireless Fidelity**

Appendix A

List of Figures

Appendix B

List of Tables

Appendix C

Measurement Report

The channel measurement is done at three different places in the TU Delft EWI buildings, which are power lab, canteen and library during 07.03.2011~ 11.03.2011. Following are the details for each place.

The whole measurements are using the time window 2us and the sampling frequency is 20GHz. The number of average is 512 for each channel impulse response. One LNA is used before Rx antenna. The Rx antenna array is circular and with 72 elements. The radius of the array is 0.3m.

- **Power lab**

The Tx antenna is kept at the same position for each measurement and the Rx antenna is moving for different position to measure the channel. There are 5 positions for LOS scenario and *5* positions for NLOS scenario. The Rx side is using circular antenna array, therefore, the total number of channel impulse response I measured is 10*72=720 for the power lab scenario. The power lab measurement environment is showed in Figure A-1. And the transmitting and receiving sides are showed in Figure A-2. The details of each measurement location are presented in Table A-1.

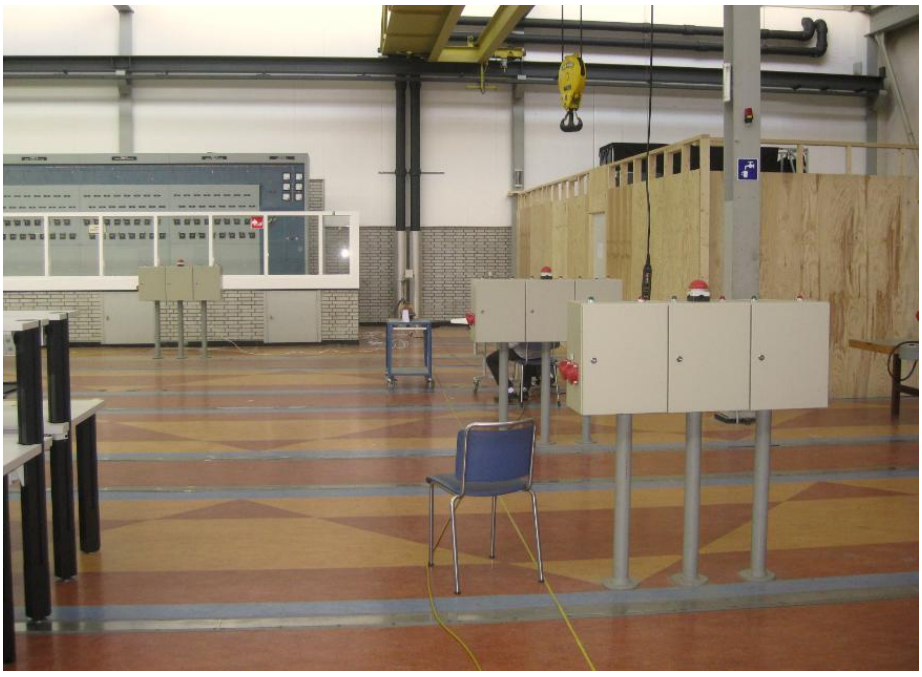

Figure A-1: power lab measurement environment

Figure A-2: Tx side (left) and Rx side (right) at power lab scenario

- **EWI canteen**

The Tx antenna is kept at the same position for each measurement and the Rx antenna is moving for different position to measure the channel. There are 5 positions for LOS scenario and 5 positions for NLOS scenario. The Rx side is using circular antenna array, therefore, the total number of channel impulse response I measured is 10*72=720 for the power lab scenario. The canteen measurement environment is showed in Figure A-3. And the transmitting and receiving sides are showed in Figure A-4. The details of each measurement location are presented in Table A-2.

Figure A-3: EWI canteen measurement environment

Figure A-4: Tx side (left) and Rx side (right) at EWI canteen scenario

Table A-1: Details of each measurement position in power lab scenario

Tx	Location/m	Antenna gain	Beam width	Number of antennas
Directional Horn Antenna	(0, 0, 1.15)	10dB	Directional(30deg)	1

Rx	Location/m	Antenna gain	Beam width	Type(number of elements)	scenario	Tx direction
Biconic antenna	(1,23,1.01)	~1dB	Omnidirectional	Circular array(72)	LOS	85deg
Biconic antenna	(1,18,1.01)	~1dB	Omnidirectional	Circular array(72)	LOS	86deg
Biconic antenna	(0.3,13,1.01)	~1dB	Omnidirectional	Circular array(72)	LOS	88deg
Biconic antenna	(-1.8,8,1.01)	~1dB	Omnidirectional	Circular array(72)	LOS	103deg
Biconic antenna	(-2,5,1.01)	~1dB	Omnidirectional	Circular array(72)	LOS	112deg
Biconic antenna	(-0.9,23,1.01)	~1dB	Omnidirectional	Circular array(72)	NLOS	92deg
Biconic antenna	(-1.0,18,1.01)	~1dB	Omnidirectional	Circular array(72)	NLOS	93deg
Biconic antenna	(-1.5,13,1.01)	~1dB	Omnidirectional	Circular array(72)	NLOS	98deg
Biconic antenna	(2,8,1.01)	~1dB	Omnidirectional	Circular array(72)	NLOS	76deg
Biconic antenna	(2,5,1.01)	~1dB	Omnidirectional	Circular array(72)	NLOS	68deg

Table A-2: Details of each measurement position in power EWI canteen scenario

Tx	Location/m	Antenna gain	Beam width	Number of antennas
Directional Horn Antenna	(0, 0, 1.15)	10dB	Directional(30deg)	1

Rx	Location/m	Antenna gain	Beam width	Type(number of elements)	scenario	Tx direction
Biconic antenna	(3.3,29,1.01)	~1dB	Omnidirectional	Circular array(72)	LOS	85deg
Biconic antenna	(3.3,24,1.01)	~1dB	Omnidirectional	Circular array(72)	LOS	82deg
Biconic antenna	(3.7,19,1.01)	~1dB	Omnidirectional	Circular array(72)	LOS	76deg
Biconic antenna	(3.7,14,1.01)	~1dB	Omnidirectional	Circular array(72)	LOS	70deg
Biconic antenna	(3.5,9,1.01)	~1dB	Omnidirectional	Circular array(72)	LOS	69deg
Biconic antenna	(5.6,29,1.01)	~1dB	Omnidirectional	Circular array(72)	NLOS	79deg
Biconic antenna	(5.6,24,1.01)	~1dB	Omnidirectional	Circular array(72)	NLOS	77deg
Biconic antenna	(5.6,19,1.01)	~1dB	Omnidirectional	Circular array(72)	NLOS	74deg
Biconic antenna	(5.8,14,1.01)	~1dB	Omnidirectional	Circular array(72)	NLOS	65deg
Biconic antenna	(5.6,9,1.01)	~1dB	Omnidirectional	Circular array(72)	NLOS	58deg

- **EWI library**

The Tx antenna is kept at the same position for each measurement and the Rx antenna is moving for different position to measure the channel. There are 4 positions for LOS scenario and 4 positions for NLOS scenario. The Rx side is using circular antenna array, therefore, the total number of channel impulse response I measured is 8*72=576 for the power lab scenario. The power lab measurement environment is showed in Figure A-5. And the transmitting and receiving sides are showed in Figure A-6. The details of each measurement location are presented in Table A-3.

Figure A-5: EWI library measurement environment

Figure A-6: Tx side (left) and Rx side (right) at EWI library scenario

Table A-3: Details of each measurement position in power EWI library scenario

Tx	Location/m	Antenna gain	Beam width	Number of antennas
Directional Horn Antenna	(0, 0, 1.15)	10dB	Directional(30deg)	1

Rx	Location/m	Antenna gain	Beam width	Type(number of elements)	scenario	Tx direction

Biconic antenna	(-0.2,16.5,0.98)	~1dB	Omnidirectional	Circular array(72)	LOS	91deg
Biconic antenna	(-0.5,13,0.98)	~1dB	Omnidirectional	Circular array(72)	LOS	95deg
Biconic antenna	(-0.5,9.5,0.98)	~1dB	Omnidirectional	Circular array(72)	LOS	100deg
Biconic antenna	(-0.5,6,0.98)	~1dB	Omnidirectional	Circular array(72)	LOS	103deg
Biconic antenna	(-3.3,16.5,0.98)	~1dB	Omnidirectional	Circular array(72)	NLOS	101deg
Biconic antenna	(-3.3,13,0.98)	~1dB	Omnidirectional	Circular array(72)	NLOS	104deg
Biconic antenna	(-3.3,9.5,0.98)	~1dB	Omnidirectional	Circular array(72)	NLOS	109deg
Biconic antenna	(-3.3,6,0.98)	~1dB	Omnidirectional	Circular array(72)	NLOS	119deg

Appendix D

In this part, I list the analysis results of the frequency dependency studies on channel parameter modeling, which are not presented in the thesis main part.

Table 1: Statistics of power fading for power lab scenario

Fading						
Location		*Frequency band*				
Power lab			*1.25GHz -1.35GHz*	*1.95GHz -2.05GHz*	*2.65GHz -2.75GHz*	*3.15GHz -3.25GHz*
LOS	23m	σ	0.3912	0.4722	0.3684	0.5759
		Max.[dB]	2.7243	3.2509	3.2926	4.1755
		Min.[dB]	-4.2392	-4.6212	-7.5002	-9.0796
	18m	σ	0.3583	0.4296	0.3246	0.6415
		Max.[dB]	3.2207	3.7591	2.4630	4.1877
		Min.[dB]	-2.9529	-5.2475	-5.0739	-6.8131
	13	σ	0.3279	0.2612	0.2680	0.6455
		Max.[dB]	2.6531	2.6392	2.1668	5.1108
		Min.[dB]	-3.8590	-2.5041	-3.8603	-6.4258
	8m	σ	0.4642	0.7071	0.3721	0.7328
		Max.[dB]	3.0410	5.1795	2.6532	5.6451
		Min.[dB]	-8.1200	-6.5116	-4.6448	-6.6179
	5m	σ	0.4102	0.6278	0.7285	0.5805
		Max.[dB]	2.9801	5.2184	5.6380	4.7288
		Min.[dB]	-5.3096	-5.1230	-6.1389	-8.5383
	total	**σ**	**0.3904**	**0.4996**	**0.4123**	**0.6352**
		Max. -Min[dB]	**11.1610**	**11.6911**	**11.7769**	**13.2671**
NLOS	23m	σ	0.3735	0.3187	0.3627	0.4424
		Max.[dB]	2.4847	2.9453	3.1192	3.6392
		Min.[dB]	-6.7545	-3.6951	-4.8433	-4.1445
	18m	σ	0.4617	0.4289	0.5550	0.6490
		Max.[dB]	3.9421	3.7625	3.6007	4.6588
		Min.[dB]	-4.7394	-4.5521	-6.1378	-7.1078
	13	σ	0.3365	0.4380	0.4613	0.6753
		Max.[dB]	2.4112	3.5897	4.0313	5.1115
		Min.[dB]	-4.1896	-4.3821	-4.6079	-5.9501
	8m	σ	0.3867	0.2679	0.5820	0.6028
		Max.[dB]	2.9778	2.7906	4.2597	6.1675

		Min.[dB]	-3.1424	-2.7627	-7.0905	-6.7912
	5m	σ	0.2888	0.4726	0.6913	0.4517
		Max.[dB]	2.7129	3.6087	4.4858	3.3630
		Min.[dB]	-3.0930	-5.8778	-5.9123	-4.5853
	total	**σ**	**0.3694**	**0.3852**	**0.5305**	**0.5642**
		Max. -Min.[dB]	**9.2392**	**9.4865**	**11.3502**	**12.9587**

Table 2: Statistics of power fading for canteen scenario

Fading						
Location		*Frequency band*				
Canteen			*1.25GHz -1.35GHz*	*1.95GHz -2.05GHz*	*2.65GHz -2.75GHz*	*3.15GHz -3.25GHz*
LOS	29m	σ	0.6045	0.4318	0.6778	0.5841
		Max.[dB]	4.4441	4.5063	4.7856	4.7812
		Min.[dB]	-6.9762	-4.4465	-5.5171	-11.0718
	24m	σ	0.3627	0.3904	0.4848	0.5051
		Max.[dB]	2.8522	2.6279	3.0897	4.2446
		Min.[dB]	-3.6197	-3.9073	-7.2490	-6.3701
	19m	σ	0.5384	0.4028	0.3223	0.3823
		Max.[dB]	3.1916	3.7746	2.4651	3.4432
		Min.[dB]	-7.3590	-4.4176	-3.3881	-3.7555
	14m	σ	0.5684	0.6216	0.4291	0.5597
		Max.[dB]	4.0627	4.5461	3.3775	4.6755
		Min.[dB]	-5.8852	-6.8542	-6.2254	-9.0404
	9m	σ	0.3254	0.3518	0.4357	0.4806
		Max.[dB]	2.3439	2.9075	4.3499	3.7255
		Min.[dB]	-4.3841	-4.6226	-5.6715	-5.0659
	total	**σ**	**0.4799**	**0.4397**	**0.4699**	**0.5024**
		Max. -Min.[dB]	**11.4203**	**11.4003**	**10.3387**	**15.8530**
NLOS	29m	σ	0.4686	0.4993	0.5219	0.4589
		Max.[dB]	3.7163	4.0142	4.1457	4.1213
		Min.[dB]	-4.2906	-5.0356	-5.1928	-4.6507
	24m	σ	0.3337	0.4343	0.3525	0.3754
		Max.[dB]	2.5700	3.4692	3.1907	3.1847
		Min.[dB]	-4.0823	-6.0346	-5.0649	-4.7230
	19m	σ	0.3424	0.3690	0.3536	0.4581
		Max.[dB]	2.7652	3.0540	3.4204	3.5812
		Min.[dB]	-3.8149	-3.9448	-3.8473	-7.6304
		σ	0.4314	0.4773	0.4529	0.6018

	14m	Max.[dB]	3.9266	3.5552	3.6519	5.9728
		Min.[dB]	-4.6206	-6.5861	-7.2675	-5.2320
	9m	σ	0.5334	0.4482	0.3749	0.4432
		Max.[dB]	4.6447	3.4662	3.2356	3.9188
		Min.[dB]	-5.2831	-6.0551	-4.6376	-6.5159
	total	**σ**	**0.4219**	**0.4456**	**0.4112**	**0.4675**
		Max. -Min.[dB]	**9.9278**	**10.1413**	**10.9194**	**11.2116**

Table 3: Statistics of power fading for library scenario

Fading						
Location		*Frequency band*				
Library			*1.25GHz -1.35GHz*	*1.95GHz -2.05GHz*	*2.65GHz -2.75GHz*	*3.15GHz -3.25GHz*
LOS	16.5m	σ	0.5261	0.6999	0.5874	0.8298
		Max.[dB]	3.4406	4.4061	4.8353	4.9901
		Min.[dB]	-5.4065	-7.6956	-4.3801	-8.1561
	13m	σ	0.3959	0.4793	0.6321	0.3806
		Max.[dB]	3.0167	4.3664	5.0918	2.5868
		Min.[dB]	-4.5050	-4.7943	-7.1388	-5.3691
	9.5m	σ	0.3575	0.3700	0.4260	0.6369
		Max.[dB]	3.0541	2.8124	3.3582	5.0023
		Min.[dB]	-4.0370	-5.5156	-4.0012	-8.5377
	6m	σ	0.4528	0.5310	0.4979	0.4923
		Max.[dB]	2.5721	3.6790	4.2378	4.1615
		Min.[dB]	-6.1366	-9.0457	-6.0450	-6.2797
	total	**σ**	**0.4331**	**0.5201**	**0.5358**	**0.5849**
		Max. -Min.[dB]	**8.8471**	**12.7247**	**12.2306**	**13.5400**
NLOS	16.5m	σ	0.5534	0.4719	0.8538	1.2710
		Max.[dB]	3.5158	3.7944	5.4749	8.9770
		Min.[dB]	-6.1058	-4.3425	-7.8509	-7.6593
	13m	σ	0.5833	0.5497	0.6592	0.6167
		Max.[dB]	4.4458	3.9888	5.8763	4.9200
		Min.[dB]	-7.5498	-5.8376	-5.8453	-8.3337
	9.5m	σ	0.4870	0.9736	0.8352	0.6135
		Max.[dB]	4.0167	6.0710	6.0504	4.1492
		Min.[dB]	-5.8829	-8.5251	-7.9064	-8.7132
	6m	σ	0.5167	0.5605	0.6207	0.7444
		Max.[dB]	3.2397	4.3813	5.2272	4.2984
		Min.[dB]	-6.3437	-5.5948	-6.2682	-8.8860

	total	***σ***	**0.5351**	**0.6389**	**0.7422**	**0.8114**
		Max. -Min.[dB]	**11.9956**	**14.5961**	**13.9568**	**16.6363**

Table 4: Power fading frequency correlation for power lab scenario

Power fading frequency correlation										
Location										
Power lab		$C_{1,1}$	$C_{1,2}$	$C_{1,3}$	$C_{1,4}$	$C_{1,5}$	$C_{1,6}$	$C_{1,7}$	$C_{1,8}$	$C_{1,9}$	$C_{1,10}$
LOS	23m	1.0000	0.9723	0.9267	0.8278	0.7294	0.5106	0.2440	0.0371	-0.0708	-0.0683
	18m	1.0000	0.9353	0.5820	0.3626	0.2590	0.1170	-0.0833	-0.0987	-0.1808	-0.1415
	13m	1.0000	0.8785	0.7039	0.4089	0.2698	0.2323	0.4754	0.6012	0.6094	0.6050
	8m	1.0000	0.9661	0.8475	0.7229	0.4926	0.2331	0.1084	0.0400	0.0108	-0.1001
	5m	1.0000	0.9633	0.8639	0.7518	0.6656	0.5565	0.4425	0.3693	0.2915	0.1648
NLOS	23m	1.0000	0.8557	0.6985	0.3435	0.0704	0.0262	-0.0715	-0.0732	-0.1460	-0.2155
	18m	1.0000	0.9397	0.6415	0.3038	0.1131	-0.0203	-0.0153	-0.0053	0.0300	0.1091
	13m	1.0000	0.9422	0.7080	0.4520	0.4116	0.3550	0.1740	0.0051	-0.1322	-0.1674
	8m	1.0000	0.9097	0.8150	0.6032	0.5114	0.3204	0.4134	0.4063	0.5776	0.5079
	5m	1.0000	0.9801	0.9397	0.8564	0.8547	0.8183	0.7715	0.6472	0.5892	0.4166

Table 5: Power fading frequency correlation for Canteen scenario

Power fading frequency correlation										
Location										
Canteen		$C_{1,1}$	$C_{1,2}$	$C_{1,3}$	$C_{1,4}$	$C_{1,5}$	$C_{1,6}$	$C_{1,7}$	$C_{1,8}$	$C_{1,9}$	$C_{1,10}$
LOS	29m	1.0000	0.9222	0.8075	0.7145	0.4145	0.3252	0.1523	0.1522	0.1655	0.1775
	24m	1.0000	0.9656	0.8313	0.7096	0.5002	0.3326	0.2257	0.1779	0.0832	-0.0601
	19m	1.0000	0.8888	0.6576	0.3473	0.0622	-0.1403	-0.2877	-0.3015	-0.2748	-0.3094
	14m	1.0000	0.8246	0.2617	-0.0146	-0.1288	-0.0024	0.1207	0.1718	0.2452	0.3982
	9m	1.0000	0.9152	0.5800	0.3705	0.3492	0.2515	0.2495	0.3322	0.2767	0.1480
NLOS	29m	1.0000	0.9366	0.6798	0.5195	0.2769	0.2132	0.1962	0.1814	0.1768	-0.0897
	24m	1.0000	0.8885	0.5499	0.4638	0.4072	0.3741	0.3489	0.2744	0.3230	0.1680
	19m	1.0000	0.8992	0.6672	0.6084	0.4328	0.3119	0.2316	0.2937	0.2156	0.1240
	14m	1.0000	0.8904	0.2781	0.1675	0.1296	0.0439	0.0280	0.1606	0.1284	0.1907
	9m	1.0000	0.7993	-0.0439	-0.0281	-0.0836	-0.1002	-0.1019	0.2283	0.2456	0.2335

Table 6: Power fading frequency correlation for Library scenario

Power fading frequency correlation										
Location										
Library		$C_{1,1}$	$C_{1,2}$	$C_{1,3}$	$C_{1,4}$	$C_{1,5}$	$C_{1,6}$	$C_{1,7}$	$C_{1,8}$	$C_{1,9}$	$C_{1,10}$
LOS	16.5m	1.0000	0.9868	0.9486	0.8998	0.7948	0.6553	0.4264	0.2989	0.1883	0.0829
	13m	1.0000	0.9714	0.8768	0.7372	0.6324	0.5826	0.5681	0.5591	0.3531	0.0348
	9.5m	1.0000	1.0000	0.9539	0.8453	0.5753	0.2477	-0.0216	-0.0931	-0.0377	0.0928
	6m	1.0000	0.9194	0.5916	0.4000	0.2816	0.2442	0.2742	0.2158	0.0762	-0.0969

NLOS	16.5m	1.0000	0.9314	0.7818	0.4575	0.2191	0.1008	0.1347	0.2222	0.2924	0.2455
	13m	1.0000	0.9950	0.7050	0.4294	0.2069	0.0663	0.1198	0.1976	0.1797	0.1574
	9.5m	1.0000	0.9882	0.9207	0.8208	0.7574	0.7253	0.6503	0.6277	0.6443	0.6228
	6m	1.0000	0.8768	0.6153	0.4292	0.2852	0.1751	0.1174	0.0633	0.1293	0.1689

Table 7: Power fading frequency correlation for power lab scenario (the frequency band staring at [1.20, 1.30] GHz and then 20MHz per step increasing the center frequency to [1.38, 1.48] GHz)

Power fading frequency correlation											
Location											
Power lab		$C_{1,1}$	$C_{1,2}$	$C_{1,3}$	$C_{1,4}$	$C_{1,5}$	$C_{1,6}$	$C_{1,7}$	$C_{1,8}$	$C_{1,9}$	$C_{1,10}$
LOS	23m	1.0000	0.8887	0.7947	0.6332	0.4633	0.2912	0.0935	-0.0591	0.0074	0.0065
	18m	1.0000	0.9454	0.8750	0.6925	0.5127	0.3970	0.3153	0.3205	0.2582	0.2417
	13m	1.0000	0.9339	0.8023	0.6797	0.2744	-0.1012	-0.1517	-0.1962	-0.1826	-0.1851
	8m	1.0000	0.9855	0.9603	0.9209	0.7916	0.5303	0.2748	-0.0161	-0.2857	-0.2204
	5m	1.0000	0.9664	0.8987	0.7392	0.5711	0.5089	0.4869	0.4304	0.3849	0.4135
NLOS	23m	1.0000	0.9720	0.9088	0.7893	0.7588	0.7453	0.6980	0.7460	0.6698	0.4622
	18m	1.0000	0.9492	0.8900	0.8125	0.6058	0.4093	0.4250	0.1067	-0.0097	-0.1435
	13m	1.0000	0.7832	0.6723	0.5220	0.2205	0.2178	0.2066	0.2121	0.0583	-0.0096
	8m	1.0000	0.9840	0.9596	0.8662	0.7294	0.2293	0.2501	0.1622	-0.0804	-0.1334
	5m	1.0000	0.9649	0.8724	0.6602	0.4776	0.3980	0.3053	0.3296	0.3106	0.2774

Table 8: Statistics of *rms delay spread* at frequency band [1.25, 1.35] GHz

RMS delay spread						
Frequency band: 1.25GHz-1.35GHz						
location		*distance* [m]	*mean* [ns]	*std dev.* [ns]	*min* [ns]	*Max* [ns]
LOS	power lab	23	25.9876	6.9666	14.8434	47.0618
		18	29.0955	7.1427	14.7095	49.3425
		13	29.1341	6.0364	18.0896	45.0408
		8	29.4215	7.4963	19.2061	58.1712
		5	27.3105	6.8349	15.5864	42.9442
	canteen	29	28.4603	6.2183	16.6552	44.1714
		24	31.2805	6.5753	20.7753	46.1752
		19	26.0776	5.3461	15.3238	41.5147
		14	28.2710	5.5966	14.6876	44.6924
		9	19.8703	3.5962	13.8214	29.1045
	library	16.5	15.8506	4.8171	8.8262	26.5818
		13	17.5050	2.6395	12.1397	22.8340
		9.5	22.1525	4.4212	12.7996	31.8695
		6	16.1128	4.0038	8.5011	26.2930
	total	**6.0-29.0**	**24.7521**	**5.5494**	**8.5011**	**58.1712**

NLOS	power lab	23	43.6218	7.4764	30.5080	69.4082
		18	36.8112	7.1126	18.7390	57.6750
		13	35.6456	7.2002	22.1767	55.7021
		8	50.0190	6.8458	31.7068	62.7053
		5	40.9507	8.8741	21.0856	59.8520
	canteen	29	31.9960	8.8134	16.4868	54.1707
		24	32.1150	5.3732	22.1687	46.5749
		19	28.2888	5.1072	19.3247	40.8287
		14	29.6596	6.3653	20.2528	54.0579
		9	26.4615	6.5155	14.2924	40.3058
	library	16.5	23.9726	5.4430	14.6866	37.6411
		13	21.6421	4.4150	13.7510	31.1757
		9.5	20.1319	3.7794	12.7236	27.5486
		6	20.3112	5.1771	10.9287	35.3249
	total	**6.0-29.0**	**31.5448**	**6.3213**	**10.9287**	**69.4082**

Table 9: Statistics of *rms delay spread* at frequency band [1.95, 2.05] GHz

RMS delay spread						
Frequency band:1.95GHz-2.05GHz						
location		*Distance* [m]	*mean* [ns]	*std dev.* [ns]	*min* [ns]	*Max* [ns]
LOS	power lab	23	38.1256	6.1112	23.9191	50.7783
		18	41.7836	8.2449	27.9466	64.9642
		13	38.8221	8.7587	24.6829	54.3396
		8	35.1235	10.3385	16.7628	60.3930
		5	31.5883	8.8859	16.3928	53.4212
	canteen	29	39.1987	10.6956	20.9777	63.9289
		24	27.8493	5.4007	17.1546	41.8978
		19	38.1256	9.1081	16.9886	61.3920
		14	30.2621	12.7856	12.7088	59.5666
		9	19.4412	4.4545	11.5328	38.4416
	library	16.5	35.7374	19.1892	14.8370	90.2483
		13	37.8208	12.3611	23.2415	81.2675
		9.5	26.8863	7.1333	15.0520	52.7629
		6	20.4166	6.6627	10.9960	40.7494
	total	**6.0-29.0**	**32.9415**	**9.2950**	**10.9960**	**90.2483**
NLOS	power lab	23	38.1249	5.7101	28.6959	53.1984
		18	34.7218	7.6652	19.6062	52.7355
		13	39.3105	7.3639	23.8726	67.9788
		8	47.6691	7.1436	32.5282	63.2485
		5	38.5297	7.7870	22.5274	60.5354
		29	32.5453	7.6471	17.5314	53.7158
		24	34.2908	6.9632	24.9888	54.4713

	canteen	19	32.0610	7.4391	17.6829	53.9749
		14	34.7352	7.8033	18.2765	65.2089
		9	38.5536	7.8765	21.4421	59.3523
	Library	16.5	33.3097	5.8414	21.6759	49.9941
		13	26.3869	6.0043	16.2036	41.5889
		9.5	22.0313	5.8462	12.5923	36.2833
		6	22.6001	6.4773	11.6429	43.7411
	total	**6.0-29.0**	**33.9193**	**6.9692**	**11.6429**	**67.9788**

Table 10: Statistics of *rms delay spread* at frequency band [2.55, 2.65] GHz

RMS delay spread						
Frequency band: 2.55GHz-2.65GHz						
location		*distance* [m]	*mean* [ns]	*std dev.* [ns]	*min* [ns]	*max* [ns]
LOS	power lab	23	36.4297	8.2600	22.3906	56.2749
		18	31.7199	7.7690	17.2013	54.0687
		13	23.2454	3.7241	13.9262	33.7470
		8	24.6001	5.2177	16.6903	37.0455
		5	37.7255	12.9194	14.4776	71.4357
	canteen	29	38.5276	9.5447	20.8585	73.4581
		24	22.8226	5.4380	14.3049	38.9510
		19	29.4499	5.2970	19.8941	43.8901
		14	21.4733	7.0212	11.9042	45.7679
		9	17.7901	4.5085	8.1557	29.5992
	library	16.5	35.9399	8.6496	20.6209	53.6822
		13	55.9022	15.3538	23.5159	92.3085
		9.5	47.0565	8.6954	31.9159	66.1317
		6	36.4576	9.6796	17.5955	57.8509
	total	**6.0-29.0**	**32.7957**	**8.0056**	**8.1557**	**92.3085**
NLOS	power lab	23	40.8324	6.3196	29.0950	56.2267
		18	44.4456	10.2532	24.7398	69.9564
		13	38.4980	8.0883	23.6814	55.5435
		8	48.1058	12.7236	24.9516	75.1483
		5	36.8259	11.5116	18.6774	59.2484
	canteen	29	36.2810	8.4366	21.2542	57.9716
		24	42.7043	8.3770	28.8656	71.2201
		19	39.6278	7.1787	28.3685	59.8191
		14	42.9458	10.8601	23.4579	68.1301
		9	46.0894	8.5733	29.4569	70.7851
	library	16.5	40.6828	10.2872	23.3543	61.1959
		13	36.3241	8.3449	20.8006	54.8245
		9.5	26.8657	8.5898	12.0187	45.1331
		6	30.2565	6.9739	18.7806	51.9728
	total	**6.0-29.0**	**39.3204**	**9.0370**	**12.0187**	**75.1483**

Table 11: statistics of *rms delay spread* at frequency band [3.15, 3.25] GHz

RMS delay spread						
Frequency band: 3.15GHz-3.25GHz						
location		*distance* [m]	*mean* [ns]	*std dev.* [ns]	*min* [ns]	*max* [ns]
LOS	power lab	23	37.3287	11.0053	19.6912	71.0996
		18	23.4339	6.7552	13.8308	39.2153
		13	28.1978	8.7675	17.0578	52.6991
		8	31.8153	10.6770	14.5920	62.3619
		5	37.8687	12.1513	20.5103	75.6998
	canteen	29	38.5099	10.5777	21.2369	69.5160
		24	40.6713	8.7521	26.3684	65.6731
		19	32.4121	8.6409	17.8708	55.3712
		14	27.3916	11.1455	13.8105	72.3681
		9	22.4640	5.9850	11.9886	37.6931
	library	16.5	21.9174	6.6325	12.4834	43.9982
		13	28.6937	6.3931	15.8567	41.9641
		9.5	23.2619	5.6489	13.4071	37.0891
		6	36.8845	11.7982	5.2659	21.4488
	total	**6.0-29.0**	**30.7751**	**8.9236**	**5.2659**	**75.6998**
NLOS	power lab	23	46.0142	7.7917	27.9121	61.9509
		18	44.1125	8.9810	23.9677	72.2230
		13	37.7478	7.4719	21.0126	59.3624
		8	46.0738	7.7552	30.0624	64.2770
		5	42.0208	8.8718	26.2339	59.3771
	canteen	29	41.2513	7.5523	25.1161	55.4357
		24	47.0745	8.4357	28.5675	68.5327
		19	43.2053	8.0104	29.2234	61.6485
		14	36.4364	9.4576	18.5012	60.6806
		9	39.8862	9.1061	21.1565	67.9202
	library	16.5	28.5995	7.0877	15.2429	44.2577
		13	25.1179	5.8540	14.6366	44.5289
		9.5	23.0948	6.0741	10.9453	39.8655
		6	27.1907	7.7994	12.6374	48.5216
	total	**6.0-29.0**	**37.7018**	**7.8749**	**10.9453**	**72.2230**

Table 12: *rms delay spread* frequency correlation for power lab scenario

RMS delay spread frequency correlation					
Location					
Power lab		$C(f_1, f_1)$	$C(f_1, f_2)$	$C(f_1, f_3)$	$C(f_1, f_4)$
LOS	23m	1	0.5019	-0.1124	-0.0816
	18m	1	-0.1887	0.0616	0.2866
	13m	1	0.3040	0.1248	-0.0809
	8m	1	-0.0856	0.0835	0.1689
	5m	1	-0.1126	0.3271	0.2913
NLOS	23m	1	0.0890	-0.1991	0.0739
	18m	1	0.0648	0.0177	0.0063
	13m	1	0.1174	0.0531	0.0840
	8m	1	-0.1232	-0.0253	0.2812
	5m	1	-0.1425	0.2093	0.0466

Table 13: *rms delay spread* frequency correlation for canteen scenario

RMS delay spread frequency correlation					
Location					
Canteen		$C(f_1, f_1)$	$C(f_1, f_2)$	$C(f_1, f_3)$	$C(f_1, f_4)$
LOS	29m	1	-0.4126	0.1139	0.0153
	24m	1	-0.0858	0.2296	-0.0352
	19m	1	-0.2797	0.2710	0.0514
	14m	1	-0.1334	-0.1232	0.1578
	9m	1	0.2424	-0.2864	-0.1340
NLOS	29m	1	-0.1431	-0.0092	0.1331
	24m	1	0.0283	-0.1307	-0.0866
	19m	1	-0.3348	-0.3167	0.0355
	14m	1	0.1061	0.1940	0.0427
	9m	1	-0.0599	0.0856	0.1333

Table 14: *rms delay spread* frequency correlation for library scenario

RMS delay spread frequency correlation					
Location					
library		$C(f_1, f_1)$	$C(f_1, f_2)$	$C(f_1, f_3)$	$C(f_1, f_4)$
LOS	16.5m	1	-0.5991	0.5459	0.5745
	13m	1	-0.0649	-0.0235	0.0136
	9.5m	1	0.3122	0.1184	-0.2202
	6m	1	-0.1499	0.0288	-0.0598
NLOS	16.5m	1	-0.0079	0.3956	0.2507
	13m	1	0.1399	0.1764	-0.0053
	9.5m	1	0.0252	-0.0966	-0.0955
	6m	1	-0.2003	-0.2732	-0.1853